USCEE REPORT #271

Fourier Coding of Images

by

Harry C. Andrews

June 1968

Signal and Image Processing Institute
UNIVERSITY OF SOUTHERN CALIFORNIA
Department of Electrical Engineering-Systems
3740 McClintock Avenue, Room 404
Los Angeles, CA 90089-2564 U.S.A.

ABSTRACT

The transmission of two dimensional images over large distances from far ranging space probes has become an important factor in space exploratory research. A common requirement for such transmission systems is a large bandwidth, low noise interference communication link for pleasing reception.

Standard communication systems transmit images as they are normally viewed by light sensing devices such as cameras, photosensitive emulsions, and the human eye. This dissertation presents the results of investigations into the feasibility of transmitting the Fourier transform of an image rather than the spatial domain representation. The motivations behind the study of image transmission in the Fourier domain are threefold. First, the Fourier transform tends to compact the image energy in the Fourier domain such that large bandwidth reductions can be obtained. Second, noise energy introduced in the Fourier domain tends to spread over the entire retransformed image, and thus becomes less offensive to the eye. Finally, image enhancement can be accomplished by using nonlinear quantization and coding techniques on the Fourier domain.

In this dissertation a proof of the equality of entropy in the spatial and Fourier domains of an image is derived. Adaptive quantization methods which compensate for the tremendous dynamic range of information in the Fourier domain are developed. A high speed two dimensional Fourier transforming computer algorithm is designed, and experimental results are obtained through a digital computer implementation of the Fourier coding communication system. Experimental verification of the equal entropy concepts provided by information theoretic principles is presented.

A noise immunity coding technique is designed for the Fourier domain utilizing the concepts of error correcting codes. Considerably better quality transmission over noisy channels is experienced with the Fourier coding technique as opposed to spatial domain techniques.

Very large bandwidth reductions are obtained by filtering in the Fourier domain. In addition a novel sequential image construction communication system is presented utilizing the bandwidth reduction potentialities of the Fourier domain.

Image enhancement and evaluation techniques are presented. Correlated noise is removed from images by spatial filtering in the Fourier domain. The matched filter, which maximizes the signal to noise ratio for additive noise, is implemented as a tool for evaluating pre-processed and post-processed images by indicating the degree of correlation between the two images.

The results of this research indicate that the Fourier coding of images is a feasible concept for image transmission. Fourier coding provides an inherent noise immunity and permits a significant bandwidth reduction without tolerable image degradation. Finally, Fourier domain processing techniques can be utilized to remove image defects.

TABLE OF CONTENTS

LIST OF FIGURES

ACKNOWLEDGEMENT

The author wishes to acknowledge the advice and encouragement provided by the members of his guidance committee throughout the period of this research: Professors I. S. Reed and T. E. Harris. The author particularly appreciates the interest shown by his chairman, Professor W. K. Pratt, in the development and implementation of the research project reported here.

The experimental portion of this research was invaluably assisted by the huge software programming effort provided by Mr. D. J. Ketcham. In addition, the kind assistance of the Jet Propulsion Laboratory and Mr. F. C. Billingsley in obtaining digitized images for test scenes is greatly appreciated.

This research was supported to a significant degree by a NASA Research Grant NGR-05-018-044, and the author wishes to acknowledge this kind assistance.

CHAPTER 1

INTRODUCTION

1.1 Research Motivation

Television has become an increasingly important means of communication in scientific, military, and commercial applications. Recently, particular emphasis has been placed on spacecraft exploratory missions in which television pictures are transmitted over great distances. Important problems in the transmission of television for such an application are the high bandwidth and low noise interference requirements for quality reception.

Over the years many investigations have been made into the reduction of bandwidth in the transmission of video scenes [1]. The investigations have often made use of the communication model depicted in figure 1-1 in which a video source is quantized, coded, transmitted over a channel, and then decoded for reconstruction. Diverse quantizing, scanning, coding, and modulation schemes have been developed [1]. These techniques have been restricted to processing in the spatial domain of an image or scene. The spatial domain is the two dimensional coordinate system associated with a scene as normally viewed by the eye or optical scanning device.

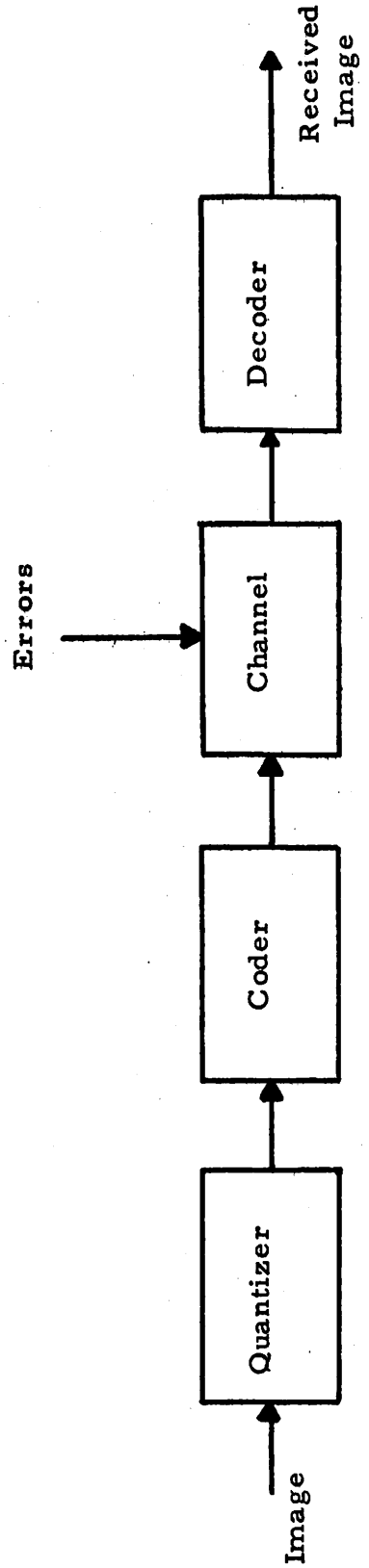

Figure 1-1.--Spatial Domain Communication Model

Generally, results have not been favorable using spatial domain methods.

The research reported here deals with the general communication model of figure 1-2. The approach taken to the communication problem is different from earlier efforts and affords further insight into the video bandwidth-transmission problem. Rather than investigating properties of a scene, characterized by a bounded positive real two dimensional function, the properties of the two dimensional Fourier transform of the scene are studied. This introduces the frequency domain of an image as that coordinate system which corresponds to the Fourier transform of the image. The question then arises as to what properties, if any, of the frequency domain will allow for more efficient video transmission in terms of noise immunity, bandwidth reduction, more efficient coding, and improved quality reconstruction.

The motivations behind the study of image transmission in the Fourier domain are threefold. First, the Fourier transform, in general, tends to compact the image energy in the frequency domain such that more efficient scanning can be implemented. Second, noise energy introduced in the frequency domain spreads its energy over the entire retransformed image thus becoming less offensive to the human eye. Finally, image enhancement can be accomplished during the transmission process by using nonlinear quantizing and coding

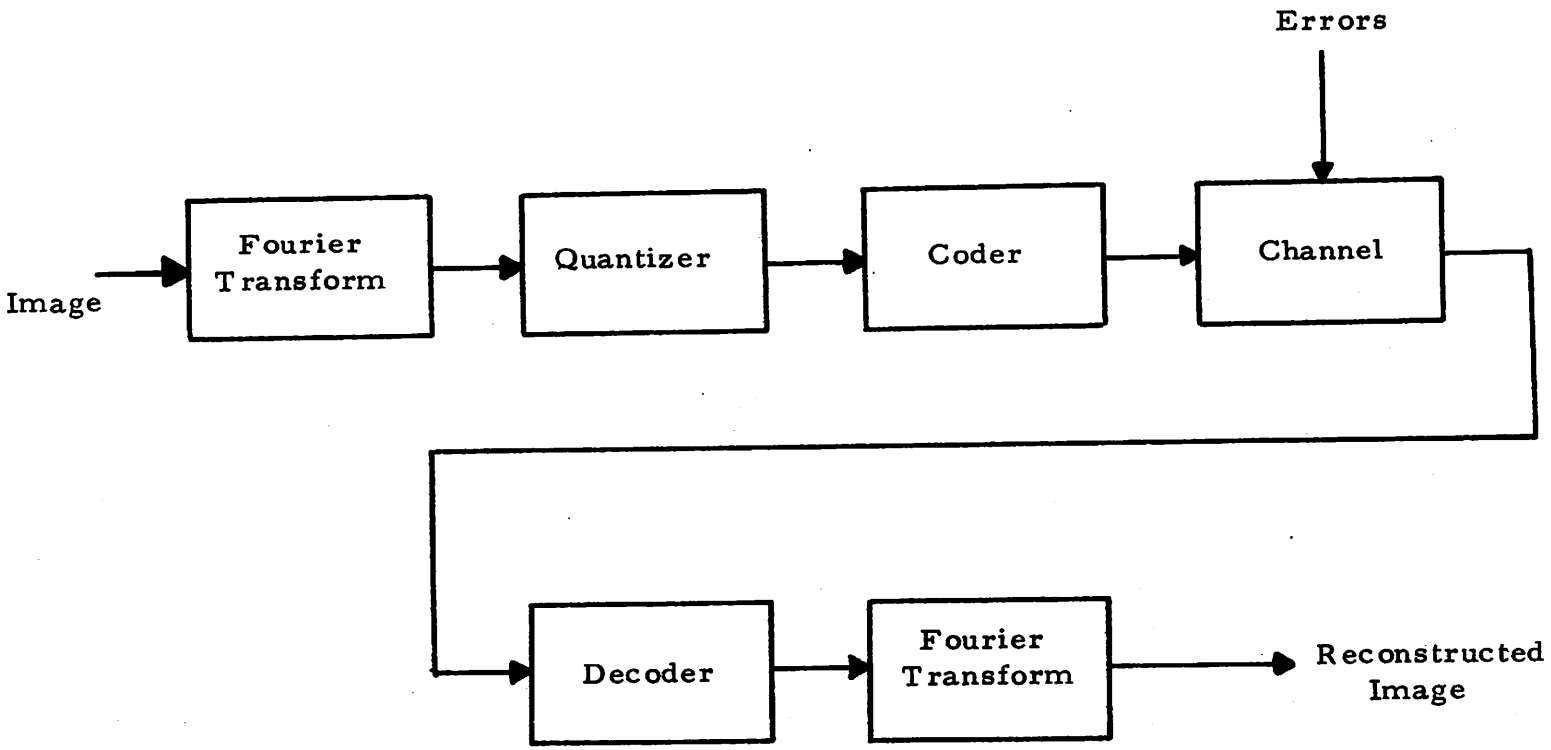

Figure 1-2.--Fourier Domain Communication Model

schemes.

1.2 Research Problem

The problem presented for research consists of an analytic and experimental investigation of the feasibility of transmitting the Fourier domain of an image as an improvement to normal spatial domain transmission. The analytic portion of the research is involved with studying the properties of the Fourier domain from an information theoretic viewpoint in order to derive necessary guidelines for developing the communication techniques needed for successful transmission of that domain over a communication link. In addition, entropy concepts are developed and density functions derived in order to construct quantization and coding rules for transmission. The experimental portion of the research is oriented toward the implementation of techniques suggested by analytic derivations. This task includes verification of equal bandwidth requirements in both the spatial and Fourier domains and implementation of quantization, noise immunity, and bandwidth reduction coding rules. The experimentation could have been performed by analog optical data processing. However, it was felt that with the considerable flexibility and dynamic range of digital computers, the more successful results would be obtained from a completely digital experimental approach. A digital computer facility has been developed solely for

this research project. Required hardware modifications for picture processing have been made to the digital computer so that two dimensional displays are possible. Additionally, a large software programming effort has been undertaken to develop the requisite programs for image processing, communication channel simulation, and receiver reconstruction simulation. The experimental digital effort is based on the development of an efficient Fourier transform program without which the computer computation time would have been far too extensive to initiate even the smallest portion of experimental results presented here.

1.3 Chapter Descriptions

Chapter 1 consists of the introduction to this report, and broadly outlines the research problem and objectives of investigation.

Chapter 2 presents a discussion of two dimensional Fourier transforms. Discrete Fourier transforms are defined and a one dimensional high speed computer algorithm is derived. The one dimensional algorithm is incorporated into a two dimensional format, and experimental verification is presented in support of the validity of the computerized transformation.

Chapter 3 analyzes the deterministic properties of the Fourier domain due to certain restrictions on the spatial domain. This chapter includes the study of symmetry, dynamic range, and

nonnegative-definite functions associated with the frequency domain. An entropy calculation is presented verifying that, from an information theoretic viewpoint, the entropy or uncertainty of the spatial domain and frequency domain is identical.

Chapter 4 develops two methods of quantitative image evaluation. The first is based on statistical parameters, and the second is based on a two dimensional matched filtering concept. Experimental results are compared with the subjective viewing properties of the human eye.

Chapter 5 includes a derivation of the first and second moments of the spectral components in the frequency domain. A probability density distribution is described whose variance changes as a function of frequency. This distribution forms the basis of a frequency adaptive quantization law. An expression for minimum quantization noise is derived and results of experimental quantization rules are presented. These results substantiate the equal bandwidth requirements for both the spatial and Fourier domains.

Chapter 6 presents results of investigations into the inherent noise immunity of Fourier image coding. Specifically, binary symmetric channel noise is discussed; and a coding technique is presented to obtain reasonably good quality images transmitted through a very noisy channel. In addition, techniques for correlated noise removal by processing in the frequency domain are discussed.

Chapter 7 incorporates the results of bandwidth reduction studies. A unique sequential image construction technique, which yields very large bandwidth reductions, is presented. Some drawbacks are indicated, especially in the application of spatial bandwidth reduction techniques to the frequency domain. Certain coding schemes are presented for small reduction factors, and comparisons with spatial domain results are made.

Chapter 8 summarizes the results of the research and offers suggestions for future investigations.

The appendices contain sections on hardware and software systems used in the research.

CHAPTER 2

FOURIER TRANSFORMS

2.1 Two Dimensional Fourier Transforms

The two dimensional Fourier transformation is a linear operator, and consequently lends itself to a linear systems analysis approach analogous to the time-frequency studies of the communications engineer. However, rather than operating on a one dimensional causal time function, the two dimensional Fourier transformation becomes the coupling operation between a non-causal two dimensional space domain and spatial frequency domain. Two dimensional spatial frequency concepts are not new. They have been developed extensively by the optical engineer in studies of optical data processing systems [2,3].

The two dimensional Fourier transform can be expressed mathematically as

$$F(u,v) = \int_{-\infty}^{\infty}\int f(x,y)\, \exp\{i(ux+vy)\}\, dxdy \qquad (2.1)$$

In this equation $f(x,y)$ is a two dimensional function defined on a plane with coordinates (x,y), hereafter referred to as the space domain. The space domain may be assigned the physical dimension of length

along a reference axis. $F(u,v)$ is a two dimensional function defined on a plane with coordinates (u,v), hereafter referred to as the spatial frequency or Fourier domain. The axes dimensions of the frequency domain have units of cycles per unit length. $F(u,v)$, then, is the two dimensional Fourier transform of $f(x,y)$ with respect to the Fourier kernel $\exp\{i(ux+vy)\}$.

2.2 Optical Implementation

In order to become familiar with the physical applications, and to perceive the significance of the above two dimensional transform, a brief review of optical data processing schemes will be presented. Most optical processing systems are linearly analyzed in light intensity, or amplitude and phase, depending on whether the optical elements are illuminated with incoherent or coherent optical radiation, respectively. The case of coherent illumination is of particular interest. The concepts of coherent optical systems and spatial frequencies can be explained with reference to figure 2-1. A transparency with transmittance $f(x,y)$ is illuminated by a coherent, collimated light beam so that the electric field amplitude of the light at the input plane is proportional to $f(x,y)$. The spherical lens produces an image of the transparency in the frequency plane. The light electric field amplitude, $F(u',v')$, in the frequency plane, as determined by the Kirchhoff integral of diffraction theory, is given by the Fourier

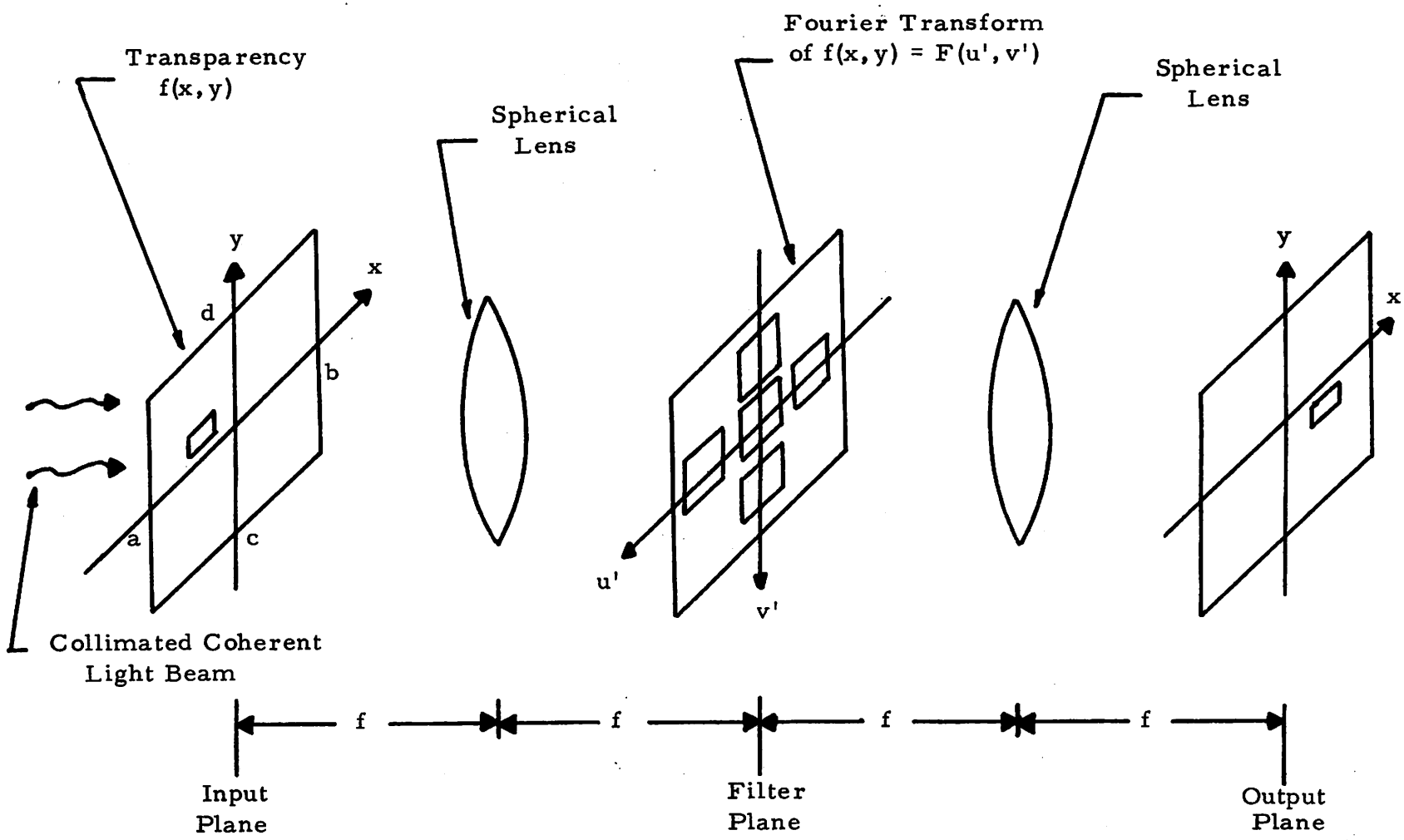

Figure 2-1.--Coherent Optical System

transform relation

$$F(u',v') = \int_c^d \int_a^b f(x,y) \exp\left\{\frac{2\pi i}{\lambda f}(u'x+v'y)\right\} dxdy \qquad (2.2)$$

where λ is the wavelength of light illuminating the transparency and f is the focal length of the lens [4, pg. 379]. This relation can be written as

$$F(u,v) = \int_c^d \int_a^b f(x,y) \exp\{i(ux+vy)\} dxdy \qquad (2.3)$$

where $u = \frac{2\pi u'}{\lambda f}$ and $v = \frac{2\pi v'}{\lambda f}$ are called the spatial frequencies in the Fourier transform frequency plane. A second spherical lens, as shown in figure 2-1, performs a second Fourier transform to return to the space domain. The image is rotated 180° because each spherical lens introduces a positive two dimensional kernel. This is mathematically expressed as

$$\mathcal{F}_2\left\{\mathcal{F}_2\{f(x,y)\}\right\} = f(-x,-y) \qquad (2.4)$$

where $\mathcal{F}_2$ implies a two dimensional Fourier transform.

In optical data processing systems the frequency content of a two dimensional signal, f(x,y), may be modified by placing a transparency, H(u,v), in the frequency plane of the function. The output,

$\mathcal{O}(-x,-y)$, of a second spherical lens, and therefore second Fourier transform, can be expressed as

$$\mathcal{O}(-x,-y) = \mathcal{F}_2\{F(u,v)H(u,v)\} \tag{2.5}$$

This physical system can be mathematically modeled by a two dimensional linear system analysis as illustrated in figure 2-2 where $h(x,y)$ is the impulse response of the filter and is equal to the Fourier transform of $H(u,v)$.

For a completely general two dimensional linear processing system, both complex (real and imaginary) inputs and outputs must be readily processable. In fact, only under special circumstances will the output of a Fourier transformation be entirely real. Unfortunately, the light sensing transducers employed in optical data processing systems are only sensitive to energy or intensity rather than phase and amplitude. Consequently, it is difficult to implement and detect complex functions optically, although some methods to exist [5]. An alternative to optical processing is found by incorporating the use of a digital computer for completely general two dimensional information processing.

2.3 Digital Fourier Transforms

A two dimensional digital Fourier transform may be represented by the equation

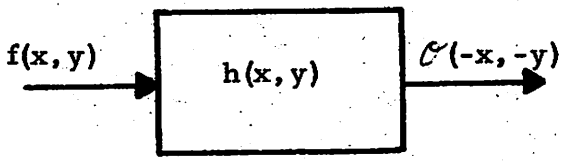

Figure 2-2. --Two Dimensional Filter

$$F(u,v) = \frac{1}{N} \sum_{x,y=0}^{N-1N-1} f(x,y) \exp\left\{\frac{2\pi i}{N}(ux+vy)\right\} \qquad (2.6)$$

The inversion formula associated with equation (2.6) is

$$f(x,y) = \frac{1}{N} \sum_{u,v=0}^{N-1N-1} F(u,v) \exp\left\{-\frac{2\pi i}{N}(ux+vy)\right\} \qquad (2.7)$$

For ease of programming, the inversion relation is not used. Instead the positive kerneled transform will always be employed, thereby introducing rotated retransformed images.

As with the continuous case, equation (2.1), f(x,y) is a two dimensional spatial function and F(u,v) is its Fourier transform. However, the functions f(x,y) and F(u,v) have, of necessity, been quantized in the space and frequency domains, respectively. The indices x, y, u, v, take on integer values running from zero to N-1. Also, equation (2.6) represents a finite transformation. The discrete two dimensional transform can be expressed in the form of

$$F(u,v) = \sum_{x,y=-N/2}^{\frac{N}{2}-1\ \frac{N}{2}-1} f(x,y) \exp\left\{\frac{2\pi i}{N}(ux+vy)\right\} \qquad (2.8)$$

with the inversion formula

$$f(x,y) = \frac{1}{N^2} \sum_{u,v=-N/2}^{\frac{N}{2}-1\ \frac{N}{2}-1} F(u,v) \exp\left\{-\frac{2\pi i}{N}(ux+vy)\right\} \qquad (2.9)$$

However, to maintain continuity, equation (2.6) will be adhered to.

An initial survey of digital Fourier transforming techniques has indicated that until very recently only brute force methods were available for producing the transformation [6]. For instance, if it is desired to compute the one dimensional finite Fourier transform of a function f(x) sampled at N points, then the finite Fourier transform is given by

$$F(u) = \frac{1}{\sqrt{N}} \sum_{x=0}^{N-1} f(x) \exp\left\{ \frac{2\pi i u x}{N} \right\} \qquad (2.10)$$

Computation of F(u) by conventional techniques requires N^2 complex additions and multiplications. Computation of F(u, v) in equation (2.6) by the brute force method requires N^4 complex additions and multiplications. To evaluate a picture of 1000 by 1000 elements requires 10^{12} complex additions and multiplications.

In 1965 Cooley and Tukey developed an algorithm which reduced the number of complex additions and multiplications in the one dimensional case to N lg N each [7][1]. The algorithm requires N to be a highly composite number and is generally taken to be equal to 2^n (a readily adaptable parameter to digital computations).

---

[1] lg represents the logarithm to the base two.

2.4 One Dimensional High Speed Fourier Transform Algorithm

In developing the experimental capability needed for Fourier coding research, a one dimensional Fourier transform algorithm was developed. The algorithm described here utilizes a modification of the Cooley-Tukey approach and requires N lg N complex additions and only $\left(\frac{N}{2}\right)\left[\text{Lg (N)-2}\right]+1$ complex multiplications for the one dimensional example [8]. This savings is significant when it is realized that a complex multiplication includes two real multiplications and four real additions. Since most computers have a longer multiply than add time, the computation period is greatly reduced. The reduction of complex multiplication operations can be achieved by evaluating spectral components in a specified order and using the fact that

$$\exp\left\{\frac{2\pi i}{N} k\right\} = - \exp\left\{\frac{2\pi i}{N}\left(k+\frac{N}{2}\right)\right\} \qquad (2.11)$$

The algorithm can be explained by letting f(x) be a one-dimensional complex function which has been sampled and stored in $N = 2^n$ locations and defining F(u) to be the spectral domain representation of the Fourier transform of f(x) given by the equation

$$F(u) = \sum_{x=0}^{N-1} f(x) \exp\left\{\frac{2\pi i}{N} xu\right\} \qquad (2.12)$$

to within a normalizing constant $\frac{1}{\sqrt{N}}$.

Now, expressing x and u in binary form,

$$x = x_{n-1}x_{n-2}\cdots x_1x_0; \qquad x_j \epsilon (0,1) \tag{2.13}$$

$$u = u_{n-1}u_{n-2}\cdots u_1u_0; \qquad u_j \epsilon (0,1) \tag{2.14}$$

and taking advantage of the integer periodic qualities of the complex exponential function, F(u) can be written as [9]

$$F(u_{n-1},\ldots,u_0) = \sum_{x_0,x_1}^{1} \sum \cdots \sum_{x_{n-2},x_{n-1}=0}^{1} \sum f(x_{n-1},\ldots,x_0)P_{n-1}P_{n-2}\cdots P_1P_0 \tag{2.15}$$

where

$$P_j = \exp\left(\frac{2\pi i}{N}\left[u_{n-1-j},\ldots,u_0,0,\ldots,0\right]x_j\right) \tag{2.16}$$

Now upon summing over the x_j, starting with the most significant bit, x_{n-1}, it is evident that the sum of equation (2.12) is made in a specific order. Performing the computation in this order allows for the storage of calculations so that no identical computation need be repeated.

Note that for each sum over x_j, the exponential, P_j, can only take on specific values as a function of the particular spectral point, u, being evaluated. In fact, as more and more x_j are summed (approaching the least significant bit of the binary representation of

x) it is evident that the exponential, P_j, takes on values defined by the shifting of the binary representation of the spectral point, u. For example, if the spectral point 001 were being evaluated, P_j would take on values defined by

$$P_j = \exp\left[\frac{2\pi i}{N}(100)x_j\right], \quad P_j = \exp\left[\frac{2\pi i}{N}(010)x_j\right] \text{ and}$$

$$P_j = \exp\left[\frac{2\pi i}{N}(001)x_j\right].$$

For convenience, $C_k \equiv \exp\frac{2\pi iK}{N}$ is defined and a table is formed in which P_j are defined for each step in the computation and for each spectral point. In constructing such a table, it is advantageous to list the spectral points as increasing binary numbers with the most significant bit on the right. In evaluating a particular spectral point, that point should be interpreted as its binary representation with the most significant bit on the left. The table for n = 4 is given in figure 2-3.

In evaluating spectral components as they are listed in the table, it is found that after evaluating point u = 0 and retaining all intermediate sums in their storage locations, the evaluation of point u = 8 requires only a single subtaction. This is because $C_j = -C_{\left(j+\frac{N}{2}\right)}$, and from the table, $C_8 = -C_0 = -1$. To evaluate spectral point u = 4 it is only necessary to back up two storage locations and perform a

Spectral Point		Exponential Factor Values				Program Number
	$u_3u_2u_1u_0$	P_3	P_2	P_1	P_0	PN
0	0 0 0 0	1	1	1	1	0
8	1 0 0 0	1	1	1	C_8	1
4	0 1 0 0	1	1	C_8	C_4	2
12	1 1 0 0	1	1	C_8	C_{12}	1
2	0 0 1 0	1	C_8	C_4	C_2	3
10	1 0 1 0	1	C_8	C_4	C_{10}	1
6	0 1 1 0	1	C_8	C_{12}	C_6	2
14	1 1 1 0	1	C_8	C_{12}	C_{14}	1
1	0 0 0 1	C_8	C_4	C_2	C_1	4
9	1 0 0 1	C_8	C_4	C_2	C_9	1
5	0 1 0 1	C_8	C_4	C_{10}	C_5	2
13	1 1 0 1	C_8	C_4	C_{10}	C_{13}	1
3	0 0 1 1	C_8	C_{12}	C_6	C_3	3
11	1 0 1 1	C_8	C_{12}	C_6	C_{11}	1
7	0 1 1 1	C_8	C_{12}	C_{14}	C_7	2
15	1 1 1 1	C_8	C_{12}	C_{14}	C_{15}	1

Figure 2-3.--Spectral Point Evaluation for N = 16

subtraction to obtain C_8 in column P_1, and then perform one multiplication to obtain C_4 in column P_0. Note that this C_4 is circled. To evaluate spectral point u = 12 only a simple subtraction is necessary as $C_4 = -C_{12}$. Continuing in this manner it is seen that all columns contain pairs of $C_j = -C_{\left(j+\frac{N}{2}\right)}$ and that whenever one of these pairs is encountered, a simple subtraction is in order. The circled constants are the locations in the algorithm in which a multiplication must take place. The number of actual multiplications that will be required for each circled constant equals two raised to the index of the column in which the circled constant appears. Thus, from the table, the total number of multiplications required is equal to $(7)2^0 + (3)2^1 + (1)2^2 = 17$ complex multiplications. In general, the number of complex multiplications is equal to

$$\sum_{k=2}^{n} (2^{k-1} - 1)2^{n-k} = \frac{N}{2}(n-2) + 1 \qquad (2.17)$$

where $N = 2^n$

As an example, Fourier transforming a function with 1024 points requires 4097 complex multiplications as compared to N lg N = 10,240 complex multiplications. With such an algorithm the number of exponential constants, C_j, that must be used is (N/2) - 1. The number of storage locations for the entire transformation is N initial

data points, N spectral data points, and N-2 temporary data points.

Implementation of the algorithm is best described with reference to figure 2-4. In designing the computer program to implement the one-dimensional algorithm, additional computation may be saved if the input is known to be real. Such a restriction on the input manifests itself as a symmetric conjugate property of the Fourier transform, and consequently only $\frac{N}{2} + 1$ spectral data points need be calculated. However, the program must be able to accept complex inputs whenever the case arises. Figure 2-4 shows the command and control for the program. The spectral point is calculated by incrementing a binary counter and interpreting the most significant bit as the least. The program numbers are obtained by an inverse sieving operation as in the example of figure 2-3. The coefficient addresses are computed when a multiplication becomes necessary. Finally, a branch to a specific program takes place. Program PN0 will always be the first program. It sequentially adds the first half of the data input to the second half, storing the results in $\frac{N}{2}$ storage locations. This operation is repeated until the final sum is stored in one storage location. This result is the average value of the original function, f(x). Program PN1 simply backs up a storage location and performs a subtraction resulting in the value for the spectral point found by adding $\frac{N}{2}$ to the prior spectral point. This can be verified

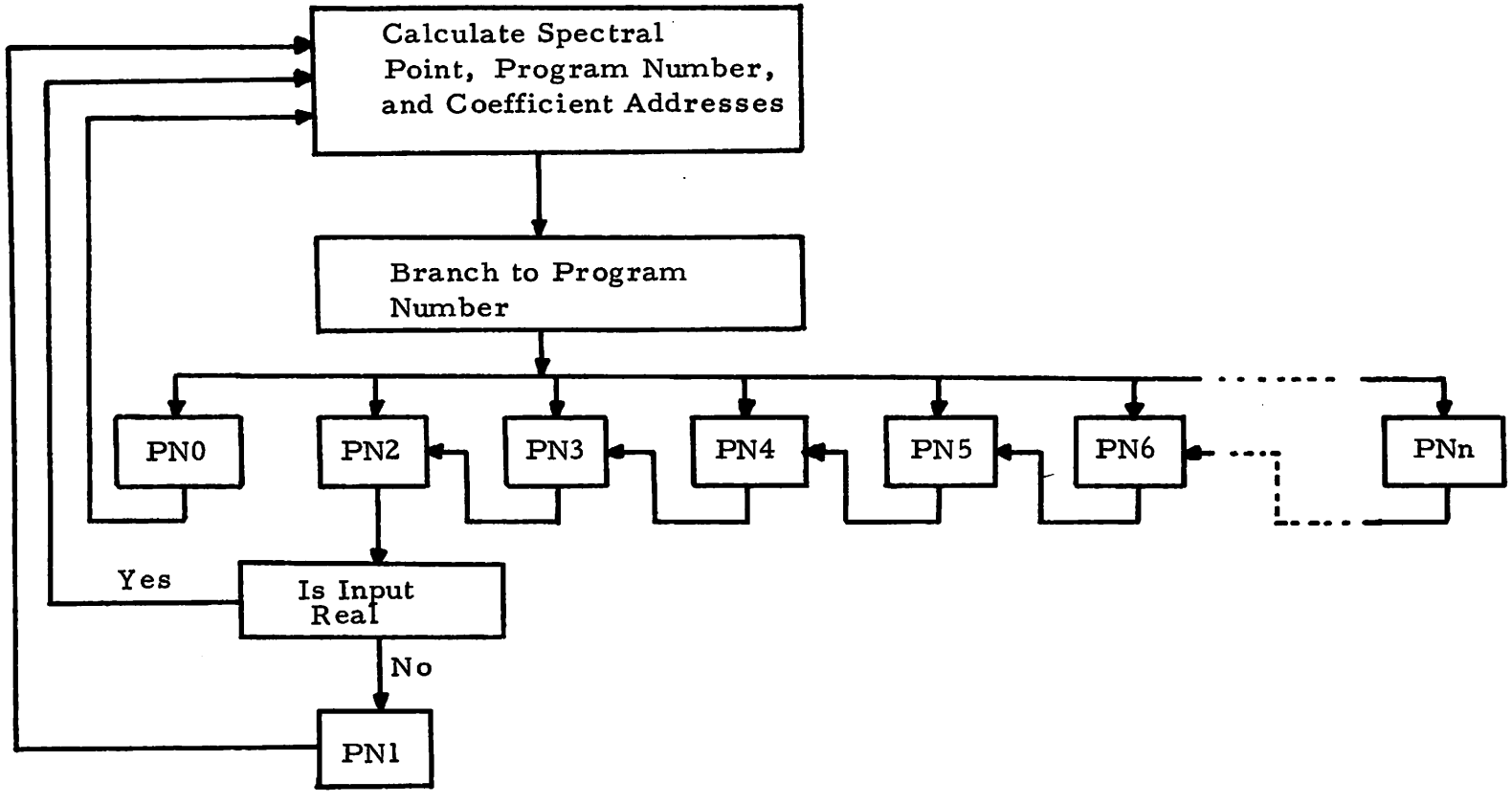

Figure 2-4. --Program Block Diagram

from figure 2-3 where program PN1 always evaluates the spectral point $\frac{N}{2} = 8$ greater than the previous spectral point. Notice that program PN1 always evaluates spectral points greater than or equal to $\frac{N}{2}$ and consequently need not be implemented, except once, for real inputs. All other programs back up a respective number of levels of storage locations, implement a series of subtractions and multiplications, and branch to the next lower program number.

2.5 Experimental Results

The one dimensional Fourier transform algorithm described in the previous section has been incorporated into a two dimensional Fourier transforming program. The operation and data flow of this program is described in the appendix. Experimental results utilizing the two dimensional program are encouraging, and are presented below.

A two dimensional real function whose Fourier transform is mathematically known is the first scene. The simplest such function is probably a square of uniform amplitude. The Fourier transform of the square is a $\left(\frac{\sin au}{au}\right)\left(\frac{\sin av}{av}\right)$ pattern in the frequency plane where a is an appropriate constant. If the square is not centered in the space domain, the frequency domain will have a phase shift associated with the pattern. In addition, as mentioned before, all optical or light sensing devices are sensitive only to

intensities and not amplitudes and phases. Therefore visual representation of the Fourier domain will contain only magnitude information with a loss of phase information. Two visual display techniques are employed. The first technique displays the square root of the sum of the squares of the real and imaginary components of each frequency sample. The second technique displays the logarithm of the magnitude of the Fourier transform. This produces a nonlinear representation of the Fourier samples but allows viewing of low magnitude information that otherwise would remain undetected. Since neither the magnitude nor logarithm of the magnitude display techniques alter the physical positioning of the Fourier transform information, these display methods have become exceedingly useful tools in studying the information distribution in the frequency domain.

Figure 2-5 contains the square test function and its Fourier display. Figure 2-5a displays the square of uniform amplitude. Figure 2-5b displays the logarithm of the magnitude of the Fourier transform of the square in figure 2-5a. The shape of the logarithmic display is a $|[(\sin au)/au][(\sin av)/av]|$ function. Notice that there is high frequency information far out on the axes of the frequency plane but very little off axis. This is intuitively justified as there are no diagonal brightness transitions in the original square. Figure 2-5c is a two level block letter scene which has been Fourier transformed. The logarithm of the magnitude of the Fourier transform is

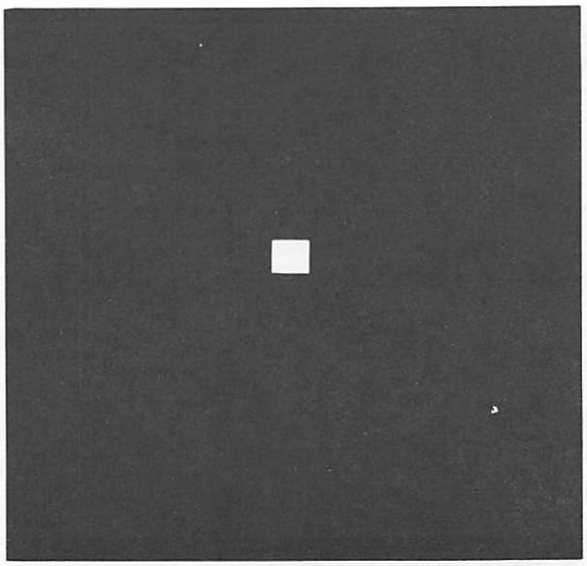

a) Square

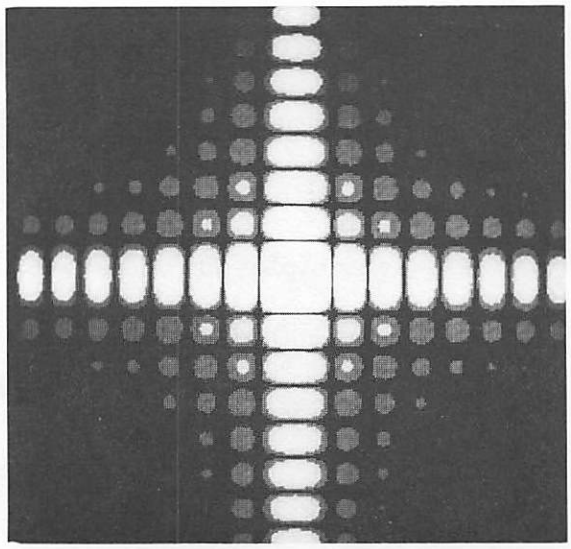

b) Logarithm of the Magnitude of the Fourier Transform of the Square

c) Block Letters "USC"

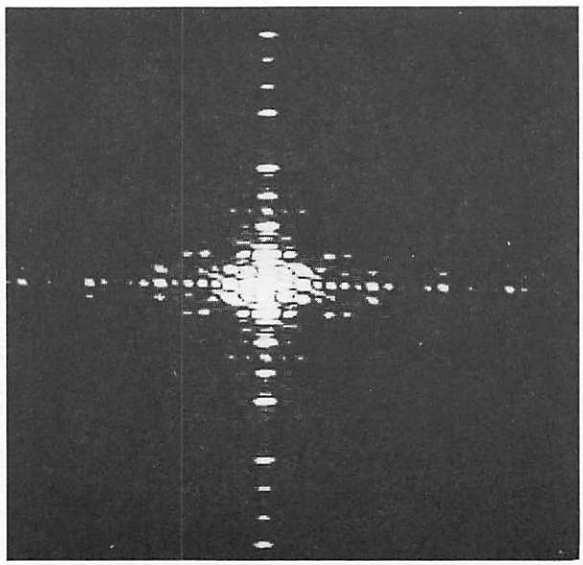

d) Logarithm of the Magnitude of the Fourier Transform of the Block Letters

Figure 2-5. -- Two Test Scenes

displayed in figure 2-5d.

It is desirable to obtain the original function from a double implementation of the two dimensional Fourier transform program. Such results are afforded by figures 2-6, 2-7, and 2-8. Figure 2-6 is a typical moon surface with a portion of the Surveyor footpad in the upper right corner. This scene has been Fourier transformed and the magnitude and the logarithm of the magnitude of the Fourier transform are displayed in figure 2-6b and 2-6c, respectively. The Fourier transform of the original scene has been introduced, in its complex form, into the two dimensional transform program; and a second Fourier transform has been taken. The result of this transformation has been rotated 180^{o} and is displayed in figure 2-6d. Figures 2-7 and 2-8 are two different moon scenes which have been double Fourier transformed. There is no noticeable degradation in either of the retransformations in these figures.

2.6 Data Processing Errors

The subject of digital Fourier transforming of images would not be complete without a discussion of the limitations due to the discrete and finite nature of the computations. The computer calculations have been carried out in simple single precision integer arithmetic. This means that all results are integer valued and

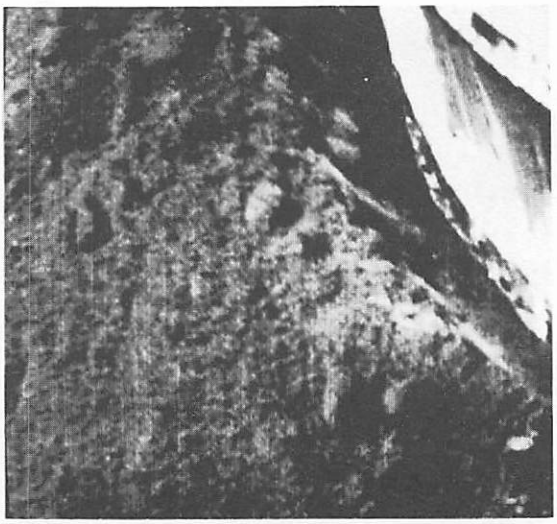

a) Surveyor Footpad

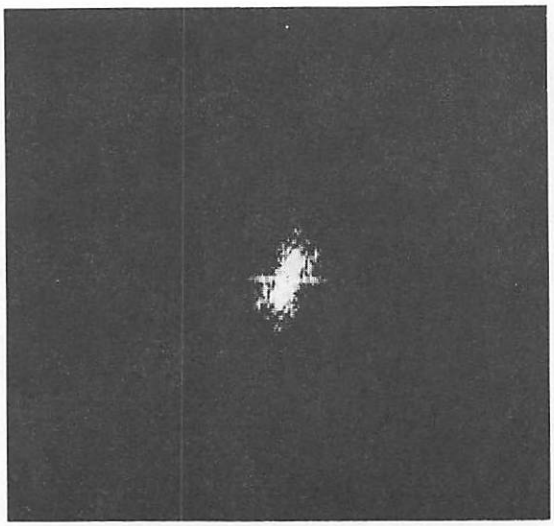

b) Magnitude of the Fourier Transform

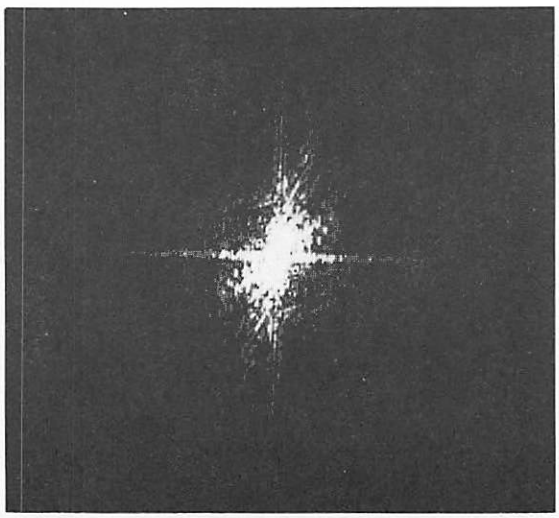

c) Logarithm of the Magnitude of the Fourier Transform

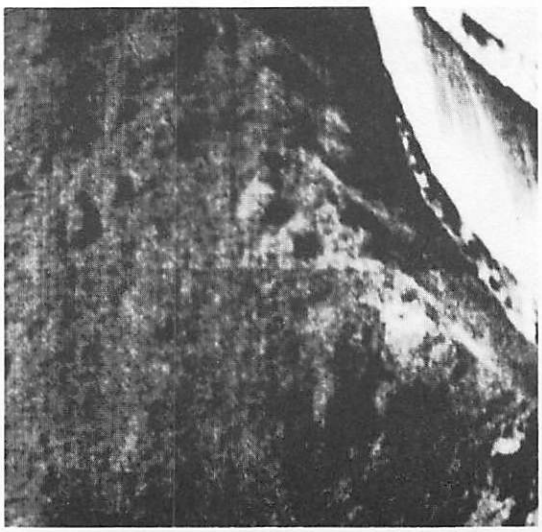

d) Double Fourier Transform

Figure 2-6. -- Fourier Transform of Footpad

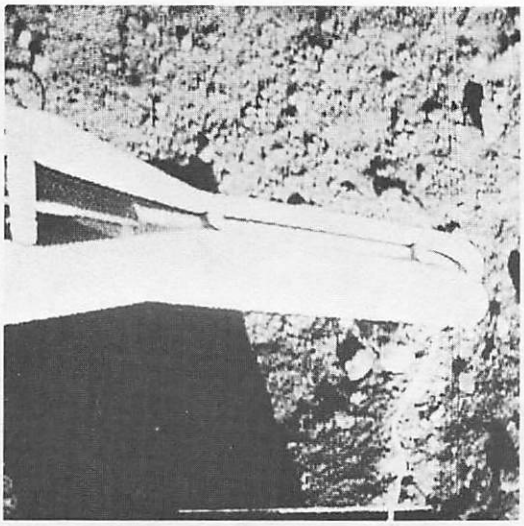

a) Surveyor Boom

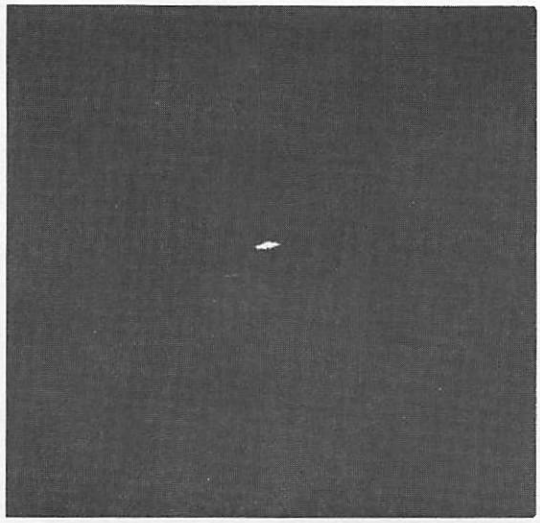

b) Magnitude of the Fourier Transform

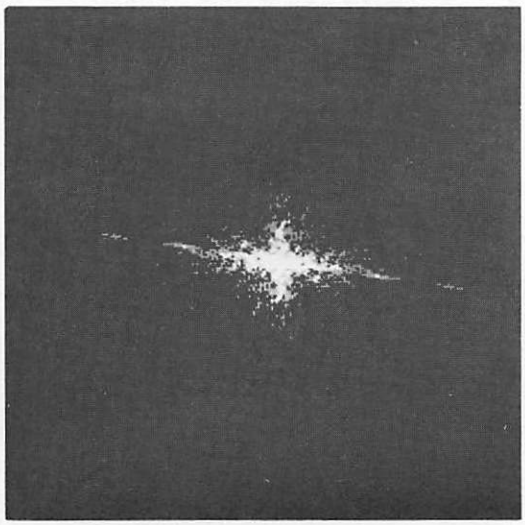

c) Logarithm of the Magnitude of the Fourier Transform

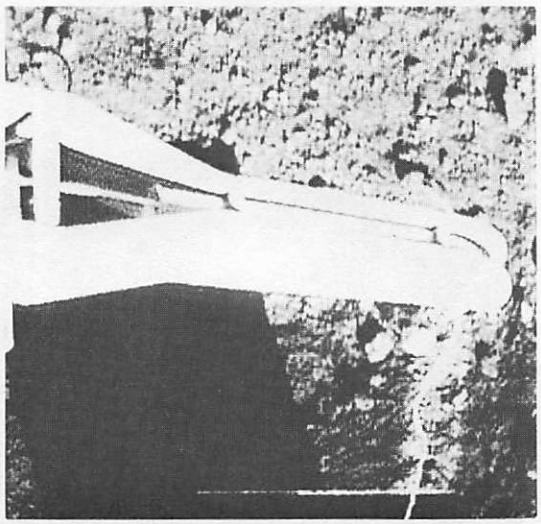

d) Double Fourier Transform

Figure 2-7. -- Fourier Transform of Boom

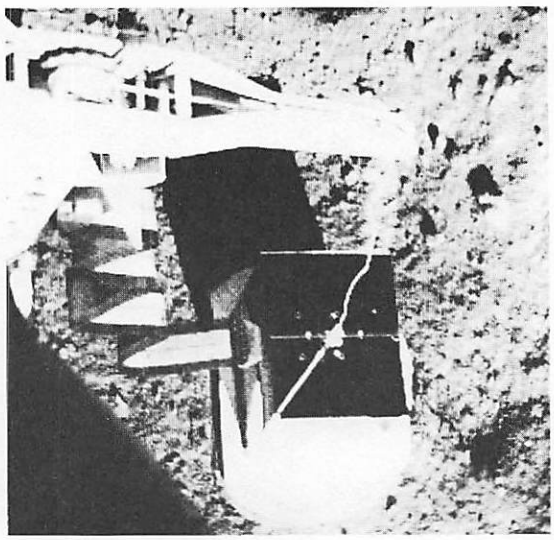

a) Surveyor Box

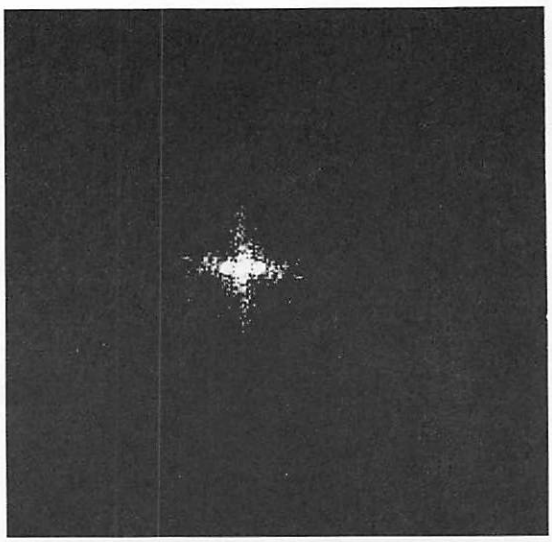

b) Magnitude of the Fourier Transform

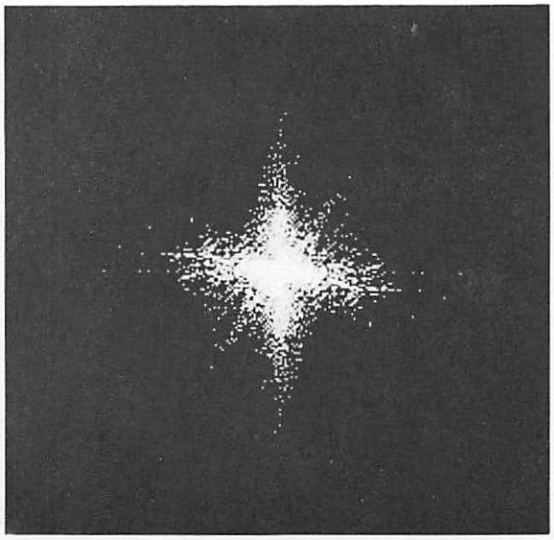

c) Logarithm of the Magnitude of the Fourier Transform

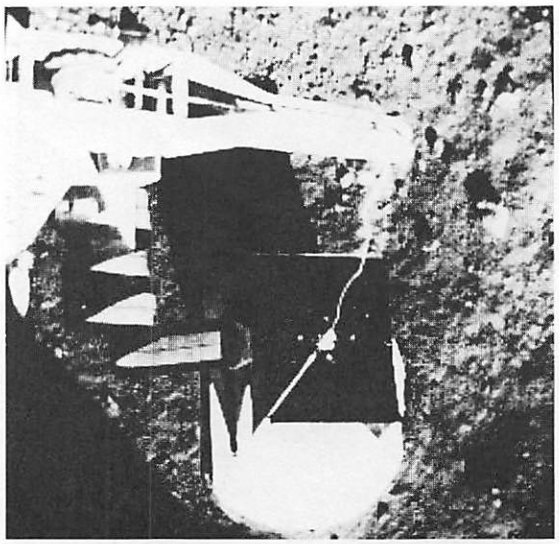

d) Double Fourier Transform

Figure 2-8. -- Fourier Transform of Box

bounded by $\pm 2^{17}$, the capacity of an eighteen bit computer register.

A problem that always arises in the use of a finite two dimensional Fourier transform algorithm is the truncation error. This type of error occurs when the normalization constant, 1/N, is used in transforming from the spatial to Fourier or Fourier to spatial domains. A partial solution to this problem is to normalize by a constant only as large as is needed to prevent overflow. Thus, the Fourier transform computation philosophy is to make maximum use of register length until the last possible moment when normalization is necessary for display purposes.

In addition to truncation errors, a certain amount of high frequency error is introduced due to the fact that only a finite number of Fourier coefficients are calculated. These high frequency errors, due to truncation of the algorithm, have been found to be quite insignificant.

An additional point concerning the nature of the finite Fourier transformation must be made. This relates to the fact that the Fourier series approximation is valid only if the scene is periodic with periodicity equal to the window of observation. This fact must be taken into consideration when viewing the energy distributions in the Fourier domain. It is possible, when the data on two parallel edges of the window of observation are quite dissimilar, to influence

the energy in the frequency domain along the perpendicular frequency axes. The periodic assumption implies that parallel edges of a scene are adjacent. Consequently, certain on axis information in the Fourier domain could be due to brightness transitions on opposite but periodically adjacent edges in the spatial domain. The effect of this phenomena can be reduced by smoothing the transitions at the edges of the observation window. Such techniques result in the development of special windows of observation. Different windows of observation, then, could result in different on axis energies in the Fourier domain. The effect of the square binary observation window used in this research is relatively insignificant and will not be developed further.

The above discussions are meant to imply that the results of the finite algorithm have been well enough behaved to glean meaningful experimental results by operations on the Fourier domain of images. However, the first step that should be taken in developing a realistic developmental model for a Fourier coding scheme would be a greater resolution algorithm and double precision arithmetic. In fact, floating point calculations should be considered for a more exact transforming program.

CHAPTER 3

PROPERTIES OF THE FREQUENCY DOMAIN

Certain deterministic properties can be derived for the frequency domain due to restrictions in the space domain. These properties, which will be used in developing Fourier coding techniques in the frequency domain, are symmetry, dynamic range, entropy, and nonnegative-definiteness.

3.1 Symmetry

The function f(x, y) describes the intensity of samples in the spatial domain of an image. Intensities are nonnegative and real; and therefore, f(x, y) is also nonnegative and real. Making use of this restriction on f(x, y), a property of conjugate symmetry can be demonstrated for the frequency domain. Let the Fourier transform of f(x, y) be expressed as

$$F(u,v) = \frac{1}{N} \sum_{x,y=0}^{N-1} \sum^{N-1} f(x,y) \left\{ \cos \frac{2\pi}{N} (ux+vy) + i \sin \frac{2\pi}{N} (ux+vy) \right\} \qquad (3.1)$$

The Fourier transform, F(u, v), can then be divided into real and imaginary components

$$F(u,v) = F_R(u,v) + i\, F_I(u,v) \tag{3.2}$$

Since f(x,y) is real

$$F_R(u,v) = \frac{1}{N} \sum_{x,y=0}^{N-1\,N-1} f(x,y) \left\{ \cos \frac{2\pi}{N} (ux+vy) \right\} \tag{3.3}$$

and

$$F_I(u,v) = \frac{1}{N} \sum_{x,y=0}^{N-1\,N-1} f(x,y) \left\{ \sin \frac{2\pi}{N} (ux+vy) \right\} \tag{3.4}$$

The cosine is even in u and v, and the sine is odd in u and v. Hence, the following relationships exist

$$F_R(u,v) = F_R(-u,-v) \tag{3.5}$$

and

$$F_I(u,v) = -F_I(-u,-v) \tag{3.6}$$

Consequently

$$F(u,v) = F^*(-u,-v) \tag{3.7}$$

where * implies the complex conjugate. Referring to figure 3-1, this symmetric conjugate relationship implies that quadrants (1) and (3) are deterministically dependent as are quadrants (2) and (4). Thus any two independent quadrants are sufficient for complete knowledge of the entire frequency domain. A visual example of this symmetry property is afforded by figure 3-2 which displays the logarithm of the magnitude of the Fourier transforms of various

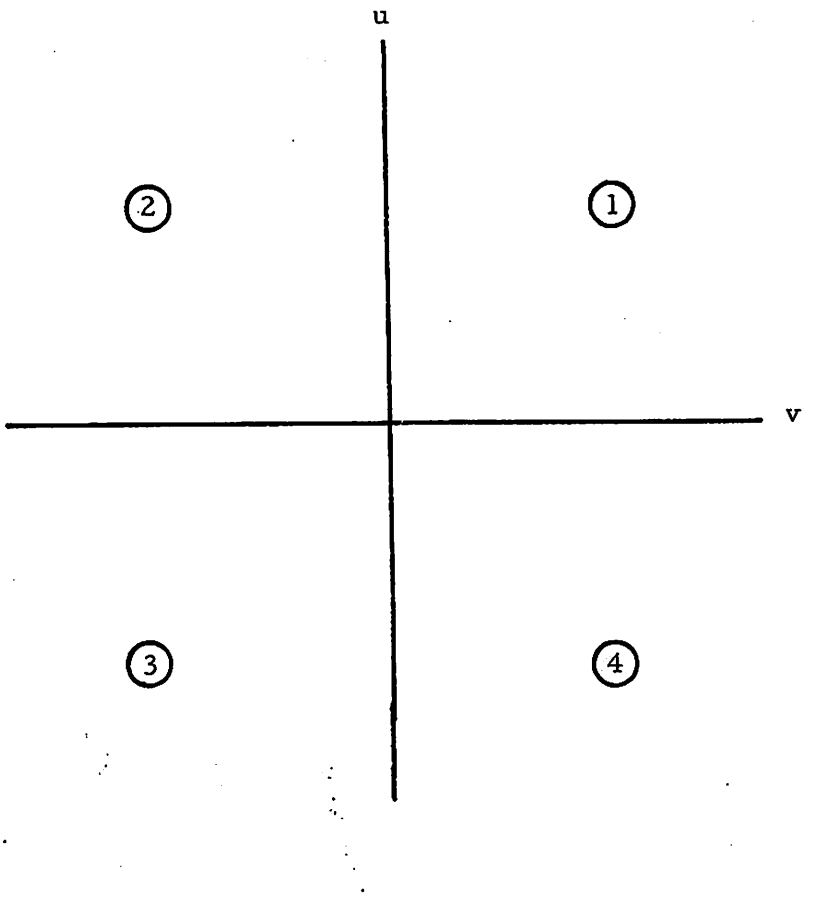

Figure 3-1.--Frequency Domain Quadrants

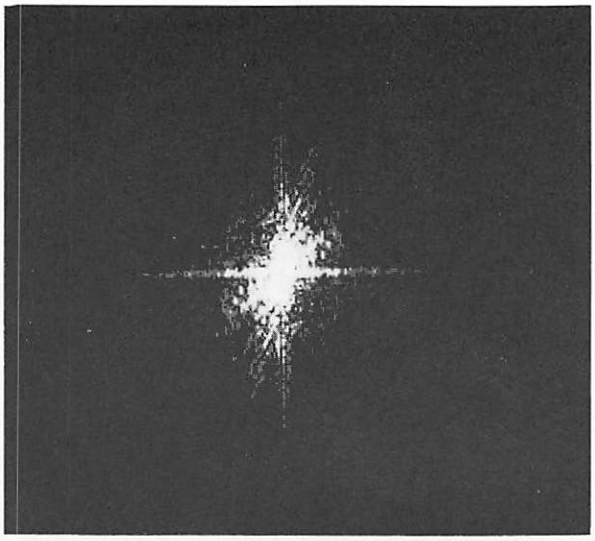

a) Footpad

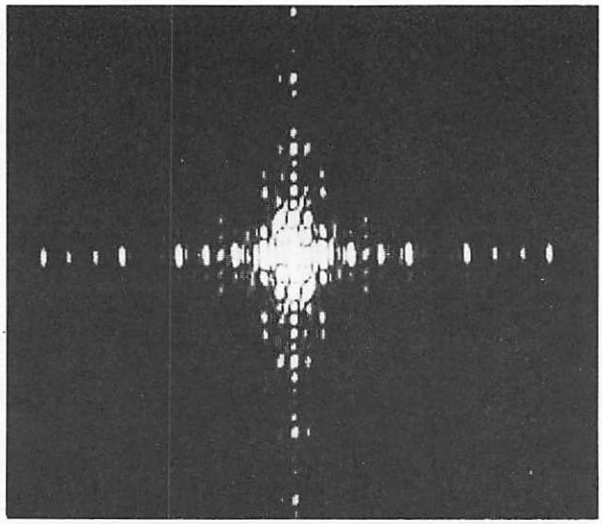

b) Block Letters "USC"

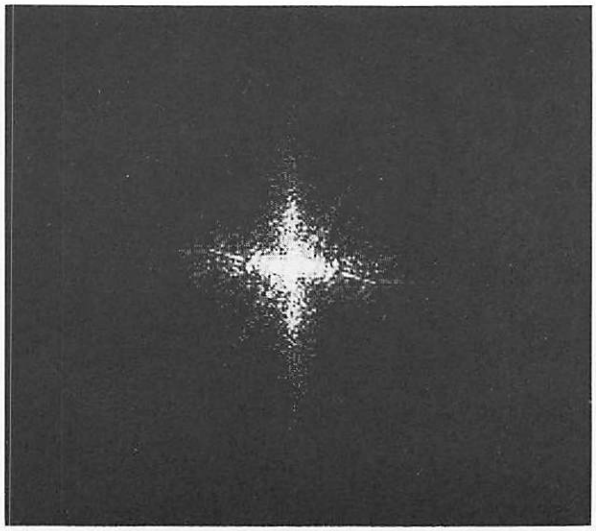

c) Surveyor Box

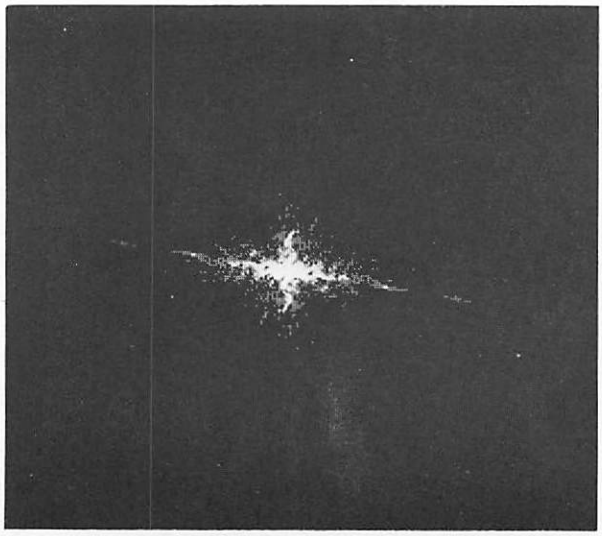

d) Surveyor Boom

Figure 3-2. -- Logarithm of the Magnitude of the Fourier Transforms of Test Scenes

test scenes. It is evident that diagonally opposite quadrants are identical due to displaying magnitude rather than phase and amplitude information.

It is possible to demonstrate that knowledge of two adjacent, and therefore, independent quadrants is sufficient for total reconstruction of the original image by an alternate proof. The proof is based upon the application of a Hilbert or quadrature filter to two dimensional functions. Let a two dimensional filter be constructed such that there is filtering power in only one dimension with impulse response given by

$$h(x,y) = \frac{1}{\pi x}\,\delta(y) \tag{3.8}$$

where $\delta(y)$ is the Dirac delta function. The transfer function of the filter is given by

$$H(u,v) \equiv \mathcal{F}_2\{h(x,y)\} = \begin{matrix} -i & u>0 \\ i & u<0 \end{matrix} \tag{3.9}$$

This transfer function represents a one dimensional quadrature filter or Hilbert transform operator in the x dimension. Referring to figure 3-3, the output of the filter, $\hat{f}(x,y)$, can be obtained from linear systems analysis as

$$\hat{f}(x,y) = f(x,y) \circledast h(x,y) \tag{3.10}$$

where $\circledast$ implies a two dimensional convolution. The Fourier

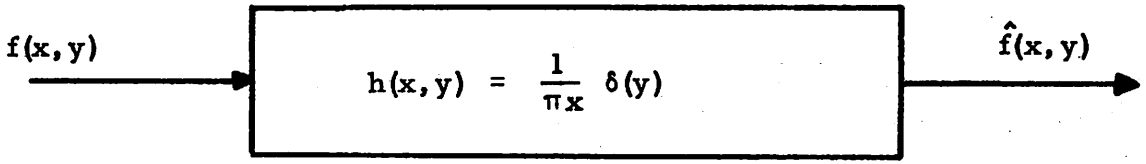

Figure 3-3.--One Dimensional Quadrature Filter in Two Dimensional Notation

transform of the output, $\hat{F}(u,v)$, is given by

$$\hat{F}(u,v) = F(u,v)\,H(u,v) \tag{3.11}$$

Now a function $z(x,y)$ is formed such that

$$Z(x,y) = f(x,y) + i\,\hat{f}(x,y) \tag{3.12}$$

is the analytic signal associated with $f(x,y)$. The Fourier transform, $Z(u,v)$, of $z(x,y)$ is given by

$$Z(u,v) = F(u,v) + i\,\hat{F}(u,v) \tag{3.13}$$

And hence, from equation (3.11)

$$Z(u,v) = F(u,v) + i\,F(u,v)\,H(u,v) \tag{3.14}$$

Finally, from equation (3.9)

$$Z(u,v) = 2\,F(u,v)\,U(u) \tag{3.15}$$

where $U(u)$ is a step function at the v axis in the u direction. The function, $z(x,y)$, can thus be obtained with the knowledge of only half of the frequency domain. The only restriction necessary to recover the original function, $f(x,y)$, from $z(x,y)$ is that $f(x,y)$ be real. Then a simple extraction of the real field from the complex $z(x,y)$ function results in the desired output. The above analysis was carried out for an arbitrary dimension x and is valid for the y dimen-

sion as well.

Both the symmetric conjugate and Hilbert approach lead to the same conclusion. Any two adjacent quadrants in the frequency domain are sufficient to reconstruct the original function when it is real. In addition, the reconstruction can be implemented in either of two modes: a two dimensional Fourier transform of half a plane can be taken and the desired function extracted from the real part of the transform, or the entire frequency domain can be regenerated using the symmetric conjugate property and then retransformed to obtain the original. The only difference between the two methods is a computational one due to the finite computer implementation, to be discussed in chapter 8.

The conclusion from the above analyses indicates that it is only necessary to transmit half the number of sample points in the frequency domain as in the spatial domain. This does not result in any type of data reduction. If the spatial domain has N^2 real samples, the frequency domain will have $N^2/2$ complex samples. Thus, there is an equal number of units of data to be transmitted in both domains.

3.2 Dynamic Range

An important subject not yet explicitly discussed is the dynamic range of values in the Fourier domain. It is of interest to introduce

an upper bound, A, on the function f(x,y). Therefore the range of values and consequently the dynamic range that a function can achieve in the space domain is from zero to A. This assumption of a bound on f(x,y), although mathematically valid, also has physical significance. For most light sensing devices the dynamic range is a real physical limitation and not an assumption for ease in calculations. Referring to equation (3.1), the range of values allowed at the origin in the frequency domain is seen to be zero to AN. For the case when f(x,y) is constant at value A the upper bound is reached, and when f(x,y) is identically zero, the lower bound is achieved. The bounds on all frequencies other than the origin are $\pm$ AN/2. These bounds are based on the condition that f(x,y) take on the value A either in phase or out of phase and take on the value zero otherwise for any given two dimensional trigonometric function. The upper bound is obtained from the in phase case and the lower bound, from the out of phase case.

The dynamic range of F(u,v) is dependent upon the normalization constant. N is adopted as the normalizing constant in equation (3.1) in order that the same equation becomes the definition of the Fourier inversion operation with a 180° rotation. In this way transformations from one domain to the other can be implemented with the same normalization constant. Actually, for computational reasons, this normalization constant is selected so that maximum use

of the computer registers is made. This technique was discussed in chapter 2. The emphatic point is that the frequency domain must be capable of handling far greater magnitude numbers than the spatial domain. This demonstrates why certain optical data processing systems have severe limitations. The dynamic range necessary for good experimental frequency domain operations is too large for most physical systems to handle. However, there are some new photographic holographic techniques that approach the required dynamic ranges of the Fourier frequency domain, but these will not be discussed here [10].

While the dynamic range of possible values is extremely large in the Fourier domain, it is interesting to note that few points can actually take on large values. As is known from Parseval's relationship, the total energies in the space and frequency domain must be equal [11, pg. 27].

$$\sum_{x,y=0}^{N-1}\sum^{N-1} [f(x,y)]^2 = \sum_{u,v=0}^{N-1}\sum^{N-1} |F(u,v)|^2 \qquad (3.16)$$

Consequently, only a few spectral points can be large because of the energy bound in the frequency domain. In other words, a few large valued spectral components will consume most of the total energy of the original spatial function. It is this fact, the redistribution of energy in the frequency domain, that allows a large amount of

bandwidth reduction in transmitting most of the original scene.

As an example of the dynamic range often obtained in the frequency domain, consider the results demonstrated by figure 3-4. Figures 3-4a and 3-4c are the magnitudes of the Fourier transforms of a square and a circle, respectively. Figures 3-4b and 3-4d are three dimensional displays of the two magnitude transforms. The analytic solutions to the magnitude squared of the Fourier transform of a square and a circle are known to be $\left(\frac{\sin au}{au}\right)^2\left(\frac{\sin av}{av}\right)^2$ and $\left(2\frac{J_1(kw)}{kw}\right)^2$, respectively. Here $J_1(\cdot)$ is a first order Bessel function and w is a radial spatial frequency. The dynamic range for the zeroth to first order, on axis lobe for these two functions is about 21:1 and 57:1. Similarly, the ratio of the zeroth to third order, on axis lobe is 120:1 and 625:1, respectively. These lobes are barely visible in the perspective displays of figure 3-4 but are present in the computer as are much higher order lobes. These examples emphasize the care which must be taken when drawing conclusions from displays of the frequency domain.

3.3 Entropy

To analyze the theoretical efficiency of transmitting the Fourier transform of a scene rather than the scene itself, it is necessary to compare the entropy of the spatial and Fourier domain information. Towards this end it would be expedient to know that it

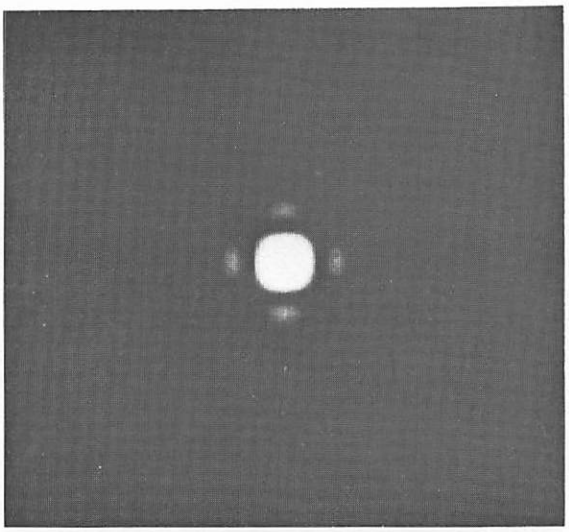

a) Magnitude of the Fourier Transform of a Square

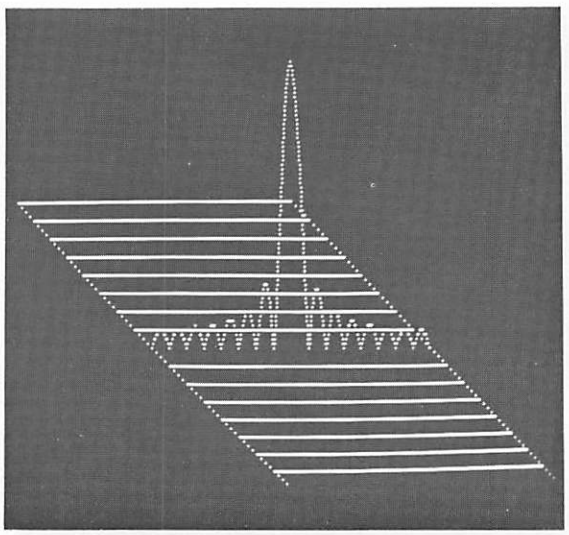

b) Perspective of the Magnitude of the Fourier Transform of the Square

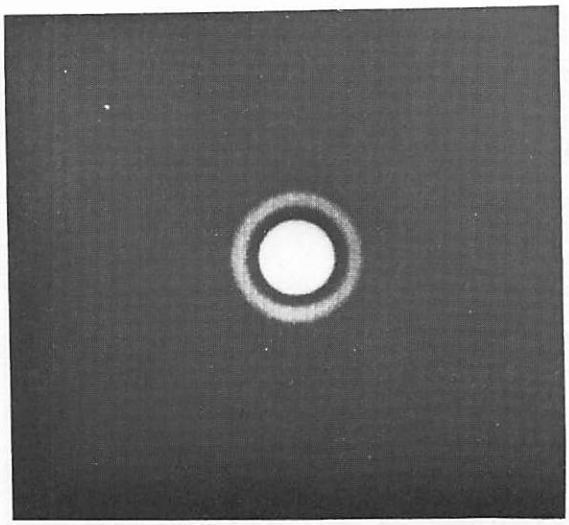

c) Magnitude of the Fourier Transform of a Circle

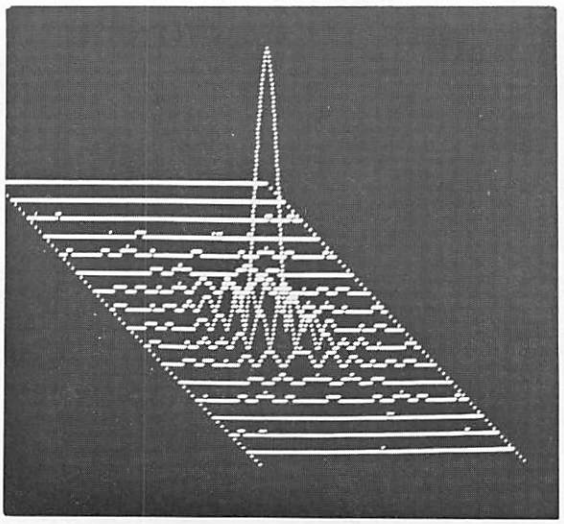

d) Perspective of the Magnitude of the Fourier Transform of the Circle

Figure 3-4. -- Illustration of Dynamic Range

is valid to assume that the entropy of a scene and the Fourier transform of the scene is identical. The proof that follows demonstrates the invariant nature of a Fourier scene and space scene as information sources of a communication system [12]. In fact, the analysis holds for any two dimensional complex bipolar function and thus is applicable to certain types of Fourier holography where complex electromagnetic optical fields are stored in two dimensions.

Introducing subscripted notation causes the Fourier definition to become

$$F_{u,v} = \frac{1}{N} \sum_{x,y=0}^{N-1\,N-1} f_{x,y} \exp\left\{\frac{2\pi i}{N}(ux+vy)\right\} \qquad (3.17)$$

Now the two dimensional functions are complex samples $\left\{f_{x,y} = a_{x,y} + ib_{x,y}\right\}$ where x,y range over the integers $\{0,1,\ldots.N-1\}$. Also $\left\{F_{u,v} = c_{u,v} + id_{u,v}\right\}$ is a sequence of complex samples; and u and v range over the same integer index set. Now consider the $f_{x,y}$ samples to be complex variables of a two dimensional space domain with joint probability density and distribution functions

$$p_f(a_{0,0},\ldots.,a_{x,y},\ldots.,a_{N-1,N-1},b_{0,0},\ldots.,b_{x,y},\ldots.,b_{N-1,N-1})$$

and

$$P_f(a_{0,0},\ldots.,a_{x,y},\ldots.,a_{N-1,N-1},b_{0,0},\ldots.,b_{x,y},\ldots.,b_{N-1,N-1})$$

respectively. Similarly, let the $F_{u,v}$ samples be complex random variables of a two dimensional frequency domain with joint probability density and distribution functions

$$p_F(c_{0,0},\ldots,c_{u,v},\ldots,c_{N-1,N-1},d_{0,0},\ldots,d_{u,v},\ldots,d_{N-1,N-1})$$

and

$$P_F(c_{0,0},\ldots,c_{u,v},\ldots,c_{N-1,N-1},d_{0,0},\ldots,d_{u,v},\ldots,d_{N-1,N-1})$$

respectively.

The entropy of the space domain scene is given by

$$H(f) = -\Sigma P_f \log P_f \tag{3.18}$$

and the entropy of the frequency domain scene by

$$H(F) = -\Sigma P_F \log P_F \tag{3.19}$$

The summations are over all possible combinations of distributions in the space and frequency domains, respectively. Reza has shown that the entropies of the two domains are related by

$$H(f) = H(F) - E\left[\log\left|J\left(\frac{F_{0,0},\ldots,F_{N-1,N-1}}{f_{0,0},\ldots,f_{N-1,N-1}}\right)\right|\right] \tag{3.20}$$

where J is the Jacobian of the transformation between the two spaces

and $E[\cdot]$ is an ensemble average [13, pg. 287]. The Jacobian relates the density functions by the following:

$$p_F = p_f / |J| \tag{3.21}$$

The problem has now been reduced to proving that the Jacobian of the transformation is unity. There are two ways to proceed at this point. An abstract analysis approach allows verification that the Jacobian is unity by noticing that the transformation is linear and proving that norms and hence inner products are preserved.[1] The second approach, presented below, shows that the Jacobian is unity from matrix theory. The Jacobian is given by

$$J = \left| \frac{\partial F_{u,v}}{\partial f_{x,y}} \right| \tag{3.22}$$

where u,v,x,y range over I, and the dimensions of the Jacobian are N^2 by N^2. Let the matrix representation of J be equal to T. Then

$$T = \frac{1}{N} \left[\frac{\partial F_{u,v}}{\partial f_{x,y}} = \exp\left\{ \frac{2\pi i}{N} (ux+vy) \right\} \right] \begin{matrix} \updownarrow\ o,v \\ \\ \updownarrow\ N-1,v \end{matrix} \tag{3.23}$$

$$\qquad\qquad \overset{\longleftrightarrow}{o,y} \qquad\qquad\qquad\qquad \overset{\longleftrightarrow}{N-1,y}$$

with indexing as illustrated. Note that the complex conjugate of T is

---

[1] See Hewitt and Stromberg, section 16 reference [14].

$$T^{*} = \frac{1}{N}\left[\exp\left\{-\frac{2\pi i}{N}(ux+vy)\right\}\right] \tag{3.24}$$

with the same indexing as for T. The transpose of the conjugate is given by

$$T^{*t} = \frac{1}{N}\left[\exp\left\{-\frac{2\pi i}{N}(ux+vy)\right\}\right]\begin{matrix}\updownarrow\ o,y \\ \updownarrow\ N-1,y\end{matrix} \tag{3.25}$$

$$\begin{matrix}\leftrightarrow \\ o,v\end{matrix} \qquad \begin{matrix}\leftrightarrow \\ N-1,v\end{matrix}$$

with indexing reversed. T and T^{*t} can be multiplied together to form

$$T^{*t}T = \frac{1}{N^2}\left[\exp\left\{-\frac{2\pi i}{N}(ux+vy)\right\}\right]\begin{matrix}\updownarrow\ o,y \\ \updownarrow\ N-1,y\end{matrix}\left[\exp\left\{\frac{2\pi i}{N}(ux+vy)\right\}\right]\begin{matrix}\updownarrow\ o,v \\ \updownarrow\ N-1,v\end{matrix} \tag{3.26}$$

$$\begin{matrix}\leftrightarrow \\ o,v\end{matrix} \qquad \begin{matrix}\leftrightarrow \\ N-1,v\end{matrix} \qquad \begin{matrix}\leftrightarrow \\ o,y\end{matrix} \qquad \begin{matrix}\leftrightarrow \\ N-1,y\end{matrix}$$

The resulting matrix, with the pq^{th} row times the rs^{th} column illustrated, is given by

$$T^{*t}T = \frac{1}{N^2}\left[\sum_{x,y=0}^{N-1\,N-1}\exp\left\{-\frac{2\pi i}{N}(px+qy)\right\}\exp\left\{\frac{2\pi i}{N}(rx+sy)\right\}\right] \tag{3.27}$$

$$T^{*t}T = \frac{1}{N^2}\left[\sum_{x=0}^{N-1}\exp\left\{\frac{2\pi i}{N}x(r-p)\right\}\sum_{y=0}^{N-1}\exp\left\{\frac{2\pi i}{N}y(s-q)\right\}\right] \tag{3.28}$$

Finally

$$T^{*t}T = \frac{1}{N^2}\begin{bmatrix} N^2 & & 0 \\ & N^2 & \\ & & \ddots \\ 0 & & N^2 \end{bmatrix} \tag{3.29}$$

by the orthogonality of the Fourier kernel except at r=p and s=q. This demonstrates that T is a unitary matrix [15, pg. 25]. The determinant of a unitary matrix is unity; and therefore, the absolute value of the Jacobian of the transformation is unity.

$$J = |T| = 1 \tag{3.30}$$

Thus the joint density functions are equal, $p_F = p_f$, and the entropies of the two spaces are now related by

$$H(f) = H(F) - E[\log |J|] = H(F) \tag{3.31}$$

Hence the frequency domain contains the same amount of information as the space domain. This result should not be construed as a solution to the coding problem in the frequency domain. The result merely states that a channel rate of x bits per picture should be achieved by transmitting either in the space of frequency domain. In general, finding a coding scheme in the frequency domain as efficient as one in the space domain is not an easy task. This topic will be discussed more fully in chapter 5.

3.4 Nonnegative-Definite

A final deterministic property of the frequency domain to be discussed is the fact that the Fourier transform of a real nonnegative function is nonnegative-definite [11, pg. 225]. In two dimensional notation this property can be expressed as

$$\sum_{m,k=1}^{n\ n} a_m a_k^* F(u_m - u_k,\ v_m - v_k) \geq 0 \tag{3.32}$$

where the a's are any complex constants, and the inequality must holds for any value of n, u_m, u_k, v_m, v_k. Proof of the necessity of the above condition can be demonstrated by the following inequality

$$0 \leq \int_{-\infty}^{\infty}\int \left| \sum_{m=1}^{n} a_m \exp\left\{i(u_m x + v_m y)\right\}\right|^2 f(x,y)\, dxdy \tag{3.33}$$

Expanding the square magnitude and interchanging the order of integration and summation yields

$$0 \leq \sum_{m,k=1}^{n\ n} a_m a_k^* \int_{-\infty}^{\infty}\int f(x,y) \exp\left\{i[x(u_m - u_k) + y(v_m - v_k)]\right\} dxdy \tag{3.34}$$

Finally

$$0 \leq \sum_{m,k=1}^{n\ n} a_m a_k^* F(u_m - u_k, v_m - v_k) \tag{3.35}$$

Proof of the sufficiency of such a condition is given by Bochner [16, pg. 207].

While the nonnegative-definite criterion is valid, testing a function to determine if it belongs to the class of nonnegative-definite functions is usually not facile. One result that the nonnegative-definite property requires of the frequency domain is that

$$F_R(0,0) \geq |F_R(u,v)| \tag{3.36a}$$

$$F_R(0,0) \geq |F_I(u,v)| \tag{3.36b}$$

This can be found by setting n=2 and using the values $a_1 = 1$ and $a_2 = 1, -1, i, -i$ for four different cases in equation (3.35). The only difference between nonnegative-definite functions and Fourier transforms of arbitrary real functions is the value at the origin of the frequency plane. Consequently, nonnegative-definiteness will not be pursued.

CHAPTER 4

IMAGE EVALUATION

A two dimensional matched filter offers a natural tool for the development of a quantitative image evaluation technique. Such a technique is developed in this chapter. In addition, two statistical image evaluation procedures are implemented for the purpose of comparison.

The advantage of having quantitative image evaluation techniques is that they take the burden of decision off the subjective evaluations of the human eye. With quantitative techniques, different experimental methods can be objectively compared and image processing systems can be quantitatively optimized. The major limitation of such evaluation procedures is that usually the ultimate receiver of an image processing system is the human eye, and it is difficult to develop quantitative models for such a receiver. In particular, the eye is more sensitive to high frequency "salt and pepper" and spatially correlated or patterned noise than it is to low frequency slowly varying and random spatial noise patterns [1]. If the same noise energy exists in both cases and if the quantitative image evaluation model is a function of total noise energy, then the

quantitative results are not going to agree with the most pleasing results as far as the eye is concerned. However, under certain circumstances correlations can be made with the results of the matched filter technique and subjective human viewing. Both the matched filter and statistical image evaluation procedures are described below.

4.1 Statistical Evaluation

There are an unlimited number of statistical functions that might be used as a quantitative measure of experimental results. For instance the difference in processed and original scenes can be formed and measurements made on this "noise difference". If all errors introduced by processing, transmitting, and reconstructing are considered to be additive noise, then the "noise difference" scene can be measured for statistical parameters. If high frequency noise is more undesirable than low frequency noise, a higher order statistical moment of the noise should be investigated. This type of statistic places more emphasis on large noise samples and thus high frequency noise on the original scene. In addition to measuring moments of the noise, a histogram of noise samples might be investigated. In this case the shape of the histogram at higher values would be of interest as this would give the relative frequency of occurence of large noise samples as versus small noise samples;

and, consequently, high frequency versus low frequency noise. For a photometric image evaluation criterion where absolute values of given picture elements are of interest, the higher order moment statistic is probably more valuable than a first order statistic. However for a photometric measurement criterion, and average over the entire image of a higher order moment statistic is probably of less value than such an average would be for a total image evaluation criterion.

The approach taken in this chapter is to develop two statistical parameters to evaluate a total image; and consequently, an average over the entire image plane will be taken. The first parameter measured will be the average of the absolute value of the error at each element in the "noise difference" plane mentioned above. If the pre-processed image is $f(x,y)$ and the post-processed image is $g(x,y)$, then

$$\frac{1}{N^2} \sum_{x=0}^{N-1} \sum_{y=0}^{N-1} |f(x,y) - g(x,y)| \tag{4.1}$$

will be referred to as the mean absolute error per element. The second parameter measured will be the average of the square error at each element in the noise plane minus the square of the mean absolute error per element. This will be referred to as the variance absolute error per element. Mathematically, this expression is

$$\frac{1}{N^2}\left\{\sum_{x=0}^{N-1}\sum_{y=0}^{N-1}[f(x,y)-g(x,y)]^2-\frac{1}{N^2}\left[\sum_{x=0}^{N-1}\sum_{y=0}^{N-1}|f(x,y)-g(x,y)|\right]^2\right\} \qquad (4.2)$$

Both these measurements have been performed for test scenes in section 4.3 of this chapter.

4.2 Two Dimensional Matched Filter

Another method that can be used to measure the quality of a processed image involves the use of a two dimensional matched filter. The concept of the matched filter originally arose in the field of communication engineering in problems of signal detection and evaluation. In the study of optimum filtering, the matched filter is derived to be the filter which maximizes the signal to noise ratio over a given interval of observation [17, pg. 239]. The matched filter is often used in pattern recognition experiments as the detecting instrument for given patterns. Two dimensional matched filtering has been performed optically with some success [5]. In two dimensions, if the pattern of signal to be detected is $f(x,y)$ with Fourier transform $F(u,v)$, then the matched filter is defined as $\frac{F^*(u,v)}{N(u,v)}$, where $N(u,v)$ is the noise power spectrum in which the signal is immersed. This spectrum can be defined as any unwanted portion of a scene. If $g(x,y)$ is the two dimensional plane from which the signal, $f(x,y)$, is to be detected, then the output, $\mathcal{O}(x,y)$,

of the matched filter is

$$\mathcal{O}(x,y) = \int_{-I}^{I}\int_{-I}^{I} G(u,v)\,\frac{F^*(u,v)}{N(u,v)}\,\exp\{i(ux+vy)\}\,du\,dv \qquad (4.3)$$

where the cell (-I, -I;I, I) is the entire picture. The true matched filter will detect phase and amplitude information and, consequently, is position as well as shape sensitive. In other words, the matched filter can detect the difference between rotationally similar characters such as "p" and "d" or "6" and "9" where the magnitude of the transform of these types of signals is identical but their phases are different. An experimental result will offer insight into the discussion. Figure 4-1a shows the signal f(x, y), the letter "d", which is the signal to be detected from the array of "p's" and "d's" of figure 4-1b. A suboptimum matched filter was constructed as F*(u, v) ignoring the noise spectrum of the "p's". Figure 4-1c is the output of the matched filter and indicates those points in the two dimensional plane where the greatest correlation with the letter "d" exists. A three dimensional display of the correlation peaks is shown in figure 4-1d. Two significant results are immediately obvious from this example. The position of the correlation peak indicates the position of the detected signal, and the height of the correlation peak indicates the degree of correlation of the detected signal with the pattern to be recognized. It is this latter property, the degree of correlation,

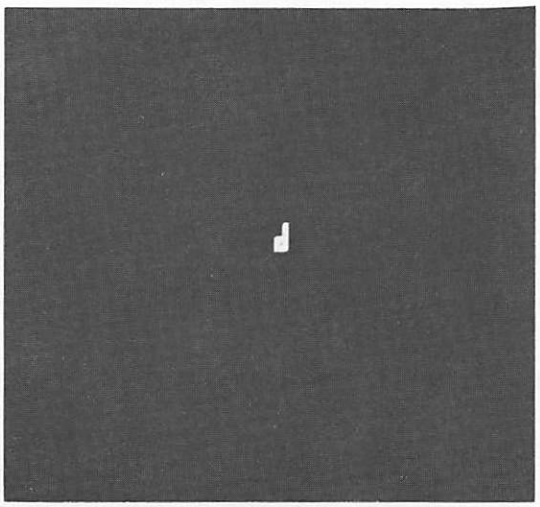

a) Signal to be Detected

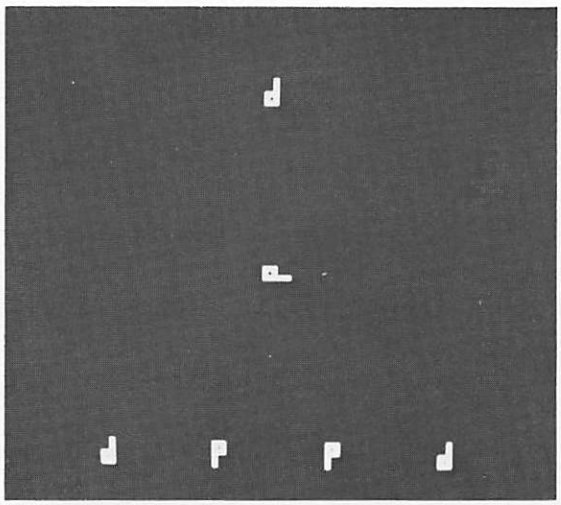

b) Array of Signals and Noise

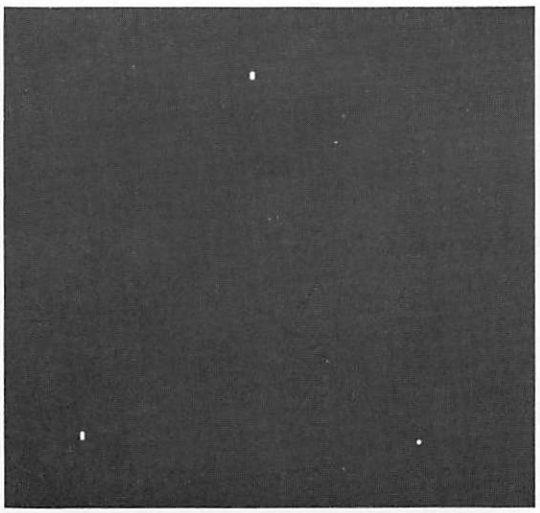

c) Filter Output

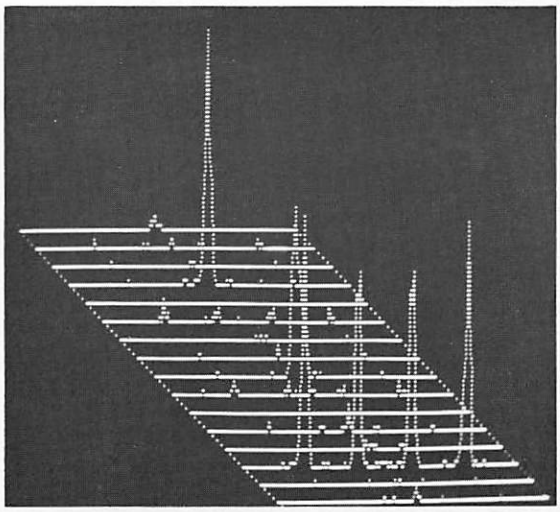

d) Perspective of Correlation Peaks

Figure 4-1. -- Matched Filter Experiment

that can be used as a measure of the processing, transmission, and reconstruction noise on the original image.

If the matched filter is used as a measure of correlation of processed to unprocessed images, then positional information is unnecessary. This can be explained by interpreting the filter as convolving the pre- and post-processed images by shifting one across the other and measuring the correlation at each shift. When the two images are synchronized in both the x and y dimension, the greatest correlation will occur and this will be at the origin. Consequently, the output of the matched filter, sampled at the origin, will indicate the degree of correlation between the two inputs. The peak correlation will occur when the filter matches an image with itself in the absence of noise. Specifically, when $\mathcal{O}(x,y)$ is the output of the filter then

$$\mathcal{O}(x,y) = \int_{-I}^{I}\int_{-I}^{I} F(u,v)F^*(u,v)\exp\{i(ux+vy)\}\,du\,dv \qquad (4.4)$$

and when the output of the filter is sampled at the origin then

$$\mathcal{O}(0,0) = \int_{-I}^{I}\int_{-I}^{I} |F(u,v)|^2\,du\,dv \qquad (4.5)$$

In other words, the best possible correlation occurs when the pre- and post-processed images are identical, and is equal to the energy

in the given image. The degree of correlation can then be normalized to the total energy for fractional representation. The output of the filter in the presence of noise is

$$\mathcal{O}(0,0) = \int_{-I}^{I}\int_{-I}^{I} \frac{F^*(u,v)G(u,v)}{N(u,v)}\,du\,dv \qquad (4.6)$$

A digital counterpart to the two dimensional matched filter has been implemented and some typical experimental results are presented below.

4.3 Experimental Comparisons

Figure 4-2 contains four images and their respective statistical and matched filtered results. The images are displayed in order of decreasing visual pleasure. The degree of correlation determined by the matched filter experiment decreases monotonically with decreasing subjectively pleasing results and appears to agree with the response of the eye. The statistical results displayed include mean and variance absolute errors per element and are obtained by subtracting the processed images from the original footpad scene. The mean absolute error results indicate that the image of figure 4-2c is better than that of figure 4-2b. This indication is not substantiated by the matched filtered results or by subjective viewing. Also the variance absolute error per element measurement indicates

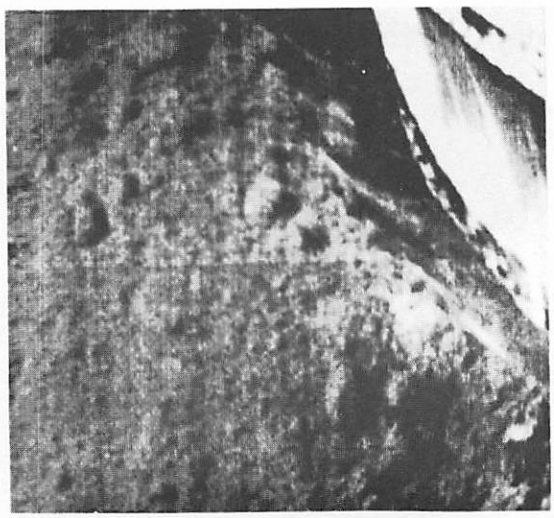

a) Matched Filter Correlation : 1.000
Mean Absolute Error per Element : 3.952
Variance Absolute Error per Element : 5.538

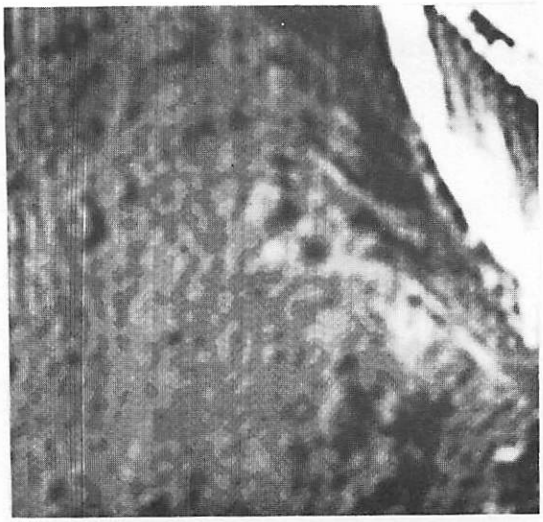

b) Matched Filter Correlation : 0.9703
Mean Absolute Error per Element : 4.930
Variance Absolute Error per Element : 5.308

c) Matched Filter Correlation : 0.9558
Mean Absolute Error per Element : 4.005
Variance Absolute Error per Element : 6.223

d) Matched Filter Correlation : 0.9494
Mean Absolute Error per Element : 4.477
Variance Absolute Error per Element : 6.550

Figure 4-2. -- Image Evaluation

image 4-2b is superior to 4-2a which is a clear discrepancy with subjective and matched filter results. Higher moment statistical measurements could be taken but the problem with such a technique lies in the fact that a few large noise errors can completely dominate all other noise effects and consequently will produce an evaluation of an image which is not based upon the entire image's domain of definition. This is exactly what has happened in figure 4-2a, where the simple process of retransforming back to the spatial domain has introduced a few large errors which have caused the variance measurement to incorrectly evaluate that image. A similar experiment has been performed on the Surveyor box and is presented in figure 4-3.

A word of caution is in order. The above results are not to be construed as proof that the matched filter is the answer to all automatic image evaluation problems. It can be used advantageously as a quantitative measure for relative results between similar processing techniques. In other words, the matched filter will discern between varying degrees of the same processing technique. This is exemplified by the earlier figures 4-2 and 4-3 where the narrower and narrower low pass filters are used to obtain the varying images of that figure. Similarly the matched filter can be used to evaluate the results introduced by varying the number of quantum levels in a given quantization scheme. The main problem with the matched

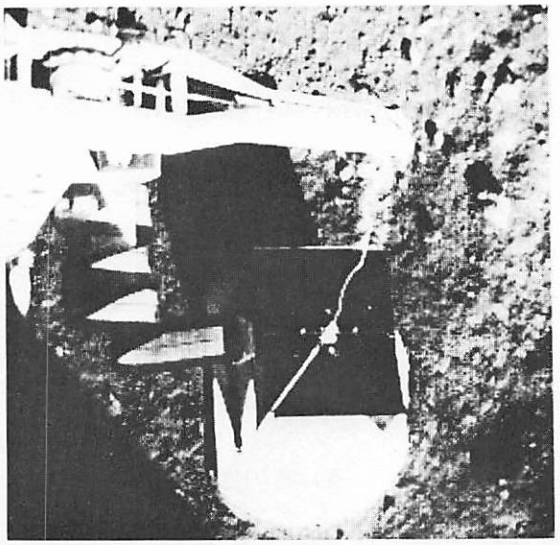

a) Matched Filter Correlation : 1.000
Mean Absolute Error per Element : 4.704
Variance Absolute Error per Element : 34.47

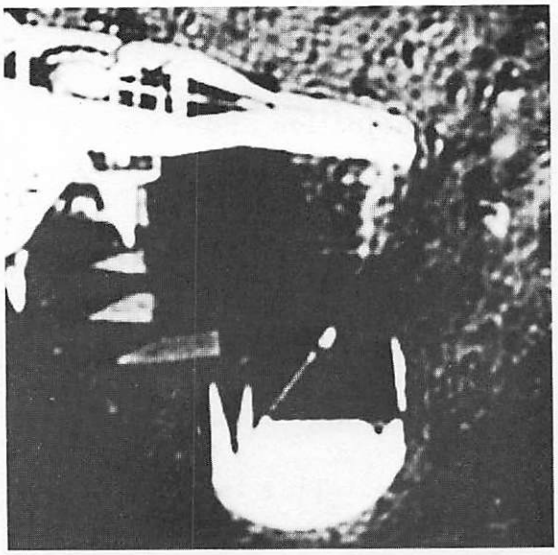

b) Matched Filter Correlation : 0.9633
Mean Absolute Error per Element : 5.229
Variance Absolute Error per Element : 20.04

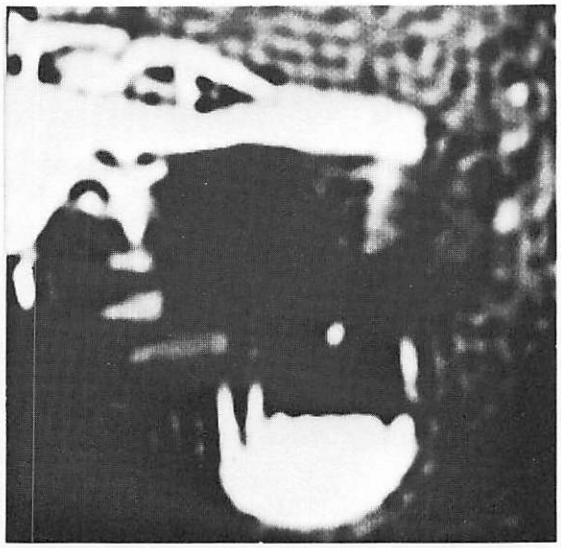

c) Matched Filter Correlation : 0.9091
Mean Absolute Error per Element : 5.619
Variance Absolute Error per Element : 22.20

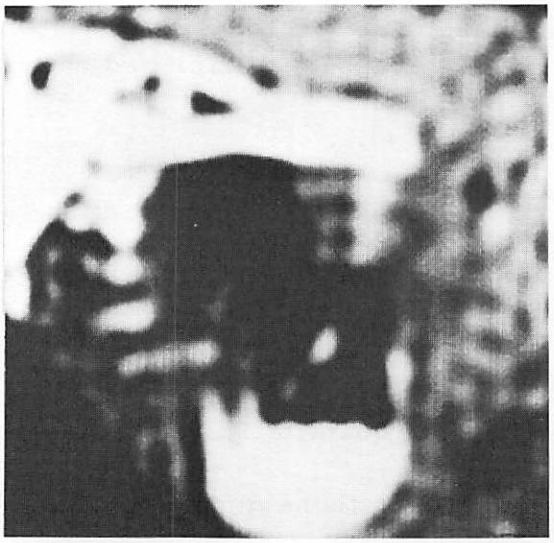

d) Matched Filter Correlation : 0.8659
Mean Absolute Error per Element : 6.974
Variance Absolute Error per Element : 27.15

Figure 4-3. -- Image Evaluation

filter is that it cannot tell if the image makes sense. Consequently, it is possible to get better matches with totally irrelevant images than with very poor but relevant ones.

It is difficult to draw a conclusion as to what techniques, if any, will offer an impartial image evaluation procedure. However, it is the conclusion of the author that if both subjective and matched filtered correlations can be used in parallel, subtle results, sometimes undetectable by the eye, can often be quantitatively evaluated successfully.

CHAPTER 5

FOURIER DOMAIN QUANTIZATION

In digital communication systems it is necessary to quantize information before it can be coded for transmission purposes, because a finite dictionary code requires a finite number of values for data input. Quantization introduces an error known as quantization noise. This error can be analyzed from a statistical viewpoint, and techniques are available for minimizing mean square quantization error. Such error minimization procedures are contingent on the selection of proper quantization levels from the probability density function of the signal to be quantized [18, pg. 641]. This chapter presents a brief stochastic analysis which results in the experimental implementation of a frequency adaptive quantization procedure. Experimental results of the procedure are presented, and an experimental tolerance for the frequency adaptive quantization parameter is demonstrated.

5.1 Stochastic Analysis

It is desirable to know as much as possible about the stochastic behavior of samples in the Fourier domain in order to derive

meaningful quantization rules for that domain. Ideally, this means determining the density function of each frequency sample in the Fourier domain. As an effort in this direction, a stochastic model is presented below.

Let $\phi(x', y')$ be a continuous two dimensional wide sense stationary random process with a bounded and continuous power spectral density, $D(u, v)$, where u and v are real. It is desired to observe the process over the two dimensional window, $(-I, -I; I, I)$, and to sample the process at N^2 uniformly spaced points within the window of observation. A new process, $F_{N,I}(u, v)$ depending on both the window of observation and the sampling period within the window, is formed according to the following

$$F_{N,I}(u,v) = \frac{1}{N} \sum_{x,y=0}^{N-1\,N-1} \phi\left(\frac{xI}{N}, \frac{yI}{N}\right) \exp\left\{\frac{2\pi iI}{N}(ux+vy)\right\} \qquad (5.1)$$

Investigation of the variance of $F_{N,I}(u, v)$ yields the following result in terms of a covariance function, ρ, on the process, ϕ.

$$\sigma^2_{F_{N,I}}(u,v) = \frac{1}{N^2} \sum_{\tau,T=0}^{N-1\,N-1} \epsilon_\tau \epsilon_T (n,\tau)(N-T)\, \rho\left(\frac{\tau I}{N}, \frac{TI}{N}\right) \cos\frac{2\pi I}{N}(u\tau+vT) \qquad (5.2)$$

where τ and T are integer values representing the two dimensional shift in the sampled function $\phi\left(\frac{xI}{N}, \frac{yI}{N}\right)$ with itself. ϵ_τ and ϵ_T are Neumann factors taking the values $\epsilon_0 = 1$ and $\epsilon_\tau = 2$ for all $\tau \neq 0$.

Equation (5.2) can be expressed as

$$\sigma^2_{F_{N,I}}(u,v) = \sum_{\tau,T=0}^{N-1\,N-1} \epsilon_\tau \epsilon_T \left(1-\frac{\tau I}{NI}\right)\left(1-\frac{TI}{NI}\right)\rho\left(\frac{\tau I}{N},\frac{TI}{N}\right)\cos\frac{2\pi I}{N}(u\tau+vT) \tag{5.3}$$

This is recognized as the Riemann approximating summation for large N for the following

$$S_I(u,v) = c\int_{-I}^{I}\int_{-I}^{I}\left(1-\frac{|z_1|}{I}\right)\left(1-\frac{|z_2|}{I}\right)\rho(z_1,z_2)\cos 2\pi(uz_1+vz_2)\,dz_1\,dz_2 \tag{5.4}$$

where c is a normalization constant and the continuous variables z_1 and z_2 have replaced the sampled variables $\frac{\tau I}{N}$ and $\frac{TI}{N}$, respectively. From Bochner's theorem it is known that

$$\rho(z_1,z_2) = R\int_{-\infty}^{\infty}\int_{-\infty}^{\infty} D(u,v)\exp\left\{-2\pi i(uz_1+vz_2)\right\}du\,dv \tag{5.5}$$

where R is a constant chosen so that D(u,v) is a probability density function [16, pg. 207]. Replacing the covariance function in equation (5.5) yields

$$S_I(u,v) = CR\int_{-\infty}^{\infty}\int_{-\infty}^{\infty} D(u-u',v-v')K_I(u',v')\,du'\,dv' \tag{5.6}$$

where K_I is the two dimensional product Kejer kernel. It is known that $S_I(u,v)$ approaches cR D(u,v) uniformly on compact sets as I

approaches infinity [19, pg. 2]. Consequently, it is not unreasonable to assume that the variance, $\sigma^2_{F_{N,I}}(u,v)$, behaves approximately as the power spectral density of the process, $\emptyset$.

The results of this analysis have been obtained by first letting the sampling interval approach zero and then letting the window of observation grow. It is important to mention that if the relaxation or correlation radius of the covariance function, ρ, is small compared to the interval of observation, then it is reasonable to assume that the variance, $\sigma^2_{F_{N,I}}(u,v)$, is already close to the power spectral density without increasing the observation window. A similar result can be obtained for the function $F(u,v)$ defined in equation (2.6) by scaling the window of observation to unity and noting that $f(x,y)$ is the sampled version of the continuous process, $\emptyset$. In such a case

$$\sigma^2_{F_N}(u,v) = \sum_{\tau,T=0}^{N-1\,N-1} \epsilon_\tau \epsilon_T \left(1-\frac{\tau}{N}\right)\left(1-\frac{T}{N}\right)\rho\left(\frac{\tau}{N},\frac{T}{N}\right)\cos\frac{2\pi}{N}(u\tau+vT) \tag{5.7}$$

A somewhat different approach from that above will yield essentially the same results. This approach indicates that when the sampling interval is fixed and the interval of observation increases, the variances of the frequency domain samples appear to behave as a sampled periodic function of the continuous power spectral density $D(u,v)$. When the sampling interval is then allowed to decrease, the

periodic function of the power spectral density approaches that density. Such results again indicate that it is reasonable to assume that the variances of Fourier domain samples behave as the power spectral density of the original process.

The above stochastic model indicates that for an uncorrelated process, the spectrum tends to be flat, and the variance of the spectral components of the Fourier transform of f(x,y) are fairly constant over a large range of frequencies. Conversely, if f(x,y) is a highly correlated process, the variance of F(u,v) tends to be large toward the low frequencies and falls off rapidly toward the higher frequencies. It will be assumed that the samples, f(x,y), are identically distributed with variance V^2.

It is convenient to express equation (5.7) in an expanded form in order to investigate certain limiting conditions.

$$\rho^2_{F_N}(u,v) = \rho(0,0) + 2\sum_{\tau=1}^{N-1}\left(1-\frac{\tau}{N}\right)\rho\left(\frac{\tau}{N},0\right)\cos\frac{2\pi u\tau}{N}$$

$$+ 2\sum_{T=1}^{N-1}\left(1-\frac{T}{N}\right)\rho\left(0,\frac{T}{N}\right)\cos\frac{2\pi vT}{N} \qquad (5.8)$$

$$+ 4\sum_{\tau,T=1}^{N-1}\sum^{N-1}\left(1-\frac{\tau}{N}\right)\left(1-\frac{T}{N}\right)\rho\left(\frac{\tau}{N},\frac{T}{N}\right)\cos\frac{2\pi}{N}(u\tau+vT)$$

In the case of a random process, f(x,y), which is constantly correlated in one direction, x, with correlation K, and totally uncorrelated

in the other direction, the variance becomes

$$\sigma^2_{F_N}(u,v) = \rho(0,0) - K + NK\,\delta(u) \tag{5.9}$$

and for the case where $\rho(0,0) = K = V^2$, the variance of the identically distributed samples, $f(x,y)$, then

$$\sigma^2_{F_N}(u,v) = V^2 N\,\delta(u) \tag{5.10}$$

Equation (5.9) indicates that for highly correlated processes in one dimension the off axis variances are reduced by an amount equal to the one dimensional correlation, K, and the variances on the axis corresponding to the correlated direction are increased by an amount proportional to the correlation K. For the case where the one dimensional correlation equals the variance of the process, equation (5.10), all off axis variances are zero and large variances are experienced on the correlation axis. For constant correlation, K, in both directions the variance behaves as

$$\sigma^2_{F_N}(u,v) = \rho(0,0) - K + N^2 K\,\delta(u,v) \tag{5.11}$$

and when the correlation equals the variance of the $f(x,y)$ process, the resulting frequency sample variance is

$$\sigma^2_{F_N}(u,v) = N^2 V^2\,\delta(u,v) \tag{5.12}$$

These results indicate that a process f(x, y) with constant correlation equal to its variance in all directions is a deterministic constant with a Fourier transform equal to the Kronecker delta function at the origin.

Another limiting condition that is of interest is the case of total statistical independence of all samples in the process f(x, y). In this case the variance of F(u, v) becomes

$$\sigma^2_{F_N}(u,v) = V^2 \tag{5.13}$$

This result indicates that for a statistically independent process all frequencies have identical variances. Under the condition of statistical independence of the samples, f(x, y), the variance is sufficient to determine the distribution of frequency components. A Central Limit Theorem is valid assuming the f(x, y) samples are bounded and identically distributed, and in the limit the distribution of the function F(u, v) becomes normal [20, pg. 294].

It is of interest to determine how closely to the normal the distributions of frequency samples behave for correlation in the process f(x, y). Work has been done in this area in the one dimensional case from the point of view of a strong mixing criterion for an ergodic process [21, pg. 191]. Also, Diananda and others have proven theorems for limiting normal distributions for the r-dependent

one dimensional random process [22]. Expansion to the two dimensional case is probable, but is not undertaken here. Instead, an experimental approximation is introduced at this point. It is assumed that the samples in the frequency domain take on a normal density for the sake of implementation of a quantizing scheme. This assumption, while not rigorously derived, is experimentally justified as the future work will verify.

Under the normal approximation, the second moment calculations are sufficient to completely define the distribution at each frequency sample. Consequently, all frequency samples will have a normal density varying only as a function of spectral frequency through the varying second moments. Therefore the probability density of the amplitudes of the Fourier samples are

$$P_{F_R}(z) = P_{F_I}(z) = \frac{1}{\sqrt{2\pi}\,\sigma_{F_N}(u,v)} \exp\left\{-z^2/2\sigma^2_{F_N}(u,v)\right\} \qquad (5.14)$$

and F_R and F_I are obtained from the equation

$$F(u,v) = F_R(u,v) + i\,F_I(u,v) \qquad (5.15)$$

It is useful to express $F(u,v)$ in terms of its magnitude and phase.

$$F(u,v) = M(u,v) \exp\{i\theta(u,v)\} \qquad (5.16)$$

where

$$M(u,v) = \sqrt{F_R^2(u,v) + F_I^2(u,v)} \tag{5.17}$$

and

$$\theta(u,v) = \tan^{-1}\left\{\frac{F_I(u,v)}{F_R(u,v)}\right\} \tag{5.18}$$

From the definition of $F_R(u,v)$ and $F_I(u,v)$, these random variables are orthogonal for a given u and v. Also, from the assumption of a normal distribution on both $F_R(u,v)$ and $F_I(u,v)$, the two random variables are independent for a given u and v. In other words, the processes $F_R(u,v)$ and $F_I(u,v)$ as a function of u and v are not independent processes, but when sampled at the same frequency, are independent[1]. Consequently, the random variable $M(u,v)$ becomes Rayleigh distributed with parameter $\sigma^2_{F_N}(u,v)$

$$P_M(z) = \frac{z}{\sigma^2_{F_N}(u,v)} \exp\left\{-z^2/2\sigma^2_{F_N}(u,v)\right\} U(z) \tag{5.19}$$

where $U(z)$ is the unit step function in z. Because of the independence of $F_R(u,v)$ and $F_I(u,v)$ at a given u and v, the random variable $\theta(u,v)$ is equally likely to take on any value from zero to 2π and consequently is uniformly distributed and independent of frequency.

$$P_\theta(z) = \begin{cases} \frac{1}{2\pi} & 0 \le z \le 2\pi \\ 0 & \text{otherwise} \end{cases} \tag{5.20}$$

---

[1] Davenport and Root, [23, pg. 161].

5.2 Experimental Implementation

The analytic results of the previous section of this chapter indicate that a likely quantization rule is a quantizing technique for each Fourier domain sample, which varies as a function of spatial frequency. The individual quantizer for each frequency sample is found to behave as the power spectral density of the original process at that given frequency. Therefore it is necessary to know the covariance function or its transform before quantizing can take place. To this end an experimental determination of the covariance function was made of the footpad moon scene test image displayed earlier in chapter 2. The results suggest that the correlation of a given picture sample is zero for samples greater than fifteen elements away, and the shape of the covariance approaches that of a two dimensional Gaussian surface. Therefore, as an approximation, a suitable power spectral density is a two dimensional Gaussian function. Such a function has been incorporated as the variance plane for the experimental quantization rules presented in this chapter.

A comment should be inserted here concerning the experimental use of the Gaussian density. From one dimensional linear prediction theory it is known that a Gaussian spectrum implies a deterministic process as defined by the Paley-Wiener theorem [24]. The fact that some of the experimental results of this report are

based on a two dimensional Gaussian spectrum does not mean that the process f(x, y) is deterministic. The results only provide empirical evidence that the Gaussian spectrum is an appropriate experimental approximation to the f(x, y) process.

The actual quantization rule developed for experimental implementation is not derived to minimize mean square quantization error. Instead the quantization law is one in which the quantum levels are set according to an equally likely probability of being in any given quantum interval. While such a rule is not optimum in the minimum quantization noise sense, it does offer a uniform distribution of quantum levels to any type of transmission channel noise.

Since the original spatial scene was coded to 64 levels, 64 levels will be the number of quantum intervals sought in the frequency domain quantization in order to attain an equal number of code words necessary for transmission in each domain. Figure 5-1 illustrates three quantization rules. The first is a simple six bit linear quantization law constant over the entire frequency plane. This method, presented for comparative purposes, approximates the rule that would be used if the original scene were totally statistically independent. It linearly quantizes each sample point to one of 64 levels determined by the maximum value in the frequency plane. The second rule quantizes each of the real and imaginary components of

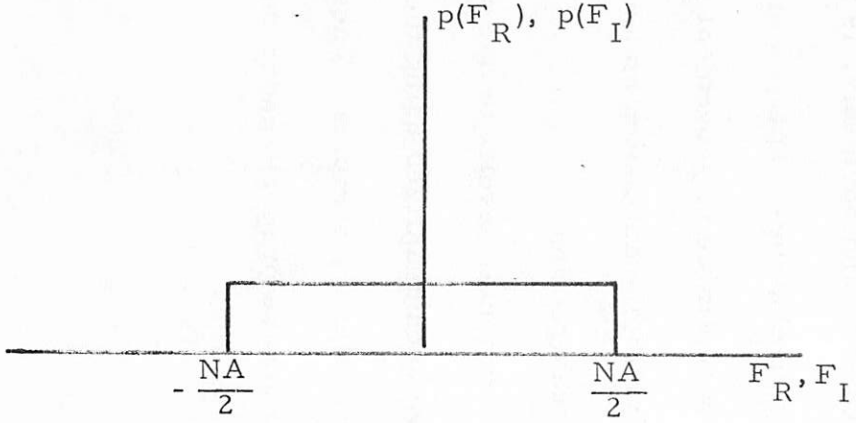

a) Linear Real and Imaginary

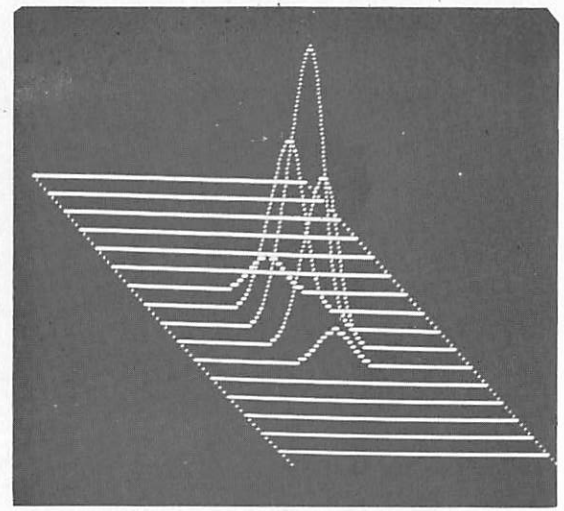

b) Perspective of Variance, $\sigma(u, v)$

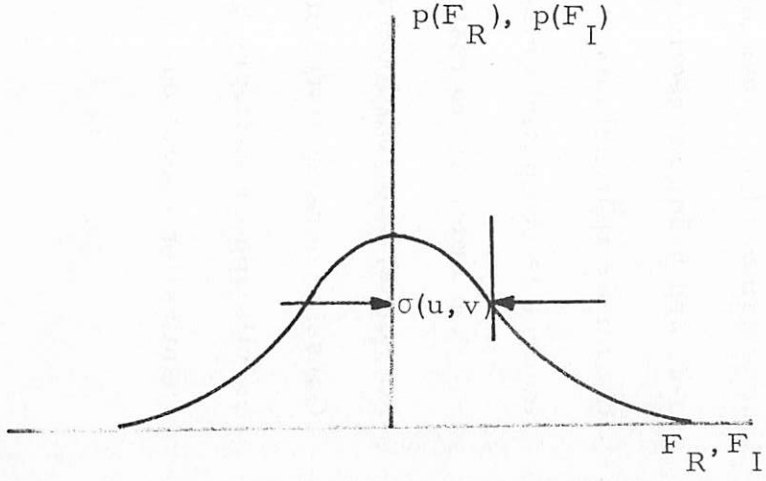

c) Gaussian Real and Imaginary

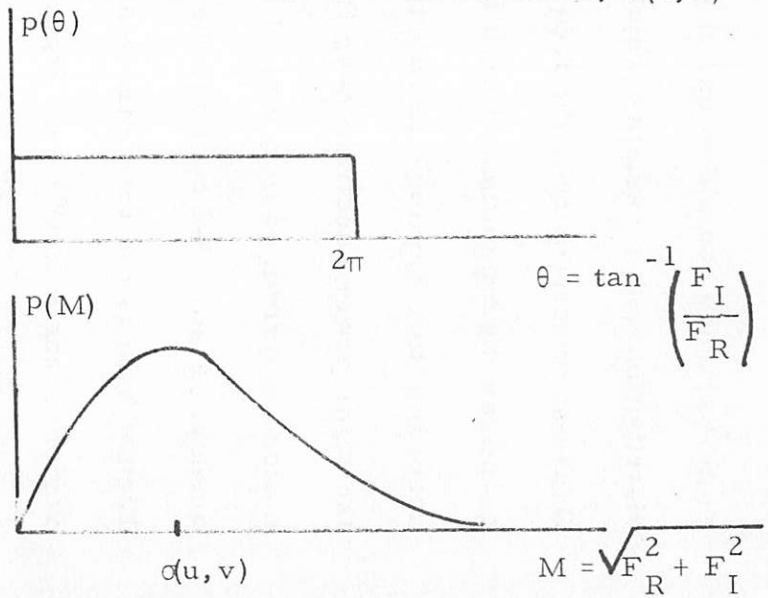

d) Rayleigh Magnitude and Linear Phase

Figure 5-1. -- Fourier Domain Quantization Techniques

each frequency sample to one of 64 levels according to a Gaussian distribution with a variance which changes as the two dimensional Gaussian spectrum over the frequency domain. The third scheme quantizes the magnitude of each frequency sample to one of 64 levels according to a Rayleigh distribution whose variance also changes as the same power spectrum over the frequency domain. The phase is uniformly quantized to one of 64 levels independent of spatial frequency. Figure 5-2 contains the results of the above three rules. Figure 5-2a is the reconstructed moon scene using the full computer register length of 18 bits. Figure 5-2b is the reconstructed moon scene using the linear quantization scheme, and obviously, is not acceptable. The Gaussian and Rayleigh techniques displayed in figures 5-2c and 5-2d, respectively, show considerable improvement over the linear approach. Little, if any, visible quantization noise is evident as compared to the 18 bit reconstruction.

In order not to restrict the experimental results to one particular scene, two additional images have been quantized using the Gaussian density distribution for the frequency samples. These results appear in figure 5-3 and also behave properly under the quantization operation.

a) No Quantization

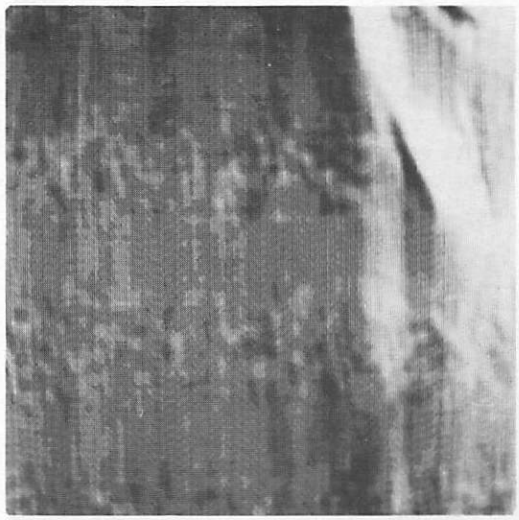

b) 64 Level Linear Quantization

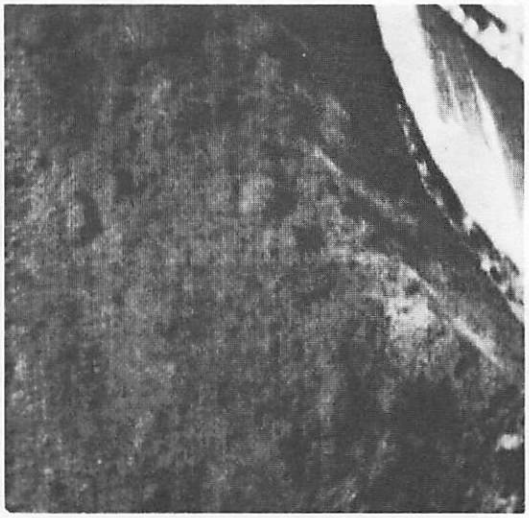

c) 64 Level Gaussian Real and Imaginary Quantization

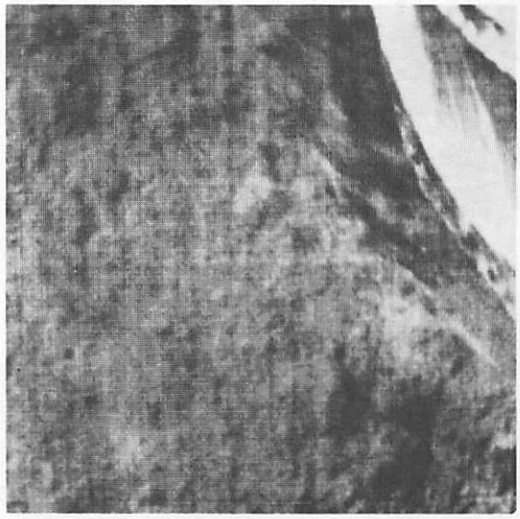

d) 64 Level Rayleigh Magnitude and Linear Phase Quantization.

Figure 5-2. -- Examples of Quantization for Footpad

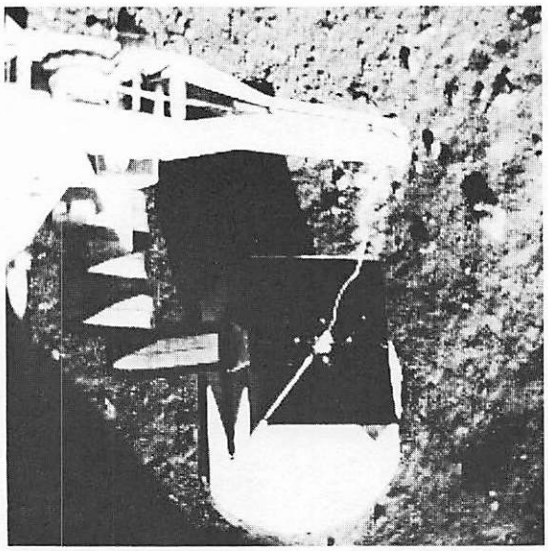

a) No Quantization

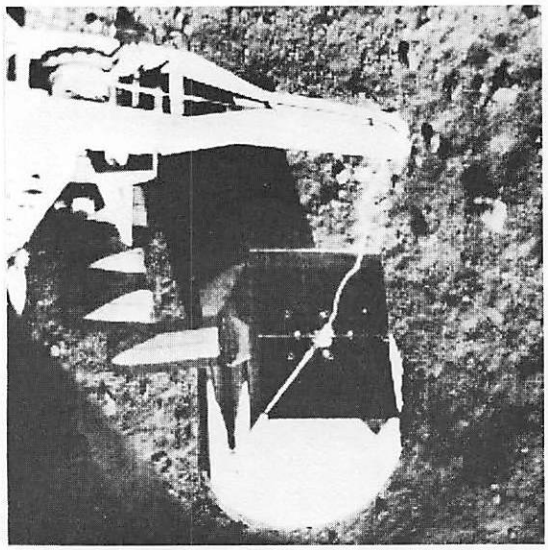

b) 6 Bit Quantization

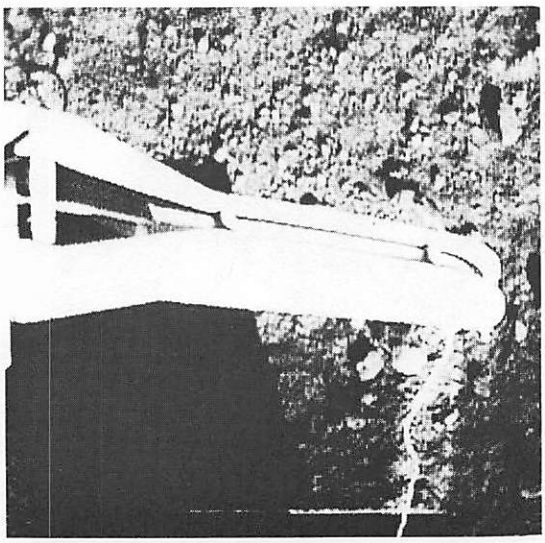

c) No Quantization

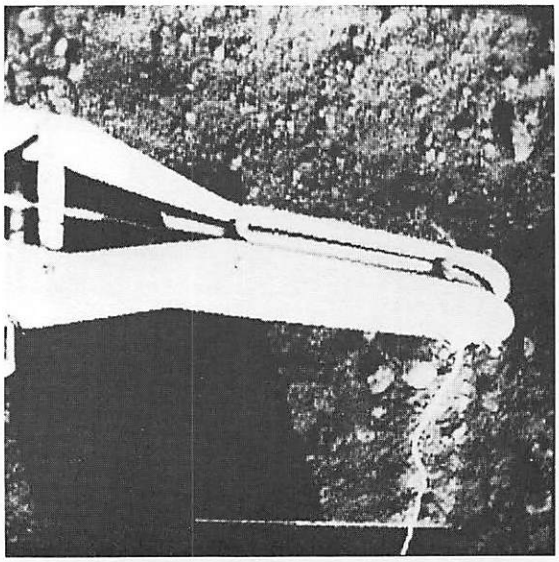

d) 6 Bit Quantization

Figure 5-3 64 Level Gaussian Quantization

5.3 Invariance to σ Plane

One result of this chapter has been the derivation of a quantization scheme based upon a variance which is a function of frequency. Therefore, a variance or σ plane is used to define the variance of the density function from which quantum levels are determined at every spatial frequency. The variance or σ plane behaves as the spectrum of the covariance function of the original process, $f(x,y)$. The problem of determining the variance plane on some distance spacecraft could far outweigh the advantages of Fourier coding, and, from a practical point of view could prejudice all Fourier coding techniques. It is the purpose of this section to develop an approach which will allow for an approximation to the variance plane with good experimental reconstructions. The following heuristic arguments are used as an introduction to the experimental results that follow.

First, the σ plane must be symmetric about the origin due to the nature of the Fourier transform of the covariance function. Second, there is no a priori knowledge to indicate that a particular direction will have a higher degree of correlation than any other direction. Consequently, the σ plane should be circularly symmetric. Finally, there is no a priori knowledge to indicate that a particular periodicity will be prevelant in the unknown image. Therefore, the σ plane should be monotonically increasing. A likely candidate for

the σ plane is a two dimensional Gaussian surface with u and v variances equal. Such a surface indicates that the original covariance function was also Gaussian, a not too unnatural assumption. The remaining question is how rapidly should the Gaussian curve fall off in the σ plane? This question is related to the degree of correlation of the original scene. The σ plane has been reduced to one degree of freedom rather than the original $\frac{N^2}{2}$ degrees of freedom.

An experiment has been performed in order to demonstrate a certain tolerance for various degrees of different Gaussian surfaces. Also, a $\left|\left[\frac{\sin au}{au}\right]\left[\frac{\sin av}{av}\right]\right|$ plane has been used with little noticeable effect on the retransformations. Three different Gaussian surfaces were used in the experiment. The Gaussian surface variances ranged over a factor of four in value. In addition to visual reconstructions, a matched filter correlation measurement was made with respect to the intermediate Gaussian curve. The visual and correlative results are displayed in figure 5-4. From a visual consideration, all four images appear relatively unchanged. The matched filter indicates that the least degree of correlation exists in the non-Gaussian surface. However, the visual results do indicate a fairly large degree of tolerance for the σ plane, especially considering the large range of variance used for the Gaussian surfaces.

a) Gaussian Surface, Intermediate Variance, Matched Filter Correlation : 1.000

b) Gaussian Surface, Small Variance, Matched Filter Correlation : 0.3675

c) Gaussian Surface, Large Variance, Matched Filter Correlation : 0.4278

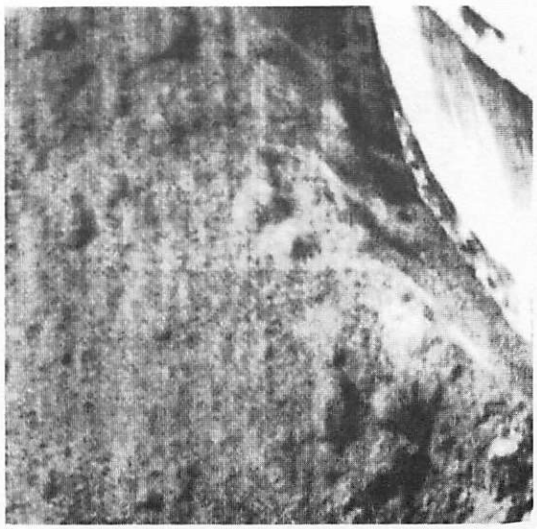

d) $\left|\left[(\sin au)/au\right]\left[(\sin av)/av\right]\right|$ Surface, Matched Filter Correlation : 0.2022

Figure 5-4. -- Gaussian Quantization with Different Variance Planes

Results such as these are encouraging in the respect that the exact spectrum is not necessary for quality reconstructions.

CHAPTER 6

NOISE EFFECTS

A major concern of communication system designers is the susceptibility of data to noise interference. It is important, then, to study the effects of noise on the Fourier coding communication system. Two particular noise patterns of interest are spatially correlated noise and spatially random noise. Spatially correlated noise will usually result from some peculiar characteristic of an image sensing device such as a vidicon mesh pattern or geometric distortion due to poor deflection amplifiers. Spatially random noise often occurs in digital communication systems as channel noise.

6.1 Binary Symmetric Channel Noise

In most digital communication systems the code alphabet consists of two symbols which are subject to perturbations in the channel, and these perturbations introduce random noise at the receiver. The binary symmetric channel is used as the noise model in the study of channel effects on Fourier coding. The classical representation of such a communication channel is given in figure 6-1 where the probability of receiving an incorrect symbol is p

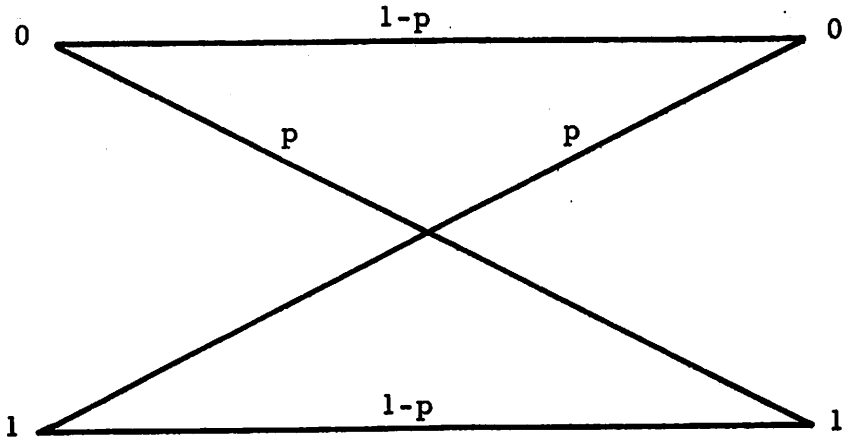

Figure 6-1.--Model of a Binary Symmetric Channel

irregardless of which symbol is transmitted.

An intuitive justification for transmitting the frequency rather than the spatial domain of an image is the fact that channel noise introduced in the Fourier transform of an image tends to be distributed evenly over the entire reconstructed image. Consequently the noise manifests itself as a low frequency effect in reconstruction. Since the eye is more sensitive to the high frequency "salt and pepper" effect of channel noise in the spatial domain, the same channel noise power in the frequency domain is somewhat less offensive. Figure 6-2a shows a mid-grey scene after having passed through a channel with probability of error of 0.1. Figure 6-2b is the Fourier transform of the output of the same channel whose input was the Fourier transform of the mid-grey scene. Both scenes have the same amount of noise energy but that energy is distributed quite differently. A quantizing and coding method can be developed to take advantage of the inherent high frequency or "salt and pepper" noise immunity that Fourier domain coding offers. As a first step in this direction a requirement will be made that each quantum level occur equally likely as any other quantum level. This quantization criterion will guarantee that each code word is equally likely to occur and will avoid any unexpected noise biasing, since the binary symmetric channel effects each code bit, and therefore each code word,

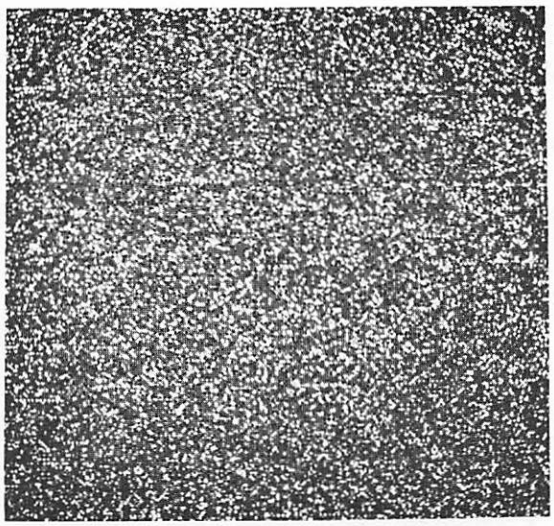

a) BSC Noise in Spatial Domain

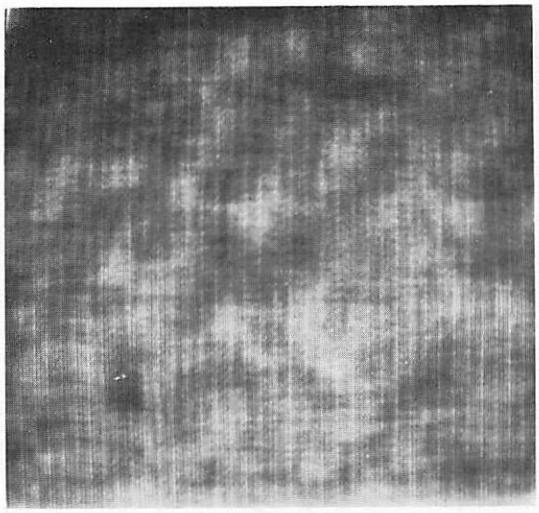

b) Fourier Transform of BSC Noise in Fourier Domain

Figure 6-2. -- Binary Symmetric Channel Noise with Error Rate $p = 10^{-1}$

independently of all others. Such a quantization requirement results in the quantization rule employed at the end of chapter 5. As was mentioned earlier, such a scheme is sub-optimum with respect to quantization error, but is better suited for channel noise immunity.

Figure 6-3 contains a series of experimental results using the Rayleigh quantization law with variance changing as a function of frequency according to the power spectrum of the original scene. The footpad and its quantized Fourier transform are passed through the same binary symmetric channel for two different error probabilities. These pictures are presented to demonstrate a further complication that must be avoided. The frequency induced noise energy is concentrated in low frequency variations which are so large that the high frequency information is lost due to normalization in reconstruction. This can be explained by the fact that the absolute, as opposed to the relative value of a bit error is much larger in the regions where the power spectrum is large. In the case of the power spectrum of the footpad, the larger values occur at the lower frequencies, and thus the lower frequency noise errors have a greater effect on the reconstructed image in the spatial domain. Further demonstration of this effect is afforded by figure 6-4. Figures 6-4a and 6-4b are the footpad noise scenes with error rates of 10^{-1} introduced in the space and frequency domain respectively. Figure 6-4c is the result of the same error rate channel noise in the frequency domain

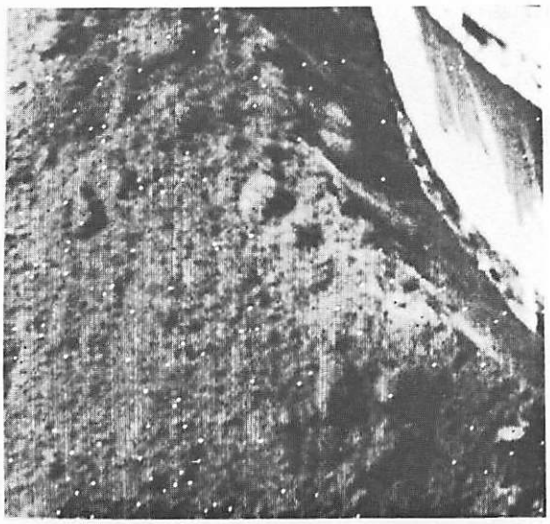

a) 10^{-3} Error Rate in the Spatial Domain

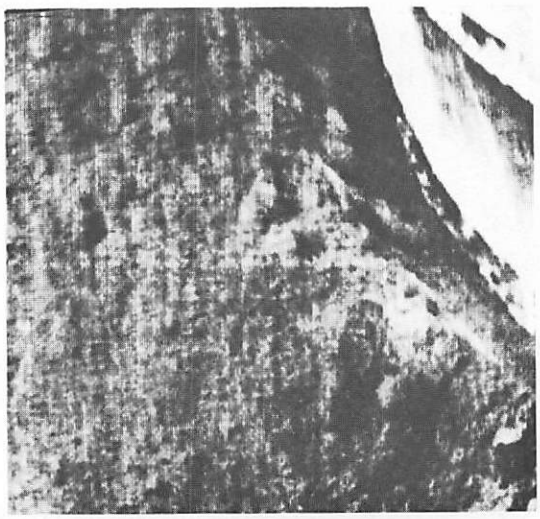

b) 10^{-3} Error Rate in the Fourier Domain

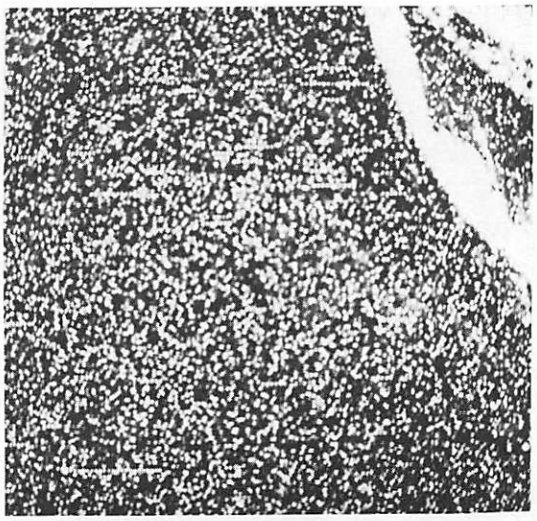

c) 10^{-1} Error Rate in the Spatial Domain

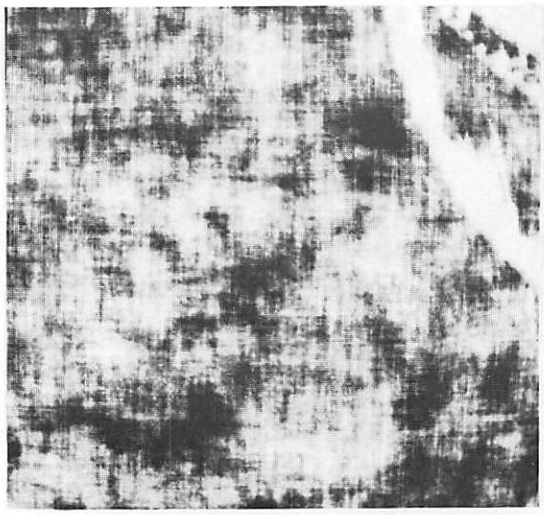

d) 10^{-1} Error Rate in the Fourier Domain

Figure 6-3. -- Binary Symmetric Channel Noise in Spatial and Fourier Domain Transmission

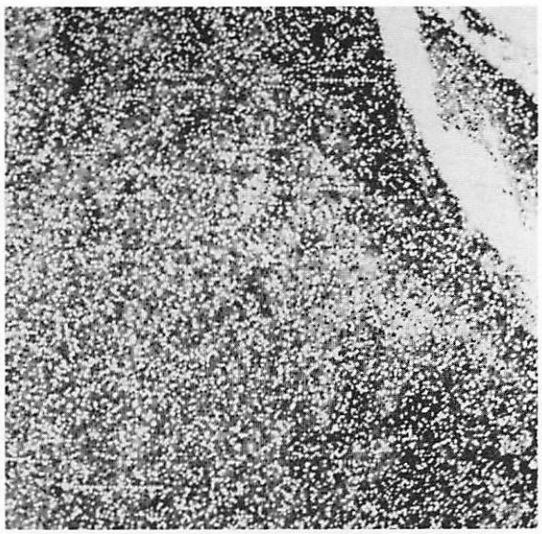

a) 10^{-1} Error Rate in the Spatial Domain

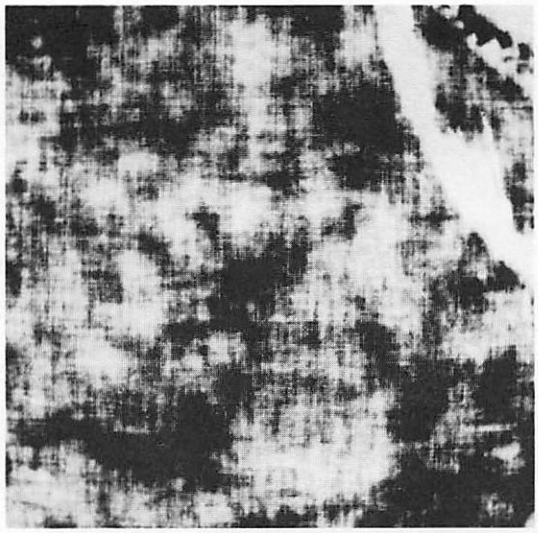

b) 10^{-1} Error Rate in the Fourier Domain

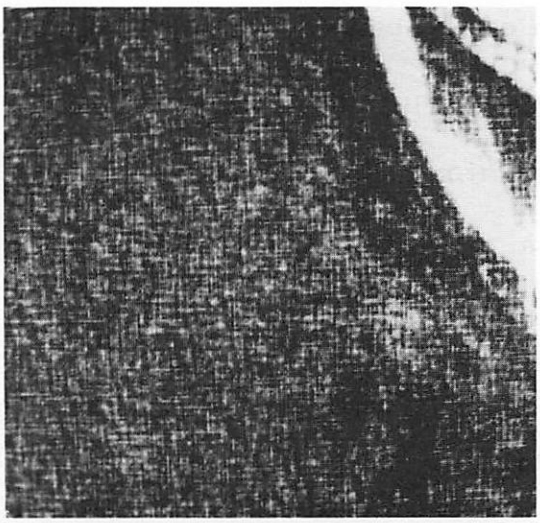

c) Reconstruction with the 800 Lowest Spatial Frequencies Errorless

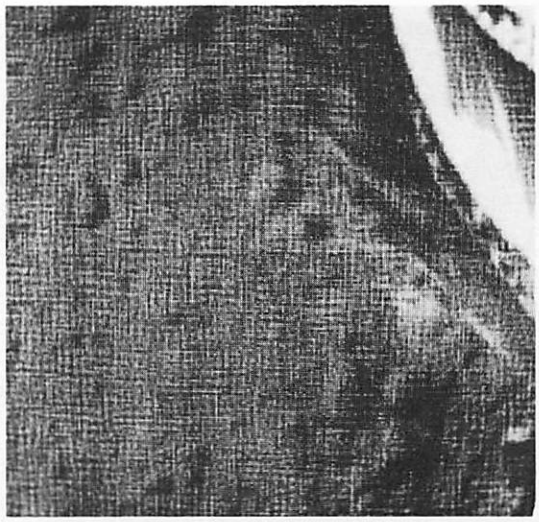

d) Reconstruction with the 6500 Lowest Spatial Frequencies Errorless

Figure 6-4. -- Effect of Low Frequency Errors

but with 20 x40 or 800 of the lowest spatial frequencies transmitted error free. It is evident from figure 6-4c that the noise energy is now concentrated in the higher frequencies. Figure 6-4d has the lowest 6500 spatial frequencies transmitted error free.

As a result of the statistical regularity of samples in the frequency domain, a much smaller amount of error correction in this domain will yield a far better noise immunity than the same amount of error correction in the spatial domain. The nature of the quantization law is such that errors in certain positions of the frequency domain are much more bothersome than in other positions due to the large statistical variance of samples at these frequencies. Therefore, it is natural to develop an error correction rule to correct for errors only in these large variance regions. One such rule would be to error correct code those frequency samples which correspond to positions in the frequency domain where the power spectrum of the covariance function indicates a high probability of large sample values. This technique alone requires an increase in bandwidth to facilitate the error correction. However, it has been found that the small increase in bandwidth in the Fourier domain will result in far better reconstructions than the same increase in the spatial domain.

It is important to emphasize that the coding technique used for the Fourier domain should be tailored to a particular channel capacity. If the channel noise has an error rate less than about 10^{-3},

then it appears that no error correction is necessary as in figure 6-3b. However, under the circumstances of a high error rate, it often becomes more desirable to transmit as many error corrected samples as possible at the expense of not transmitting the entire frequency plane. Using such a system, corrected, but not necessarily errorless, data could be received until normal picture bandwidth has been reached, at which time transmission is terminated. In order to implement such a scheme, an error correcting code must be selected. The code selected will depend on how much of the frequency domain will be omitted due to the increased error correcting capability of the code. The main point of this discussion is to illustrate the variety of coding implementations possible for different channel conditions.

A specific example of the potential of the Fourier coding technique is presented below. A high error rate channel is assumed with rate $p = 4 \times 10^{-2}$. The equal bandwidth criterion is assumed. Consequently, the Fourier coding technique requires the exact same bandwidth as conventional spatial domain transmission systems. The error correcting code must have at least six information bits. Two such codes which become candidates for implementation are a first order Reed Muller code and a Bose Chaudhuri-Hocquenghem code, (BCH) [25; 26, pg. 162]. The particular Reed Muller code of interest is a (32,6) code in which the minimum distance between

code words is sixteen, and therefore, the code is capable of correcting a total of seven errors. The BCH code is a (31,6) code and is also capable of correcting seven errors. The BCH code will be used in the following discussion. Utilizing an error correcting code capable of seven error corrections does not mean that the six information bits will be received over the noisy channel error free. Since each code word length has been increased to thirty-one bits, eight or more errors per code word cannot be guaranteed to be corrected. The probability of having eight or more errors in the BCH code is given by the partial sum of the binomial distribution

$$P(8 \text{ or more errors}) = \sum_{i=8}^{31} \binom{31}{i} p^i (1-p)^{31-i} \qquad (6.1)$$

where p is the binary symmetry channel error rate. This probability is an upper bound for the incorrect reception of a code word since the possibility of correct reception for greater than seven errors still exists but is unknown. For the specific channel error rate of 4×10^{-2}, the error corrected data samples will be received with probability of error no greater than 2.26×10^{-5} [27]. Figure 6-5 displays the results of this error correcting procedure. Figure 6-5a and 6-5c are two test scenes whose spatial domains are transmitted through the binary symmetric channel with the above error rate. Figure 6-5b and 6-5d are the error correction Fourier domain

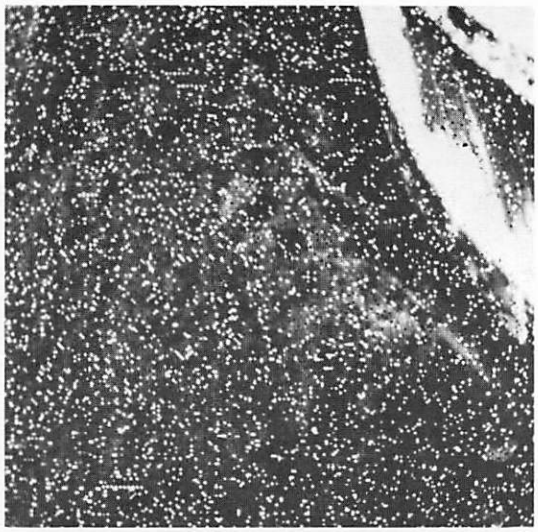

a) 4×10^{-2} Error Rate in the Spatial Domain

b) Error Corrected Retransformation

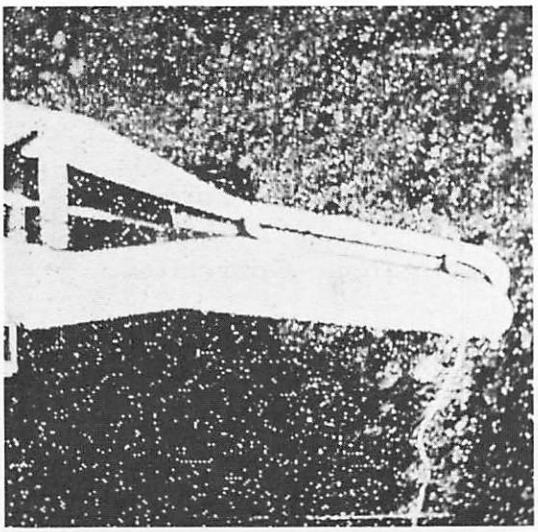

c) 4×10^{-2} Error Rate in the Spatial Domain

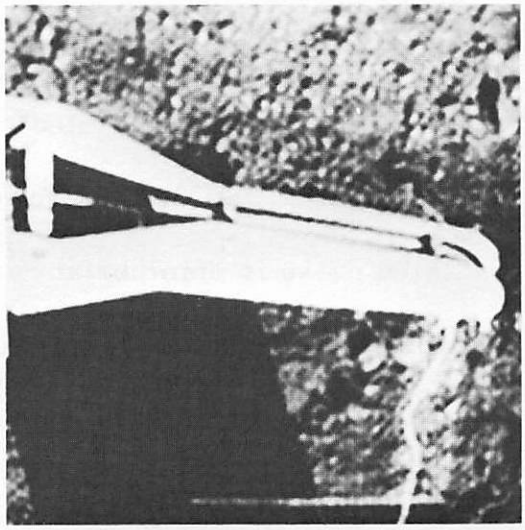

d) Error Corrected Retransformation

Figure 6-5. -- Equal Bandwidth Error Correction Technique

transmission results for each of the test scenes. While there is a loss of high frequency information in figures 6-5b and 6-5d, there is a marked improvement over the spatial coding in figures 6-5a and 6-5c. It is evident that this particular type of coding offers a considerable advantage for very noisy communication channels.

6.2 Correlated Noise

Removal of certain noise patterns is possible in the frequency domain. Such a technique is especially successful when the noise has a high degree of correlation. In this section spatially correlated noise will be any unwanted characteristic of an image that has a reasonably well defined power spectrum. The source of the correlated noise is unimportant and need not be investigated. Correlated noise removal techniques can be implemented by multiplication of a filter transfer function with the Fourier transform of an image, or by the energy subtraction of certain portions of the frequency domain of an image.

Multiplication filtering can take the simple form of frequency band filtering or the more complicated form of matched filtering as discussed earlier in chapter 4. An example of a smoothly varying low pass filter in which there is more filtering power in one dimension than in the other is afforded by figure 6-6. Examples of very

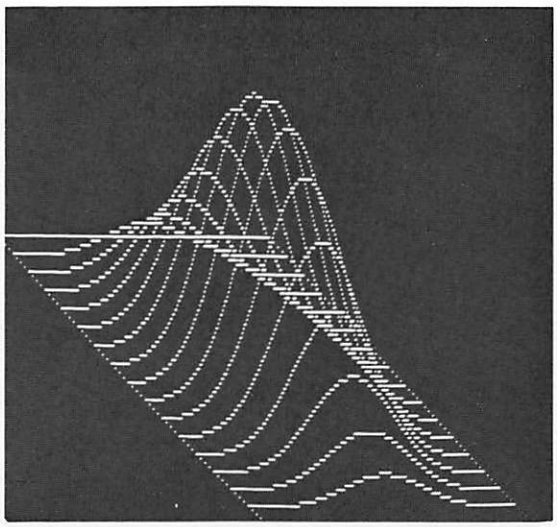

Figure 6-6. -- Nonlinear Multiplicative Filter

simple low and high pass filtering are given by figure 6-7. The low pass filter used was a 40 x40 square aperture binary mask which had the value 1 in the square and zero outside of the square. The inverse of this filter was used as the high pass filter. Figure 6-7a is the original scene and contains the block letters "USC". Figure 6-7b is the logarithm of the magnitude of the Fourier transform of "USC". Figures 6-7c and 6-7d are the low pass and high pass filtered versions of the original, respectively.

Often a low pass filter can be used successfully for noise removal in the presence of a tremendous amount of high frequency noise. Figure 6-8 demonstrates this capability. Figure 6-8a is a two level "USC" block letter scene which has an incorrect element on the average of one every fourth sample. The noise tends to be of a high frequency nature with no particular dimensional correlation visible. A simple 40 x40 low pass filter will yield the results of figure 6-8b. This technique can also be used for high frequency noise removal in grey-scale scenes. Figure 6-8c is the result of transmitting the Surveyor box scene through a channel with error rate $p = 10^{-1}$. The low pass filtering of this scene results in figure 6-8d where a circular filter of radius 51 frequency samples has been used. This technique allows viewing of low frequency information otherwise obscured by the high frequency noise.

As was mentioned earlier, certain noise patterns can be

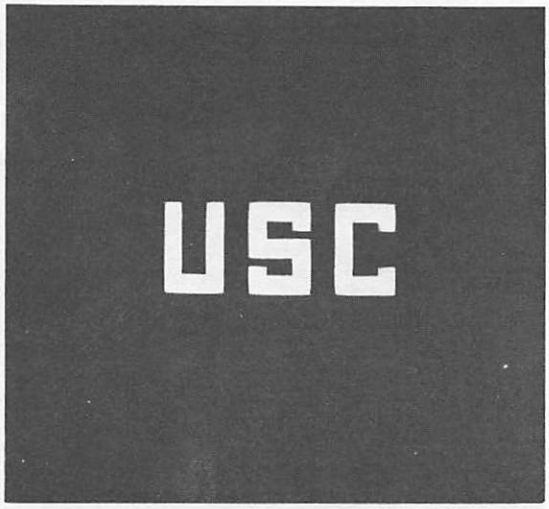

a) Block Letters "USC"

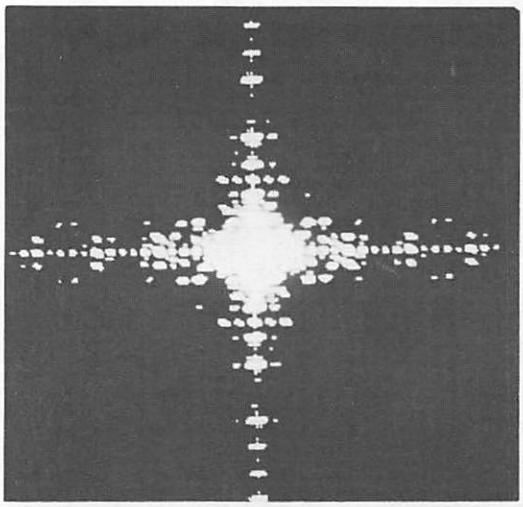

b) Logarithm of the Magnitude of the Fourier Transform

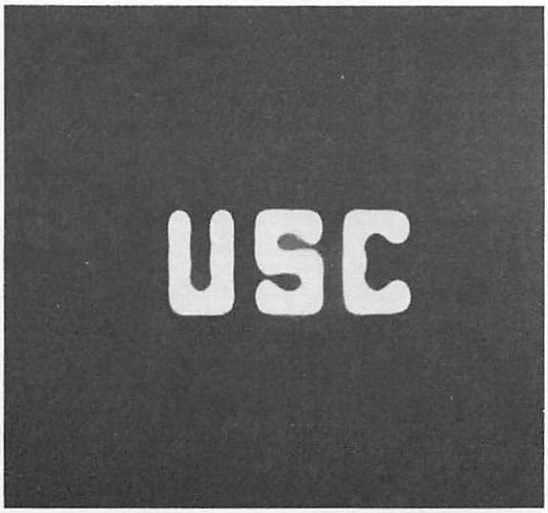

c) Low Pass Filtered Reconstruction (40 x 40 Binary Mask Filter)

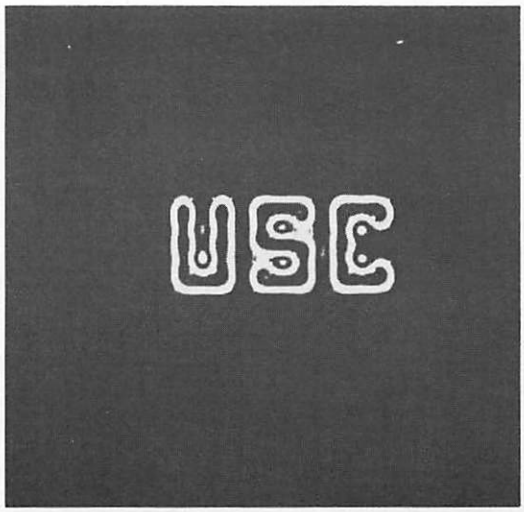

d) High Pass Filtered Reconstruction (Inverse 40 x 40 Binary Mask Filter)

Figure 6-7. -- Fourier Domain Filtering

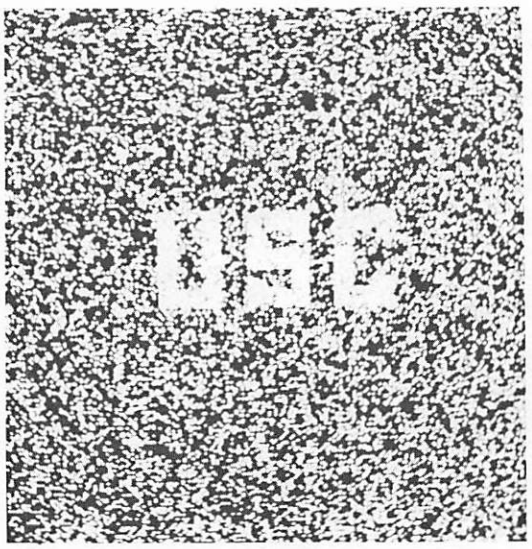

a) Two Level "USC" with Error Rate $p = \frac{1}{4}$

b) Low Pass Filtered Reconstruction (40 x 40 Binary Mask Filter)

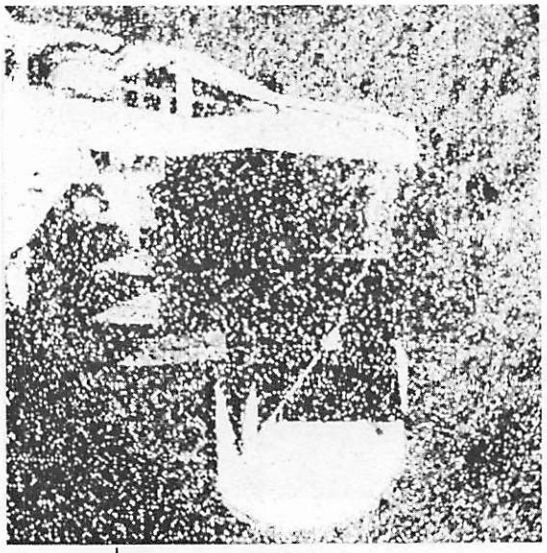

c) 10^{-1} Error Rate in the Spatial Domain

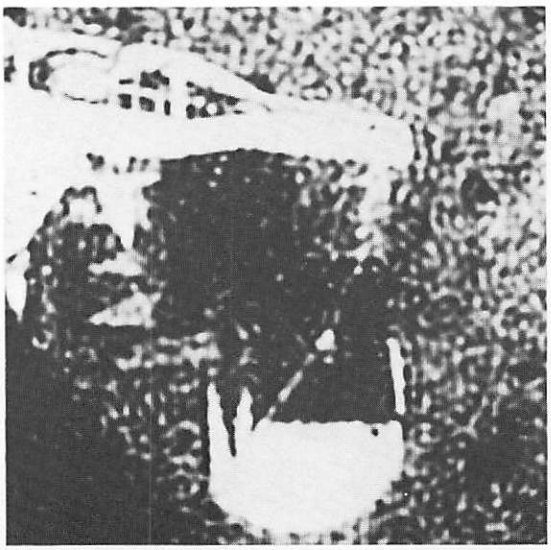

d) Low Pass Filtered Reconstruction (Circular Binary Mask Filter, Radius = 51)

Figure 6-8. -- High Frequency Noise Filtering

removed by an energy subtraction in the frequency areas of large noise content. This procedure might be used when it is desirable to remove noise of a given spectral frequency, but not remove image information at that frequency. The energy subtraction noise removal method is only recommended when very exact noise power spectral density information is available, because, subtraction of too much energy or energy at the wrong frequency will result in total image degradation corresponding to application of the superposition principle. An example in which the subtaction technique is possible is afforded by Figure 6-9. Figure 6-9a shows the footpad scene with a highly correlated one dimensional noise pattern that is quite periodic. Because the period and direction can be accurately measured, a noise spectrum can be properly determined. A subtraction of energy in this part of the frequency domain will then result in figure 6-9b. Similar results can be obtained for two dimensionally correlated noise as seen from figures 6-9c and 6-9d respectively.

6.3 Conclusions

The experimental results of this chapter indicate that processing in the Fourier domain offers advantages for noise improvement techniques. Specifically, for high channel error rates, transmission of only error corrected data permits far superior reconstructions

a) One Dimensionally Correlated Noise (Cosine [a(x+y)] Where a = .125 Cycles/Picture Element)

b) Noise Removed

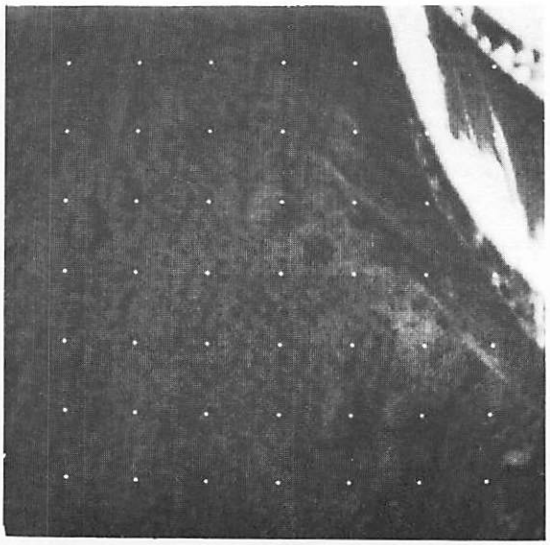

c) Two Dimensionally Correlated Noise (x, y Periodicity = 32 Picture Elements)

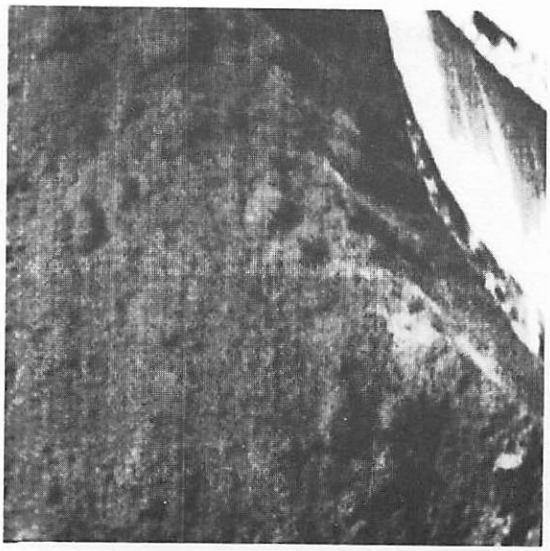

d) Noise Removed

Figure 6-9. -- Spatially Correlated Noise Removal

than spatial domain coding. The frequencies that are error corrected are a function of the power spectrum of the image, but the power spectrum can easily be approximated by a simple Gaussian function, and need not be known a priori. For channel error rates low enough, no error correction is necessary and the noise power is averaged out over the entire retransformed plane.

In the area of correlated noise removal several examples are presented to show the ease with which spatial filtering can be implemented. The results of these spatial filtering techniques are limited only by the lack of knowledge of the noise power spectrum. The advantage of computer implementation of two dimensional spatial filtering lies in the large dynamic range of the filter domain and thus a large variety of filtering possibilities.

CHAPTER 7

BANDWIDTH REDUCTION

In the investigations of the previous chapters analytic and experimental results have pointed to the advantage of using the statistical regularity of frequency samples in the Fourier domain. This has held true in developing quantization and noise immunity coding methods. It seems logical, then, that a similar technique might be pursued in the study of bandwidth reduction in the frequency domain. It will be shown that very large bandwidth reductions can be obtained in the Fourier domain with far less picture degradation than in the spatial domain for the same bandwidth reduction factor. These results are valid for severe bandwidth limited communication systems. More pleasing results can also be obtained with much smaller bandwidth reduction factors. Four different techniques are investigated below. The first technique simply indicates the quality of reconstructions obtainable from binary mask low pass filters. A scanning algorithm method is described in which a sequential image construction communication system is developed. A section of the chapter is devoted to applying spatial domain bandwidth reduction techniques to the Fourier domain; and finally, coding and quantization

techniques are discussed with respect to bandwidth reductions.

7.1 Fixed Aperture Bandwidth Reductions

Probably the most obvious method of saving bandwidth in a Fourier communication system is to not transmit the high frequency information. This is equivalent to low pass filtering an image, and will result in blurred retransformations. The technique will be referred to as a fixed aperture method. Most of the image energy is compacted into few low frequencies, and therefore a large percentage of total image energy can be transmitted with a surprisingly small bandwidth requirement. In addition, the large bandwidth reductions obtainable by the fixed aperture method are superior to the same reductions applied only in the spatial domain.

The experimental results presented in this section have been obtained with circular apertures centered about the origin of the Fourier domain. Using such apertures, energy distributions as a function of radial spatial frequency have been taken for different test scenes. These results are presented in figure 7-1 in which the energy within a given radial frequency is plotted. The radial frequency axis has been converted to a percentage of total bandwidth axis for display purposes. It is evident from this figure that a very large percentage of image energy is concentrated in a very small portion of the bandwidth in the frequency domain. It is this fact that

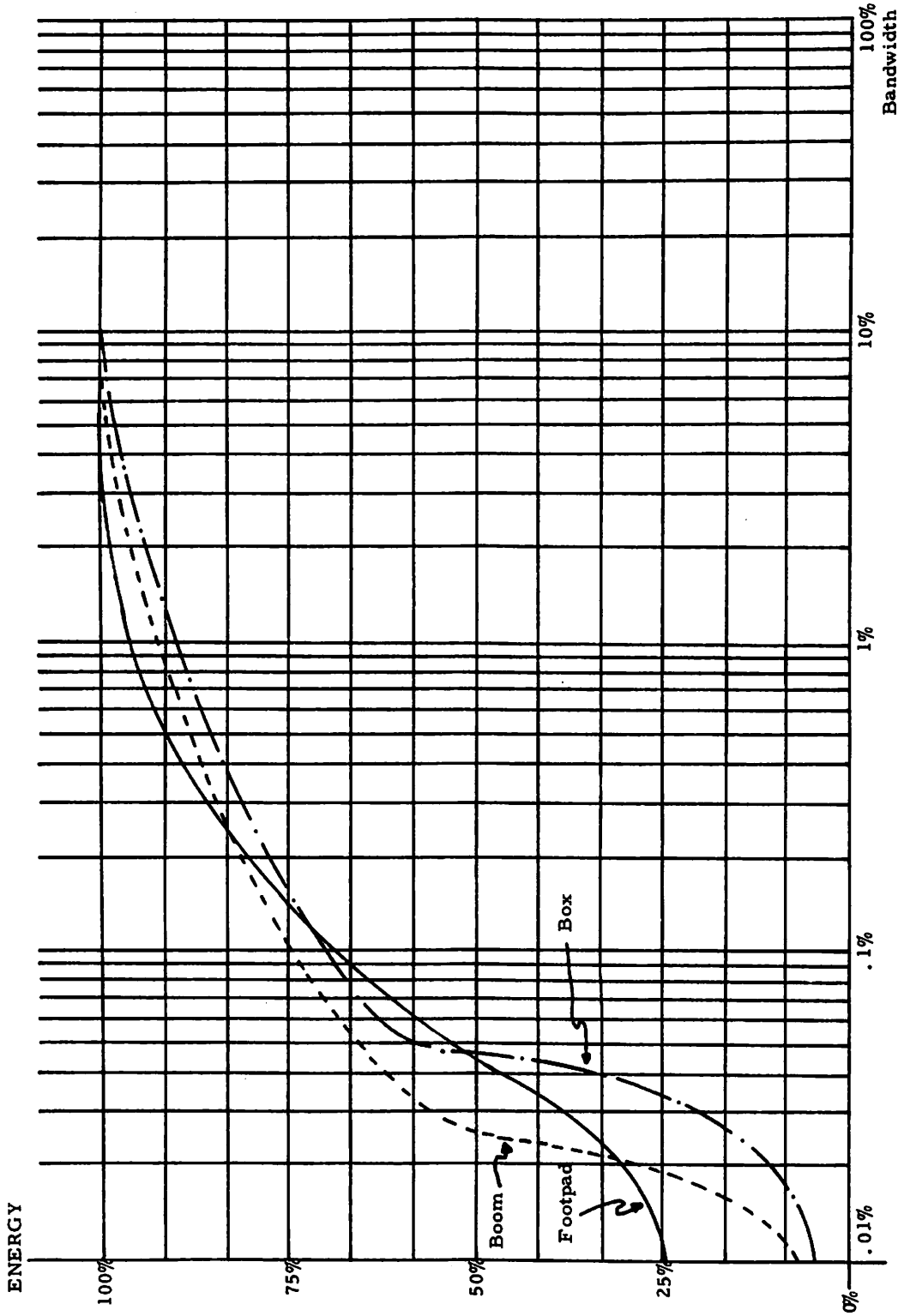

Figure 7-1. --Image Energy as a Function of Bandwidth Transmitted

allows the development of noise immunity techniques as in chapter 6 and the aperture bandwidth reduction techniques in this chapter. Figures 7-2 and 7-3 present results for two test scenes. The bandwidth reductions and amount of image energy transmitted are listed in the captions. Figure 7-4 presents two different bandwidth reduction factors for both the Fourier and spatial domains. A sample and hold technique has been used to implement the reductions in the spatial domains.

7.2 Scanning Algorithms

The particular bandwidth reduction technique which is incorporated in the Fourier domain depends entirely on the degree of resolution which is desired in the reconstruction after transmission. It should be emphasized that any modification to the Fourier domain, even if only at a single spectral point, affects the entire reconstruction. For this reason high resolution reconstructions are difficult to obtain for any significant amount of bandwidth reduction. However, one promising technique for Fourier domain bandwidth reduction is afforded when a severe bandwidth reduction is necessary due to large communication distances, or possibly, due to a desire to initially investigate a scene before full bandwidth transmission is decided upon. Under such conditions certain scanning algorithms can be developed so that a very high percentage of the energy of a picture

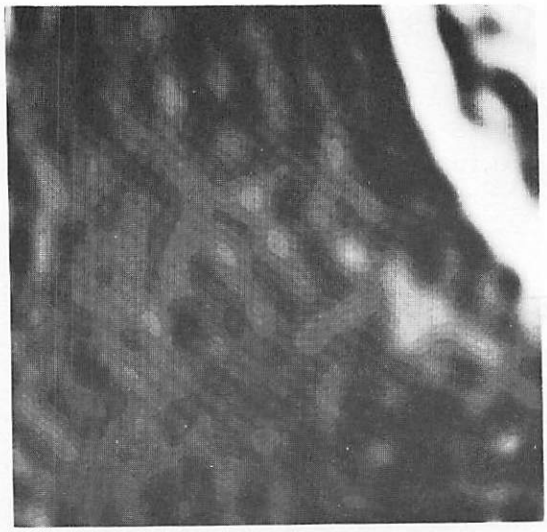

a) Bandwidth Reduction 64:1
98.3% Image Energy Transmitted

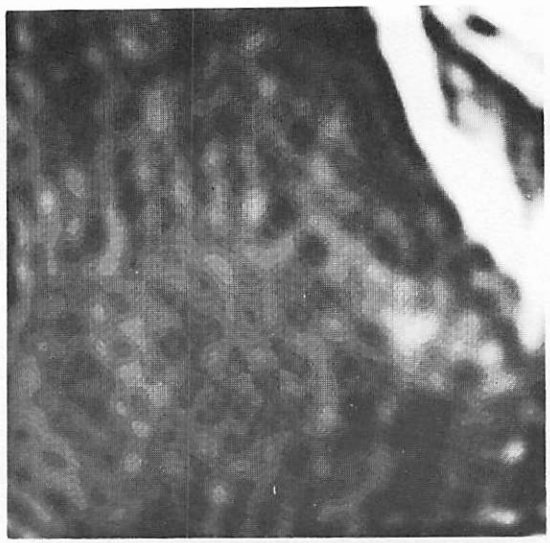

b) Bandwidth Reduction 32:1
99.5% Image Energy Transmitted

c) Bandwidth Reduction 16:1
99.8% Image Energy Transmitted

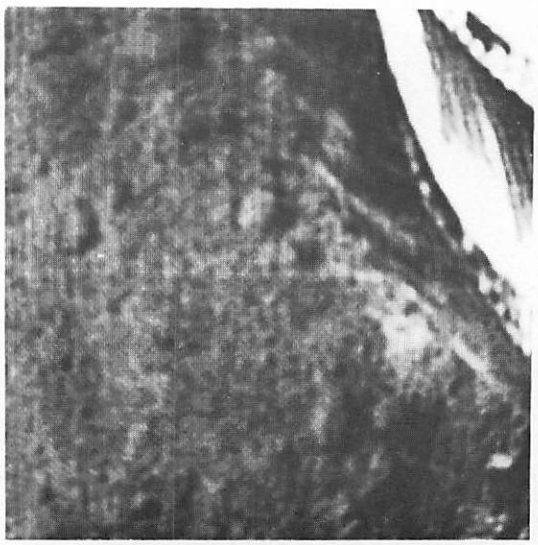

d) Bandwidth Reduction 4:1
99.9% Image Energy Transmitted

Figure 7-2. -- Bandwidth Reductions with Circular Apertures

a) Bandwidth Reduction 64:1
92% Image Energy Transmitted

b) Bandwidth Reduction 32:1
95% Image Energy Transmitted

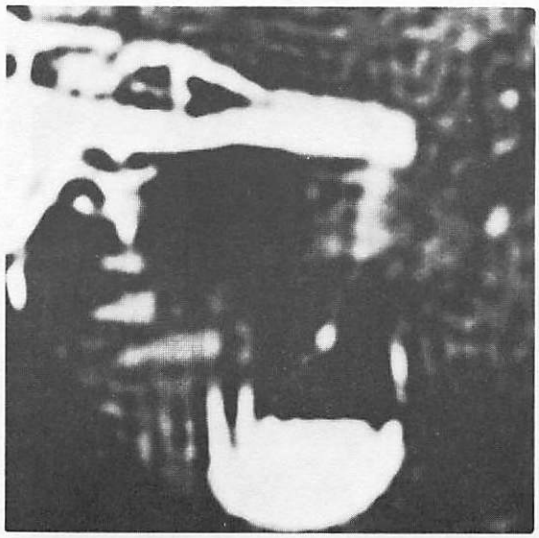

c) Bandwidth Reduction 16:1
98.3% Image Energy Transmitted

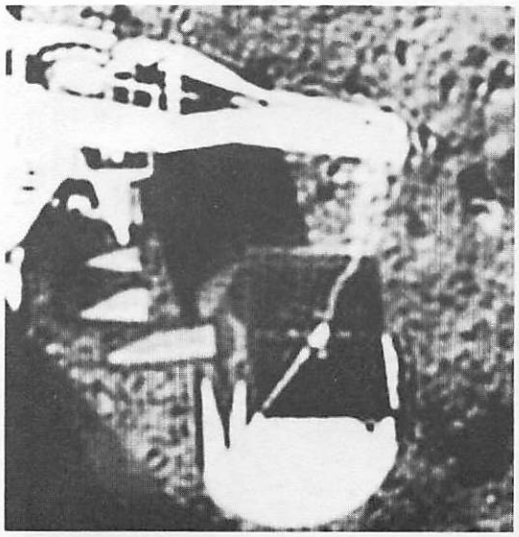

d) Bandwidth Reduction 4:1
99.8% Image Energy Transmitted

Figure 7-3. -- Bandwidth Reductions with Circular Apertures

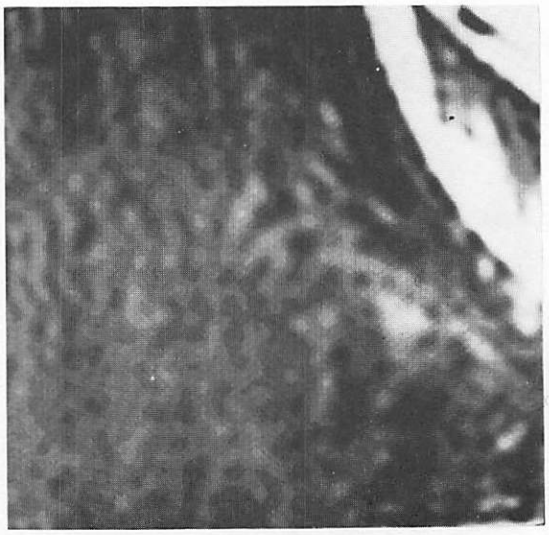

a) Fourier Domain 36:1

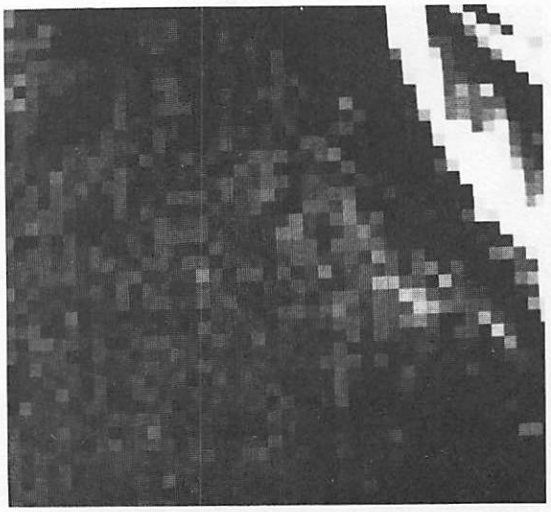

b) Spatial Domain 36:1

c) Fourier Domain 4:1

d) Spatial Domain 4:1

Figure 7-4. -- Equivalent Spatial and Fourier Domain Bandwidth Reductions

can be transmitted with very few data points. A scanning algorithm is an order of transmission of spectral points which usually would follow the peaks in the power spectrum if known. As an example, figure 7-5 contains two Fourier domain scenes and suggested scanning algorithms in each case. Notice that the scanning algorithms tend to follow the high energy frequency samples as would be indicated by the power spectrum of the process. Since the energy in the spatial and Fourier domains is identical, a transmission technique can be devised so that a cumulative record of energy transmitted is retained. In this way transmission can be terminated at any desired percentage of total energy available. If the second algorithm presented in figure 7-5 is used, the results are the same as those obtained in section 7.1 for fixed circular apertures. Referring to figures 7-2 and 7-3 it is evident that recognizable reconstructions are obtained for even the largest bandwidth reductions. The reconstructions would be valid enough to base a decision as to the advantage of transmitting more of the spectral points for better reconstructions or saving bandwidth and focusing the camera on a new scene. In this way a scene can be sequentially built up to obtain better and better resolution until the total Fourier domain has been transmitted or until bandwidth constraints are exceeded. Figures 7-2 and 7-3 demonstrate the results of this type of construction of transmitted scenes.

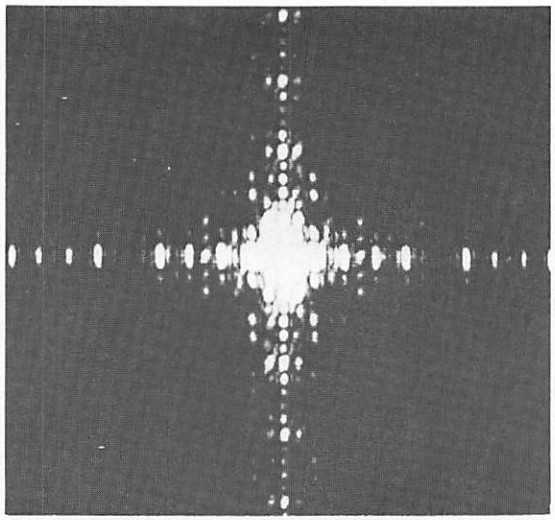

a) Logarithm of the Magnitude of the Fourier Transform of "USC"

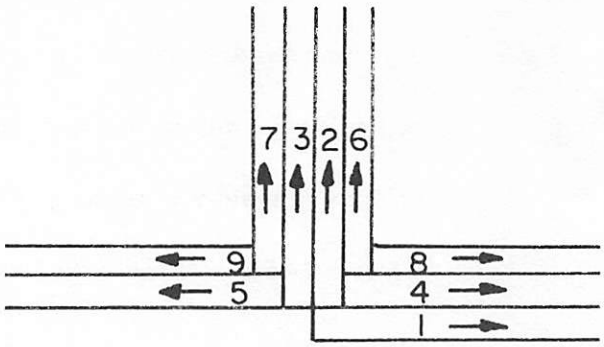

b) Rectangular Scanning Algorithm

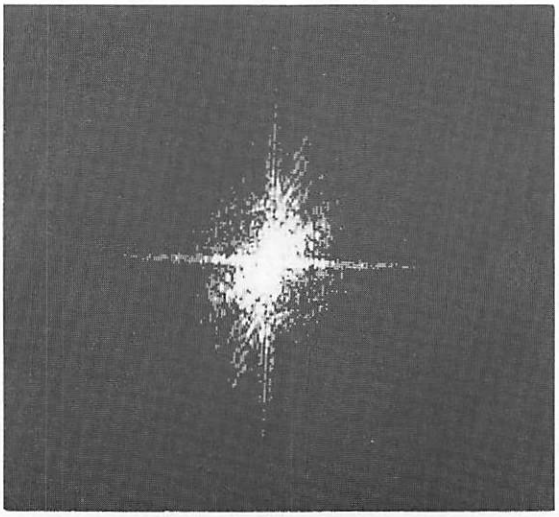

c) Logarithm of the Magnitude of the Fourier Transform of the Footpad

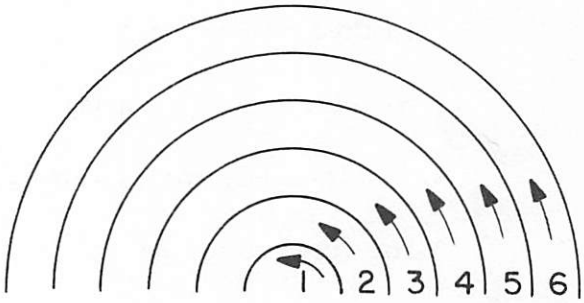

d) Circular Scanning Algorithm

Figure 7-5. -- Scanning Algorithms

7.3 Spatial Techniques in the Fourier Domain

A tremendous amount of research effort has been expended in developing bandwidth reduction techniques in the spatial domain [1,28-32]. Therefore, it seems practical to attempt to apply these techniques to the frequency domain. As an example, edge detection is useful in spatial domain bandwidth reduction techniques. An edge is defined as a change in the value of a picture sample, and the edges and their positions are coded and transmitted in this bandwidth reduction method. The difficulties of adapting such a technique to the Fourier domain are immediately obvious when defining frequency edges due to the very large dynamic ranges of this domain. This same dynamic range, coupled with changing sign, causes a severe problem in any type of predictive coding for real and imaginary frequency components, because knowledge of one sample does not significantly reduce the entropy concerning adjacent samples. One suggestion is that the magnitude function, $M(u,v)$, discussed in chapter 5, might be well enough behaved to apply predictive or interpolative sampling. A sample and hold scheme has been implemented on the magnitude of each Fourier sample while retaining complete phase information. The results are displayed in figure 7-6a and indicate poor retransformation. While the magnitude is better behaved than either the real or imaginary components of each

a) Sample and Hold on Magnitude Only

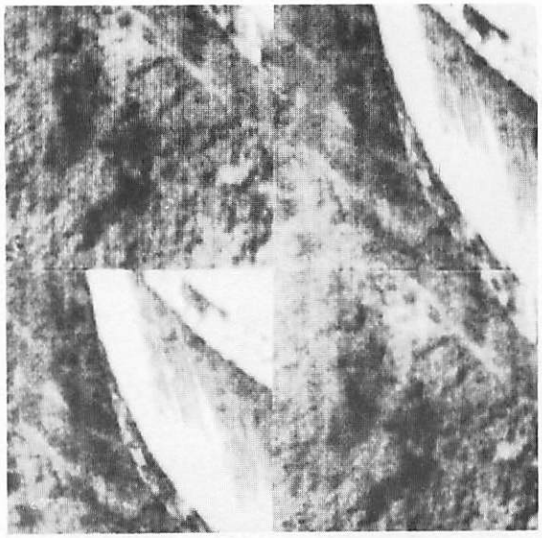

b) Checkerboard Sampling

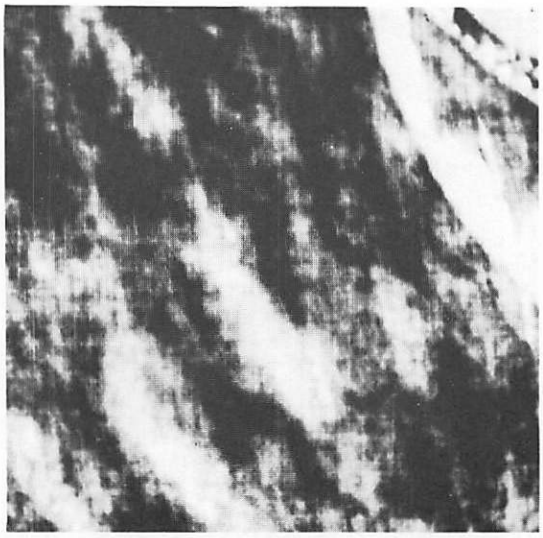

c) Random Sampling

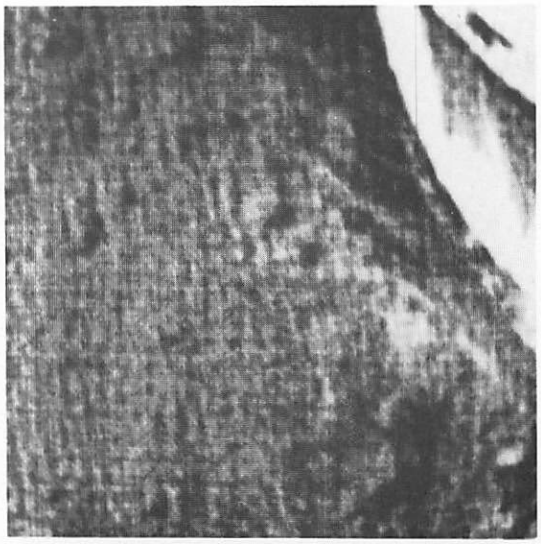

d) Random Sampling of High Frequencies

Figure 7-6. -- Spatial Domain Techniques Applied to the Fourier Domain for a Bandwidth Reduction of 2:1

frequency sample, its variance is changing with the covariance power spectrum as a function of frequency, and thus does not lend itself to sample and hold techniques.

Most of the deterministic sampling techniques used in spatial bandwidth reduction schemes are undesirable for use in the Fourier domain. As an example of a deterministic sampling technique, consider sampling in a checkerboard fashion over the two dimensional Fourier plane. The sampling function, S(u,v), can then be represented as

$$S(u,v) = \frac{1 + (-1)^{u+v}}{2} \tag{7.1}$$

and takes on the value zero or one depending on whether u+v is odd or even respectively. The sampled frequency plane can then be represented as the product of F(u,v) and S(u,v) and the retransformed image, g(x,y), becomes

$$g(x,y) = \frac{1}{N} \sum_{u,v=0}^{N-1} \sum F(u,v) \left[\frac{1+(-1)^{u+v}}{2} \right] \exp \left\{ \frac{2\pi i}{N} (ux+vy) \right\} \tag{7.2}$$

Since (-1) can be equated to exp (iπ), equation (7.2) can be further reduced to

$$g(x,y) = \frac{1}{2} \left[f(x,y) + \frac{1}{N} \sum_{u,v=0}^{N-1} \sum F(u,v) \exp \left\{ \frac{2\pi i}{N} \left(ux+u+vy+v\right) \right\} \right] \tag{7.3}$$

where f(x, y) is the two dimensional Fourier transform of F(u, v). The result of the second term within the square brackets becomes a Fourier transformation with a phase shift, thereby introducing a space shift in the spatial domain.

$$g(x,y) = \frac{1}{2}\left[f(x,y) + f\left(x+\frac{N}{2},\ y+\frac{N}{2}\right)\right] \tag{7.4}$$

A vivid example of this type of sampling is shown in figure 7-6b. Close examination of this figure reveals that equation (7.4) has been experimentally verified.

In general any sampling function, S(u, v) can be expressed as

$$S(u,v) = \frac{1 + W(u,v)}{2} \tag{7.5}$$

where W(u, v) takes on the value ± 1 as some function of frequencies u and v. Consequently, the retransformation of the sampled frequency plane will be

$$g(x,y) = \frac{1}{2}\left[f(x,y) + f(x,y) \circledast w(x,y)\right] \tag{7.6}$$

where $\circledast$ implies a two dimensional spatial convolution. If the term $f(x,y) \circledast w(x,y)$ is taken to be noise, then the average noise power will be a function of the original signal, f(x, y), and will be fairly strong. Thus any deterministic sampling procedure will affect the

convolution noise in a deterministic manner. A nondeterministic sampling procedure that might be envisioned is one in which w(u, v) becomes a random variable over the frequency plane. If this random variable is highly uncorrelated, then the noise power is spread out over the reconstructed image. Such a technique was implemented by developing a random binary plane where 50% of the frequency components were sampled at random positions. The reconstructed image is displayed in figure 7-6c. Notice that the effect of convolving the overpowering footpad section of the image across the plane is clearly visible. This can also be interpreted as the fact that the error introduced in the low frequency portion of the Fourier domain, by not sampling there, induces an absolute amplitude noise that saturates the higher frequency information. The next step in the random sampling procedure is to random sample only the high frequencies. This has been done with considerable improvement over figure 7-6c and is presented in figure 7-6d. Although the improvement is great over figure 7-6c, the image reconstruction is still poor for the small amount of bandwidth gained.

7.4 Coding

In chapter 5 a quantization process was developed which allowed the entire frequency domain to be coded in six bits. The retransformations, figures 5-2 and 5-3, were comparable, ignoring truncation

error, to the original image; and therefore, equal bandwidth requirements were achieved for the spatial and Fourier domains. A bandwidth reduction is possible by reducing the number of quantization levels or by reducing the number of code words for certain frequencies. Combinations of these two techniques have been implemented, and are presented below.

An example of the first technique, shown in figure 7-7b, is to quantize the entire plane into 32 instead of 64 levels according to a frequency varying power spectrum. This technique obviously results in greater quantization noise. About 16.7% of the bandwidth has been saved. Notice that there appears to be diagonal low frequency modulation from the lower left corner to the upper right corner caused by the quantization error.

The second technique to be implemented is one that codes certain frequency samples to just four bits even though they have been quantized to 64 levels. This means that any code word greater than seven is changed to code word seven and the proper sign bit affixed. The frequencies for which this coding scheme is used are those spectral points which are indicated to have small absolute values by the power spectrum plane. Such a coding technique does not add to the quantization noise but does introduce a coding error at certain frequencies. The results of this technique are indicated in figure 7-7c. The bandwidth saved is 23.5%. Notice that this technique has

a) 64 Level Gaussian Quantization. No Bandwidth Reduction

b) 32 Level Gaussian Quantization. 16.7% Bandwidth Reduction

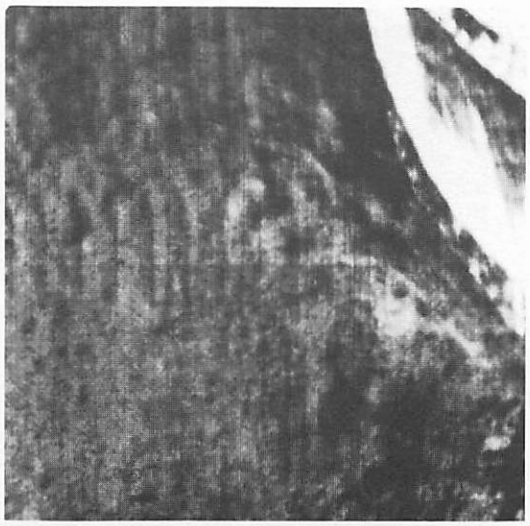

c) 64 Level Gaussian Quantization and 4 Bit Coding of High Frequencies. 23.5% Bandwidth Reduction

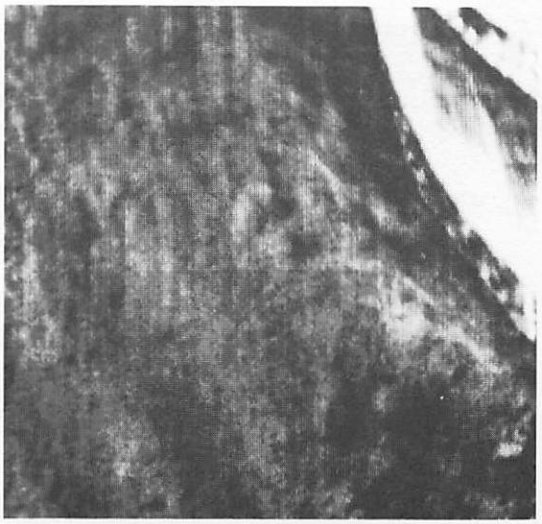

d) 32 Level Gaussian Quantization and 4 Bit Coding of High Frequencies. 35% Bandwidth Reduction.

Figure 7-7. -- Quantizing and Coding Bandwidth Reduction Techniques

introduced an undulating effect in the left center of the figure. Combination of the above two techniques results in a bandwidth reduction of 35% when a 32 level quantization scheme is combined with four bit coding at low amplitude frequencies. Results of this procedure are displayed in figure 7-7d. Figure 7-7a is a 64 level scene without bandwidth reduction transmission presented for comparison. From figure 7-7d both the diagonal modulation due to 32 level quantizing and the horizontal undulation due to four bit coding are visible. Consequently, these techniques tend to give erroneous reconstruction over the entire plane, and probably are not valuable enough as a trade off for bandwidth saved.

7.5 Conclusions

A bandwidth reduction technique has been presented which, coupled with scanning procedures, combines to form a novel and promising method of image construction with very large bandwidth reduction factors. This technique could have spacecraft applications where bandwidth is a significant factor and transmission should not be wasted on redundant images. Decisions concerning the desirability of transmitting the full bandwidth of a scene can be made after the transmission of a small portion (on the order of one sixtieth to one thirtieth) of the frequencies of the scene.

Applications of spatial bandwidth reduction techniques in the

Fourier domain have met with little success. The dynamic range in the Fourier domain results in impractical edge detection coding methods. The dynamic range coupled with rapidly changing phases, and thus signs of real and imaginary frequency components, causes most types of predictive and interpolative rules to fail, especially for any significant amount of bandwidth reduction. Sampling techniques fail because of the convolution effect in retransformation. Uncorrelated random sampling procedures result in large noise components spread over the entire space domain.

The newly developed Fourier domain coding laws offer little more promise for bandwidth reduction. Both coding and quantization noise become large when any amount of bandwidth is reduced. This, in part, can be attributed to the fact that any frequency alteration affects the whole spatial domain. While the reconstructions obtained from the bandwidth coding and quantizing schemes produce recognizable and fairly pleasing results, the amount of bandwidth saved is not enough to justify the development of the necessary frequency coding techniques.

CHAPTER 8

SUMMARY

This chapter summarizes the results of research reported in the previous chapters. In addition, a brief discussion on the philosophy of computational techniques for maximum accuracy and display purposes is presented. Finally, suggested future research stemming from the results reported here is briefly discussed.

8.1 Computation and Display

In chapter 2 it was implied that single precision integer arithmetic was satisfactory for use in the Fourier algorithm if all normalization procedures were delayed until absolutely necessary. The same philosophy has been maintained in processing the planes of data in all other computations besides Fourier transforming. An interesting dichotomy arises from using this normalization approach when making comparisons with displayed results. It can, and has happened, that certain retransformed planes of data are a closer match to the original before normalization than after. In other words, an original picture might be restricted to six bit quantization, whereas, the retransformed image could very likely contain levels

greater than 63. Unfortunately, all picture elements greater than 63 will be displayed on the output monitor modulo 64, a very distressing circumstance to the viewer. Therefore, all processed images must be normalized to 63 before viewing. But such a normalization procedure can introduce a greater discrepency between the original and post-normalized image than between the original and pre-normalized image. However, the ultimate receiver of this data processing is the human eye, and consequently numerical accuracy will often be sacrified for visual results.

Another topic of discussion is that of reconstructing images after a Fourier transformation back to the spatial domain. As indicated in chapter 3, there exist two means of reconstructing an image from a half plane of frequency data. One approach is to make the frequency plane symmetric conjugate, thereby guaranteeing a real image retransformation. The second approach is to retransform with half the Fourier plane being zero, and then extract the real field of data from the complex plane of retransformed data. This is the Hilbert transform approach. From an experimental point of view, it has been found that the former symmetric conjugate plane approach results in slightly superior image reconstructions for the following reasons. Since the frequency plane is made symmetric conjugate before retransformation, the output plane is guaranteed to be real. However, due to the finite computations involved, certain errors,

some of which will be in the imaginary fields of data, will accumulate. The numerical values that appear in the imaginary data fields are several orders of magnitude smaller than the real field data and do not affect the real data significantly. In the Hilbert retransformation approach, both real and imaginary data fields are of the same order of magnitude; the former contains the desired image and the latter contains the Hilbert transform of the image. Because of the similar orders of magnitudes, interaction between the fields of data will be more significant, and the imaginary data field will tend to have a greater influence on the real field in the Hilbert case than in the symmetric conjugate case. For this reason all of the experimental results presented have been obtained using the symmetric conjugate method.

8.2 Conclusions of Research

Chapter 1 indicated that the object of research was to investigate the feasibility of developing a Fourier image coding technique that might have advantages over spatial image coding for certain communications applications. The results of this research indicate that Fourier coding is feasible, and offers significant advantages for communicating images over certain types of channels. There are four general conclusions to this research that should be emphasized.

The first successful result is the fact that it has been

experimentally possible to verify that equal bandwidths are possible for the Fourier and spatial domains. The derivation of probability density functions for Fourier domain samples provide for the development of a frequency variable quantization scheme. Using such a scheme, a variance, or σ plane, concept was introduced which produces a different density function, and therefore quantization law for each frequency sample. The results of this investigation allow for the experimental development of equal bandwidth requirements in both spatial and Fourier domains.

The second result of the research which deserves further mention is the matched filter image evaluation technique presented in chapter 4. While research in this area needs further investigation, it should be mentioned that fairly encouraging results have been obtained. The experiment in chapter 4 reveals that the matched filter evaluation procedure correlates well with the psychophysical viewing properties of the human observer. In addition, the matched filter evaluation tool is used in chapter 5 to discern subtle differences, undetectable to the eye, in using different variance planes in the quantization scheme presented in that chapter. While the matched filter has been used with some success, it is not to be interpreted as the answer to all automatic image evaluation procedures. Since the filter does not differentiate between relevant and irrelevant images, it should not be used as an evaluation tool without the parallel use of

the human observer.

The third result of interest is the noise immunity work presented in chapter 6. In general, the Fourier domain offers greater immunity in transmission through a noisy binary symmetric channel than does the spatial domain. For very low error rates the Fourier domain is superior because the small amount of noise energy introduced in the frequency domain is averaged over the entire spatial domain in retransformation, and thus becomes less offensive to the eye than the equivalent "salt and pepper" noise introduced directly into the spatial domain. For extremely high error rates it becomes desirable to introduce an error correcting code system. The additional bandwidth required for parity bits in a code word is recovered by transmitting a comparable number of fewer data points. This is advantageous in the frequency domain since the fewer data points transmitted still contain over 90% of the energy in the complete image. The result of this technique is an error reduced retransformed image which is incomplete in its higher frequencies. However, the error reduced 90% energy retransformed image is far superior to the spatially transmitted error abundant 100% energy image, as verified by the results of chapter 6.

The final result obtained from this research is the method of bandwidth reduction and sequential image construction presented in chapter 7. It was pointed out that most spatial domain techniques

are undesirable when applied to the Fourier domain. In fact the only promising Fourier domain bandwidth reduction technique seems to be the expedient of not transmitting certain data points. The advantage of this technique is that a large percentage of image energy can be transmitted with a large bandwidth reduction, thereby allowing retransformed images to be more complete than an image from an equivalent bandwidth reduction on the spatial domain alone. This capability of transmitting a high percentage of energy with a small percentage of data points allows the development of an efficient sequential image construction technique which becomes valuable over communication channels where high energy and wide bandwidth are expensive commodities. In particular, if a spacecraft is to transmit images from a distant planet to earth, an energy constraint seems likely. With the sequential image construction technique a few data points will give the viewer a good idea of the image on the distant planet. If the image looks interesting, more frequency data points can be transmitted and a better image constructed. This technique can be continued until the entire bandwidth of the image is reached or until the viewer is satisfied with the results. If the first image is uninteresting, the spacecraft camera can be commanded to a new scene and a second image can be constructed. This sequential image construction technique will allow a feedback communication system

to be developed in which the operator on earth has close control on the most efficient way to conserve power and bandwidth in space-crafts on distant planets in video communication.

The four highlighted results discussed above were primarily made possible through the use of the high speed Fourier algorithm presented in chapter 2. The speed of the algorithm has allowed numerous two dimensional Fourier transformations that otherwise would have been impossible to obtain. The algorithm is a modified version of the Cooley-Tukey approach often cited in the computer literature [7]. It is presented in detail because of the reduction in number of complex multiplications over complex addition which is a large factor in some computer systems.

8.3 Future Research

It is anticipated that the results of the research presented here will be the forerunner to further research and development in the areas of Fourier coding. Future work need not be restricted to two dimensional data transmission, but could apply to more conventional one dimensional systems or more unconventional three dimensional systems such as are envisioned in future holographic communication techniques. Areas in which immediate effort should be expended include the development of high speed two dimensional algorithms, and special purpose Fourier transforming computers. In addition,

frame differencing techniques, where only new data in temporally adjacent frames of television information is transmitted, should be investigated making use of the Fourier domain.

APPENDIX

The appendix contains the experimental information necessary to develop a laboratory facility capable of reproducing the results reported in this dissertation. Detail is not included but brief descriptions of both hardware and software systems are provided.

A.1 Hardware Equipment

The basic piece of hardware equipment used in the experimental phase of this research is a general purpose digital computer. The computer along with the other hardware systems used is displayed in block diagram form in figure A-1. The computer consists of a central processor and a nearly autonomous buffer. The memory cycle time is three microseconds with a memory storage capacity of 8192 eighteen bit computer words. There are six registers which all have eighteen bit word lengths and consequently single precision integer values are bounded by $\pm 2^{17}-1$. Since two dimensional processing requires a tremendous amount of bulk storage, six magnetic tape units are incorporated in the computer peripheral equipment. In addition, other standard digital I/O equipment necessary for program preparation is available. This equipment includes an input-output typewriter, high speed card reader, line printer, and

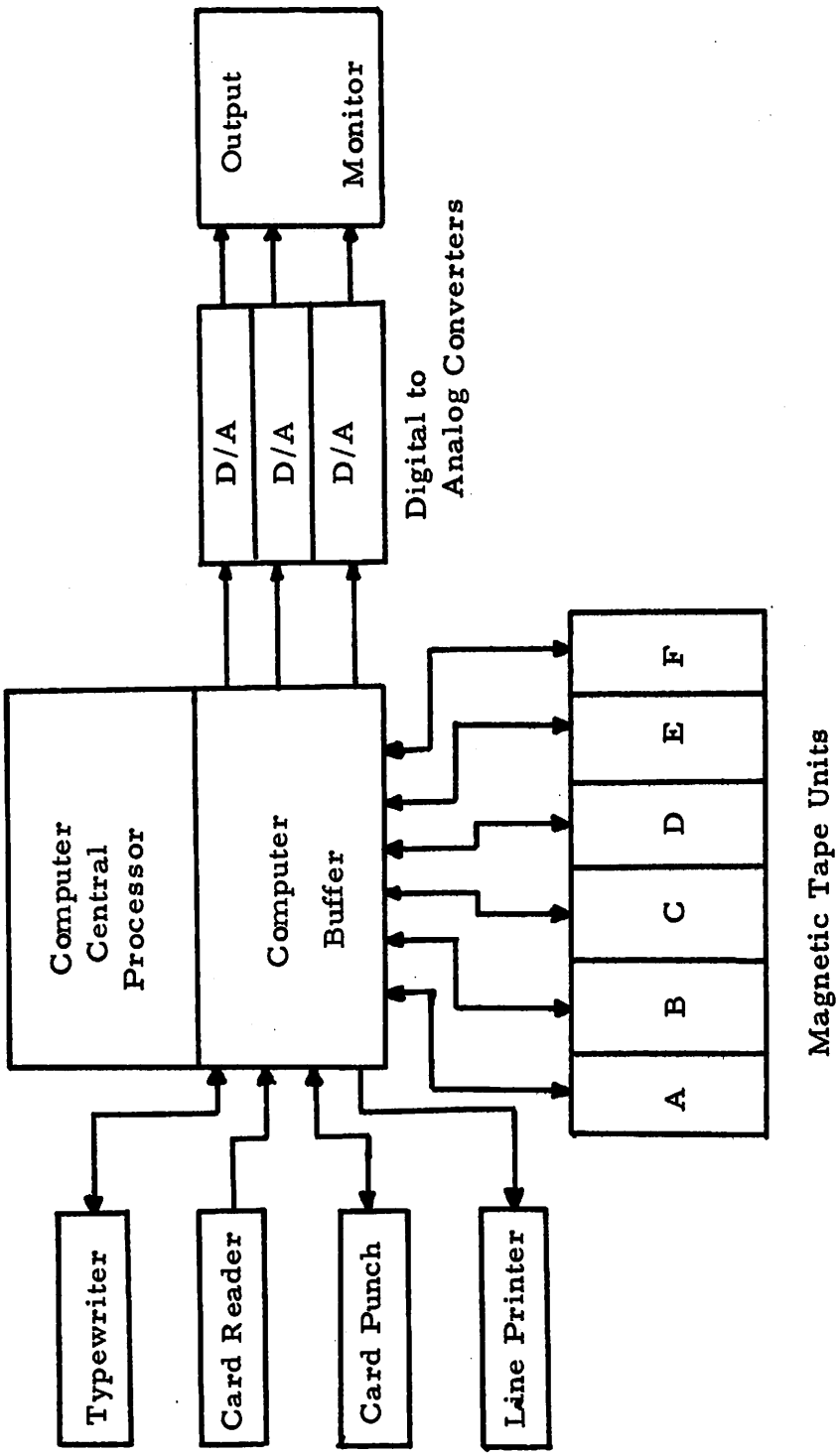

Figure A-1.--Research Computer Hardware System

card punch. The above equipment comprises an information processing system designed and built by Thompson-Ramo-Wooldridge Inc. and designated the TRW 530. All specifications for equipment and operations are included in their literature pertaining to this system. In addition to the above standard computer facility, a digital to two dimensional optical converter is necessary. Such a device has been built and has been used for all photographic work. Three digital to analog converters are driven by the computer to provide analog X and Y sweep and Z axis video voltages to an eight by ten inch cathode ray tube monitor. The picture to be displayed is placed on a magnetic tape unit which is then commanded to transfer its data to the output cathode ray tube monitor. A camera is then focussed on the monitor and a time exposure taken to record the picture on photographic film.

A.2 Two Dimensional Fourier Program

The Fourier algorithm described in chapter 2 is for a one-dimensional case. For a two-dimensional transformation the algorithm is simply used 2N times. A two-dimensional Fourier transform program has been developed to Fourier transform $f(x,y)$ into $F(u,v)$ using the above algorithm.

The two-dimensional Fourier transform program presented

here is described with particular reference to figure A-2 depicting control and data flow of the program. The program is quite versatile and consequently requires certain operator inputs. Specifically the operator defines the following three inputs.

1) Dimensions of input (i.e., number of samples in the x and y direction. The number of samples N in each direction must be a power of two, $N = 2^n$ for any n)

2) Real or complex input (i.e., whether each sample is real or complex)

3) Normalizing constant. This decision is necessary in order that high frequency low amplitude information is not lost due to normalization; or alternately, so that overflow does not occur.

Once the operator has specified the input format the control program takes over and the entire program is now automatic. The control program generates the complex coefficient adresses, controls individual program sequencing, and generates spectral point storage addresses. To perform these functions the control program must accept the operator input parameters, store and type output messages, set up the proper variables as a function of the input parameters and test and initialize all magnetic tapes. A subfunction of the control program is to output, under control of a test switch,

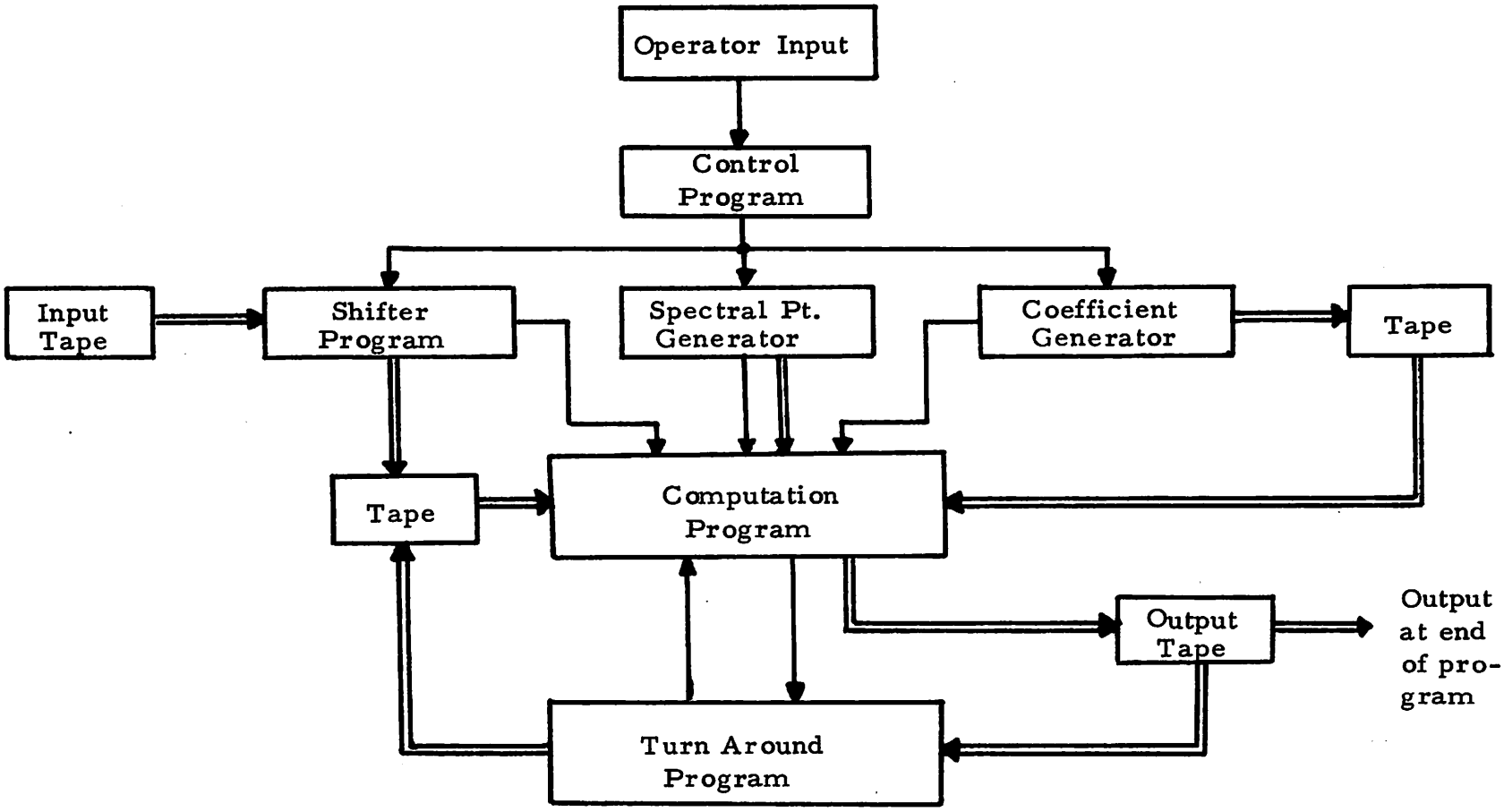

Figure A-2.--Two Dimensional Fourier Transform Program

the Fourier values and spectral points as well as the program number designations. This information is typed on the line printer and is only used for debugging purposes. The control program initiates the shifter program, the spectral point generator, and the coefficient generator. The order in which each of these three programs occurs is immaterial as all three must be complete before the computation program can commence.

The shifter program takes the input function which is stored on magnetic tape and causes a phase shift in that information so that the Fourier transform output will be centered. This is necessary since the Fourier algorithm is designed with the origin in the upper left corner of the input function. The phase shift introduced by this program is implemented by changing the sign of the number in each position when the sum of the space coordinates, x+y, is odd. This particular phase shift will cause the frequency domain function to be shifted to the center according to the Fourier shifting theorem. This can be verified for the finite Fourier case by defining the following functions. Let

$$F(u,v) \triangleq \frac{1}{N} \sum_{x,y=0}^{N-1\,N-1} f(x,y) \exp\left\{ \frac{2\pi i}{N} (xu+yv) \right\} \qquad (A.1)$$

and let

$$G(u,v) = \frac{1}{N} \sum_{x,y=0}^{N-1\,N-1} (-1)^{x+y} f(x,y) \exp\left\{\frac{2\pi i}{N}(xu+yv)\right\} \qquad (A.2)$$

Then by the basic relations

$$(-1) = \cos\pi = e^{i\pi} \qquad (A.3a)$$

$$(-1)^x = e^{i\pi x} \qquad (A.3b)$$

$$(-1)^y = e^{i\pi y} \qquad (A.3c)$$

$$(-1)^{x+y} = e^{i\pi(x+y)} \qquad (A.3d)$$

the relation between $G(u,v)$ and $F(u,v)$ is found to be

$$G(u,v) = \frac{1}{N} \sum_{x,y=0}^{N-1\,N-1} f(x,y) \exp\left\{\frac{2\pi i}{N}(xu+yv) + i\pi(x+y)\right\} \qquad (A.4)$$

or

$$G(u,v) = \frac{1}{N} \sum_{x,y=0}^{N-1\,N-1} f(x,y) \exp\left\{\frac{2\pi i}{N} x\left(u+\frac{N}{2}\right)\right\} \exp\left\{\frac{2\pi i}{N} y\left(v+\frac{N}{2}\right)\right\} \qquad (A.5)$$

and finally

$$G(u,v) = F\left(u+\frac{N}{2},\ v+\frac{N}{2}\right) \qquad (A.6)$$

The shifter program causes the shifted input function to be written on a second tape. When this operation is completed, the program signals the computation program. The spectral point generator program generates the N output spectral points in a

particular sequence. It is this particular sequence that allows for minimum computations in the Fourier algorithm. The sequence is the same as would be obtained by counting up from zero to N in binary and interpreting each count with the significance of the binary representation reversed. When the spectral point generator has generated N points, it signals the computation program that it is finished. The coefficient generator generates the exponential coefficient $\exp\left\{\frac{2\pi i}{N} k\right\}$ for all k ranging from zero to $\frac{N}{2}-1$. These coefficients are stored on magnetic tape for use in the actual computation program.

The computation program is the essence of the two-dimensional Fourier transform program. It begins when the shifter, spectral point, and coefficient programs are complete. This program takes a one-dimensional Fourier transform of each line of the input tape and stores it on another tape. It does this by a sieve type of operation in which the initial data is added together in a certain order so that minimum computation and storage are utilized. The computation program determines which operation, PN0 through PNn, is to be used to calculate the value for a particular spectral point. An operation, PNi will call one or more of three subroutines which perform complex addition, subtraction, and multiplication. When the computation program has Fourier transformed the N lines of the input in one dimension, it passes control to the turn around

program.

The turn around program performs a 90^{o} rotation on the output of the semi-transformed data. The data is called "semi-transformed" because it has been Fourier transformed in one dimension only. The turn around program places the rotated semi-transformed data onto the input tape overwriting the data there since it has already been used. This operation prepares the data for a second pass through the computation program. The second pass produces the second dimension of the Fourier transformation and places the final result on the output tape. The entire program is now complete, and the two-dimensional Fourier transformation program turns control back to the operator.

A.3 Software Programs

The programs used in the development of the picture processing capability demonstrated in this dissertation are described below. They will be presented with their code names. The descriptions will be brief; and complete listings will not be presented as the listings are only intelligible to those knowledgable in the TRW 530 software Symbolic Instruction Assembly System (SIAS).

SYSTEM: The system program is the master set of instructions under whose control all other programs are called from the system library. The system library is a magnetic tape on which all

programs are stored according to the three letter titles as presented in this appendix. The system program is written in machine language and is read into memory whenever tape unit 0 is selected from its load point position. The program converses with the operator through the typewriter.

FOI: The one dimensional Fourier Transform program follows the algorithm presented in chapter 2. It is written in maching language for speed of computation considerations and is contained in a loop such that an entire plane of data is one dimensionally Fourier transformed.

STA: A turn around program is needed to complete the two dimensional Fourier transformation. This program takes the one dimensionally transformed result of the output of FOI and rotates the plane 90^{o}. The rotation is performed by a type of scanning routine that selects the correct elements from lines of the prerotated plane and forms new lines of rotated information.

SAN: This program scans a complex plane of data to find the positive and negative extremes. It then adds the negative extreme to the entire plane forming a totally positive complex plane. Then it extracts the real components of each complex sample and normalizes these components to six bits. This makes the output of the program a real positive plane compatible with the cathode ray tube

display system. This program is very useful for preparing doubly transformed scenes for output display as it automatically adds the necessary constant bias that was lost in not transmitting the origin frequency sample in the Fourier domain.

TRI: This machine language program is necessary for all display work. It causes a plane of data stored on a magnetic tape to be read into memory and out of memory onto the monitor. This program is used in combination with some computer hardware changes that allows a program instruction transfer of data to the typewriter to actually transfer information to the monitor.

SM1: This program forms the square root of the magnitude of each complex sample of a plane and then normalizes each number to six bits. The output of this program is real, positive, and compatible with the monitor and is used in displaying frequency domain information. One variation of this program will form the natural logarithm of the magnitude of each element in the plane and is used for obtaining knowledge of low amplitude information in the frequency domain. A second variation allows a clipping level to be selected such that all values below that level are renormalized to the maximum 6 bit thereby allowing a linear output of very low amplitude information.

S3D: This program scans a normalized real positive plane and forms an output tape that contains a three dimensional view of

the relative amplitudes of the original plane. When scanned onto the monitor, a perspective display results. Such a mechanism was used in the demonstration of dynamic range in chapter 3.

SSH: This program takes half a Fourier frequency plane and forms a full plane with two options. The first is that the second half of the new plane will be identically zero. This allows for Hilbert transform reconstruction. The second option forms the second half of the new plane as the symmetric conjugate of the first half. When this full plane is two dimensionally Fourier transformed, a real two dimensional function results.

SGA: This program quantizes each real and imaginary sample to one of an operator determined number of quantum levels from a Gaussian distribution. An individual quantum scale is used for each frequency sample and is determined by a variance function at the given frequency. The program reads in the frequency plane to be quantized on one tape and the variance plane on a second tape. A third tape is used as the output or quantized frequency domain. Two additional options are available in the program and allow for coding as well as quantizing and decoding. The coding option would be used if the frequency plane were to be subjected to some type of channel disturbance and the decoding option would act as a receiving station.

SRQ: This program operates very similarly to the Gaussian

quantization program, SGA, except the square root of the magnitude of each complex frequency sample is formed and is the quantized to one of a pre-determined number of quantum levels according to a Rayleigh distribution whose variance again changes as a function of frequency. Also the phase of each complex frequency sample is formed and quantized to one of a pre-determined number of quantum levels. This program also has two tapes as inputs and one as an output with the options of coding and decoding as desired.

SFQ: This program implements a linear quantization rule. It quantizes each real and imaginary sample linearly between plus and minus the most extreme values of the plane.

SCH: This program introduces a bit error from a uniform error probability density at any error rate from $p = 10^{-6}$ to $p = 1$. Such a program allows for the random injection of errors at a given rate of input data exactly as a binary symmetric communication channel. The program is lengthy because each bit that enters the channel requires a random number generator to be called and compared with an error threshold.

SFI: This program simple adds, subtracts, or multiplies two planes together. It is useful for filtering and noise removal applications. In particular a plane can be formed which emphasizes certain frequencies and when multiplied by the Fourier transform of a scene the output becomes a filtered frequency domain ready for

retransformation.

SLB: In the course of two dimensional picture processing it becomes imperative that intermediate results be stored for later reference. A picture library has been developed for this purpose. The library stores consecutive pictures serially line by line. An index is provided for a title and dimensions of planar data stored. The program has three options, the first of which will allow the operator to initiate a tape to begin a new library. A second option allows a picture to be stored by title and dimension at any time on the library. The third option allows the operator to read any picture from the library by title and dimension.

SJP: A more efficient library procedure has been developed for storing pictures normalized to six bits. Rather than storing a computer word of 18 bits for each picture sample, three picture samples are stored per computer word. This increases the storage efficiency threefold, but of course cannot be used to store numbers out of the 0-63 range.

SPG: Often a simple plane of data is desired for computation purposes. This program allows a plane to be formed using a simple coded typewriter input. Restrictions on the resolution of the plane are 256, 512, 1024 and samples must range between 0-999.

SGE: A much more generalized picture generating technique is afforded by this program. Data is read into the computer on cards

and any range of positive or negative samples is possible.

SHS: A program that is often used for trouble shooting as well as data gathering is the histogram program. This program reads a tape into memory and makes a histogram of the different numerical values on that tape. It will histogram a variable dimensional plane of data and can process as many as 1000 different levels. The output of the program is a printer listing of the level and frequency of occurrence of each level. In addition a normalized graph is plotted for graphic representation.

SER: A program had been written to make statistical measurements on the difference of two planes. Two tapes are used for inputs to the program and the absolute value of the difference is placed on a third tape. The maximum difference is printed by the typewriter as are both mean square and variance errors per element. A histogram can be made of the output tape thereby forming a distribution of absolute value errors.

SRO: This program rotaes a plane 180^{o}, and is necessary when the SER program is used for error measurement. The 180^{o} rotation counter balances the two 90^{o} rotations inherent in the positive Fourier transform kernel. Two tape units are used for this program, the output tape being obtained by reading the input tape backwards.

SSS: This program multiplies a spatial domain scene by $(-1)^{x+y}$ in order that the frequency domain be properly centered on the monitor display.

SGU: This program calculates a normalized two dimensional Gaussian plane and writes it on a tape. Each dimension has an independent variance allowing stretching or shrinking of either dimension. The results of the program have been used as mutliplicative filters and power spectral densities.

SEX: This program extracts either the real of imaginary field of data from a complex plane of data. It is used in evaluating Hilbert quadrature filter retransformation techniques back to the spatial domain.

SEN: This program is designed to measure the total energy in a real or complex plane of data. It can be used in measuring energy transmitted in bandwidth reduction schemes and in scanning algorithms. The input to the program is a single tape and the output is on the tyepwriter.

SMA: The digital implementation of the complex matched filter correlator is in this program. Two tapes, a master and processed frequency plane, are inputs. The program measures the correlation of the processed plane with respect to the master plane. The four significant figure output is on the typewriter.

CPY: This is a utility program that copies one tape onto another irrespective of the data format.

SCI: This program forms a circular binary filter of variable radius which has the capability of being used in bandwidth reduction and low pass or high pass filtering schemes.

SBG: This program measures the energy of a Fourier domain plane as a function of radial distance away from the origin. The output is graphical as well as numerical and is presented on the line printer.

References

1. Pratt, W. K. "A Bibliography on Television Bandwidth Reduction Studies," IEEE Transactions on Information Theory, Vol. IT-13, No. 1 (January, 1967), pp. 114-115.

2. Cutrona, L. T., Leith, E. N., Palermo, C. J., and Porcello, L. J. "Optical Data Processing and Filtering Systems," IRE Transactions on Information Theory, (June, 1960), pp. 386-400.

3. Vander Lugt, A. "Operational Notation for the Analysis and Synthesis of Optical Data-Processing Systems," Proceedings IEEE, Vol. 54, No. 8 (August, 1966), pp. 1055-1063.

4. Born, M., and Wolf, E. "Principles of Optics," Pergamon Press, New York, N.Y. (1959).

5. Vander Lugt, A. "Signal Detection by Complex Spatial Filtering," IEEE Transactions on Information Theory, Vol. IT-10, pp. 139-145.

6. Cooley, J. W., Lewis, P.A.W., and Welch, P. D. "Historical Notes on the Fast Fourier Transform," Proceedings IEEE, Vol. 55, No. 10 (October, 1967), pp. 1675-1677.

7. Cooley, J. W., and Tukey, J.W. "An Algorithm for the Machine Calculation of Complex Fourier Series," Mathematics of Computation, Vol. 19, No. 90 (1965), pp. 297-301.

8. Andrews, H. C. "A High Speed Algorithm for the Computer Generation of Fourier Transforms," IEEE Transactions on Electronic Computers, (April, 1968).

9. Forman, M. L. "Fast Fourier-Transform Technique and Its Application to Fourier Spectroscopy," Journal of the Optical Society of America, Vol. 56, No. 7 (July, 1966), pp. 978-979.

10. Leith, E. N. "Photographic Film as an Element of a Coherent Optical System," Photographic Science and Engineering, Vol. 6, No. 2 (March-April, 1962), pp. 75-80.

11. Papoulis, A. "The Fourier Integral and Its Applications," McGraw-Hill, New York, N. Y. (1962).

12. Andrews, H. C. "Entropy Considerations in the Frequency Domain," Proceedings IEEE, Vol. 56, No. 1 (January, 1968), pp. 113-114.

13. Reza, F. M. "An Introduction to Information Theory," McGraw-Hill, New York, N.Y. (1961).

14. Hewitt, E., and Stromberg, K. "Real and Abstract Analysis," Springer-Verlag, New York, N.Y. (1965).

15. Bellman, R. E. "Introduction to Matrix Analysis," McGraw-Hill, New York, N. Y. (1960).

16. Loeve, M. "Probability Theory," D. Van Nostrand, Princeton, N. J. (1955).

17. Wozencraft, J. M., and Jacobs, I. M. "Principles of Communication Engineering," John Wiley and Sons, New York, N.Y. (1965).

18. Panter, P. F. "Modulation, Noise, and Spectral Analysis Applied to Information Transmission," McGraw-Hill, New York, N.Y. (1965).

19. Bochner, S. "Harmonic Analysis and the Theory of Probability," University of California Press, Berkeley, California (1955).

20. Gnedenko, B. V. "The Theory of Probability," Chelsea Publishing Company, New York, N.Y. (1962).

21. Rozanov, Y. A. "Stationary Random Processes," Holden-Day Publishing Company, San Francisco, California (1967).

22. Diananda, P. H. "The Central Limit Theorem for m-Dependent Variables," Proceedings of the Cambridge Philosophical Society, Vol. 51 (1955), pp. 92-95.

23. Davenport, W. B., Jr., and Root, W. L. "An Introduction to the Theory of Random Signals and Noise," McGraw-Hill, New York, N.Y. (1958).

24. Paley, R.E.A.C., and Wiener, N. "Fourier Transforms in the Complex Domain," American Mathematical Society Colloquium Publication, 19, New York, N.Y. (1934).

25. Reed, I. S. "A Class of Multiple Error-Correcting Codes and the Decoding Scheme," IRE Transactions, PGIT-4 (1954), pp. 38-49.

26. Peterson, W. W. "Error Correcting Codes," The M.I.T. Press, Cambridge, Massachusetts (1961).

27. "Tables of the Binomial Probability Distribution," Department of Commerce, National Bureau of Standards, Applied Mathematics Series, No. 6 (January, 1950).

28. Roberts, L. G. "Picture Coding Using Pseudo-Random Noise," IRE Transactions on Information Theory, Vol. IT-8, No. 2 (February, 1962), pp. 145-154.

29. Lewis, N. W. "Television Bandwidth and Kell Factor," Electronic Technology, Vol. 39, No. 2 (February, 1962), pp. 44-47.

30. Goodall, W. M. "Television by Pulse Code Modulation," IRE National Convention Record (March, 1949), pp. 49-51.

31. Kretzmer, E. R. "Reduced Alphabet Representation of TV Signals," IRE Convention Record, Part 4 (1956), pp. 140-147.

32. Kay, N. D., Knapp, C. F., and Schreiber, W. F. "Synthetic Highs - An Experimental TV Bandwidth Reduction System," 84th SMPTE Convention (October, 1958), pp. 1-18.